Development and Validation of a Model to Predict the Temperature of a Photovoltaic Cell

by

TY W. NEISES

A thesis submitted in partial fulfillment of
the requirements for the degree of

MASTER OF SCIENCE
(MECHANICAL ENGINEERING)

at the

UNIVERSITY OF WISCONSIN – MADISON

2011

Approved by

_____

Professor Sanford A. Klein

_____

Professor Douglas T. Reindl

Date:_____

Abstract

The temperature of a photovoltaic module affects the efficiency of the module and is largely affected by the mounting configuration. This purpose of this project is to develop and validate a model to accurately predict the cell temperature of a module that adapts to various mounting configurations, mounting locations, and climates while only requiring readily available data from the module manufacturer. Results from this model are also compared to results from published cell temperature models.

A general energy balance model was developed to predict the cell temperature of a mono-Si BIPV module. This model was simplified and validated using field measurements into a steady state model that creates a thermal resistance network between the cell and the ends of the module. This model was also validated for a poly-Si BIPV module. Finally, the model was adapted for rack mounted modules. Annual simulation results for the two BIPV modules and two rack mounted modules showed a performance model applying the temperature output of the steady state energy balance model calculates annual performance within 2.5% of results found by the same performance model applying the measured temperature. The steady state model was found to be as accurate for rack mounted and more accurate for BIPV modules than comparable cell temperature models.

Research into model simplification resulted in a study of the procedure to calculate the NOCT of a module. This study found the procedure to be inaccurate under some testing conditions as the published correction factor charts did not agree well with the validated steady state model. Futhermore, a published cell temperature model applying NOCTs predicted by the steady state model rather than measured NOCTs produced more accurate results.

The model is also adapted for roof and building mounted modules, but has not been validated at the time of publication.

Acknowledgements

This project was only possible through contributions from others. While my limited writing talents and spatial constraints make a thorough recognition impossible, I hope the following is a sufficient summary.

I would like to thank NREL for making this project possible by sponsoring this research as well as providing datasets. Special thanks to Bill Marion for his quick responses to my questions. I would also like to thank NIST for providing datasets and hosting me for a week so that I could learn about the experimental sites and module construction. I am also grateful to Sandia for providing datasets and allowing me to participate in their PV workshop.

I am very indebted to my advisors, Professors Klein and Reindl. Sandy's intelligence and ability to clearly communicate his ideas are amazing and were often on display as he guided my research. Doug's unique combination of industrial and academic knowledge often provided a larger sense of direction and purpose to my project. I would also likely to sincerely thank them for taking an interest in and offering advice about my life outside of academia.

I am also grateful to the rest of the professors who made the SEL a stimulating learning environment. I would especially like to thank Professor Nellis for serving on my thesis committee and his dry sense of humor during his terrific heat transfer classes. I would also like to thank Professor Beckman for sharing both his extensive PV knowledge and stories of a young Sandy.

I would like to thank Greg “The Rock” Marsicek for his contributions as an undergraduate assistant. His effort and commitment was exceptional, especially considering the blandness of his assignments. Good luck as a graduate student, sir.

I am grateful to Matt Boyd for giving me a great start as an undergraduate in the SEL and providing timely advice as I followed his path through graduate school.

My classmates in the SEL were intelligent, friendly students who were always willing to help solve a problem and have a good time. I would especially like to thank the folks in 1337 who were forced to spend their days with me: Bill, Greg, Lukas, Matt, Mandy, Michael, Rote, and Will. Special thanks to Will for being my sounding board and being a good sport about losing in soccer (or football, if he prefers).

Finally, I would like to thank my family and friends for their continual support throughout my entire educational career. I would especially like to thank my parents for their encouragement and belief in me. I am also very grateful to my sister for selflessly going out of her way to take care of me during my time in Madison. Most of all, I would like to thank my fiancée, Jordan, whose love, grace, and sense of humor have kept my spirits high and encouraged me to improve.

Table of Contents

Abstract ..... **i**
Acknowledgements ..... **iii**
Table of Contents ..... **v**
List of Figures ..... **xi**
List of Tables ..... **xv**
List of Tables ..... **xv**
Nomenclature ..... **xvi**
1. Introduction **1**
1.1 Project Purpose 1
1.2 Photovoltaics 1
1.2.1 Technology 1
1.2.2 Composition 2
1.2.3 Application 3
1.3 Performance 4
1.3.1 Performance Models 6
1.3.2 Cell Temperature Models 6
1.3.2.1 Empirical Models 7
1.3.2.2 Theoretical Models 7
1.3.2.3 Semi-Empirical Models 8
1.4 Research Motivation 8
2. Development of Energy Balance Model **9**
2.1 NIST Experimental Site and Datasets 9
2.2 Energy Balance Model 11
2.3 Energy Inputs 13
2.3.1 Cell Absorbed Radiation 13
2.3.2 Cover Absorbed Radiation 14
2.4 Energy Outputs 15
2.4.1 Power Output 15
2.4.2 Convective Heat Transfer 16
2.4.2.1 Free Convection 17
2.4.2.2 Forced Convection 18

2.4.2.3 Combining Free and Forced Convection Coefficients 20
2.4.3 Radiative Heat Transfer 21
2.5 Consideration of Spatial Temperature Gradients 22
2.6 Consideration of Thermal Capacitance 25
2.7 Determining an Appropriate Nodal Structure 26
2.8 Specifying the Model Structure, Correlations, and Input Data Type 29
2.8.1 Wind Speed Input 30
2.8.2 Hourly Data 31
2.8.3 Long-term Simulation Procedure 32
2.8.4 Statistical Analysis 33
2.8.5 Results 34
2.8.5.1 Combining Free and Forced Convection Coefficients 34
2.8.5.2 Free and Forced Convection Coefficients 34
2.8.5.3 Transient and Steady State Models 35
2.8.5.4 Five Minute and Hourly Datasets 36
2.9 Verification of Results 37
2.9.1 Poly-Si Module Performance Data and Material Properties 38
2.9.2 Long-term Simulation Results 38
2.9.3 Emissivity of ETFE cover 40
2.10 Summary 40
3. Reducing Model Inputs to Available TMY Data 43
3.1 Estimating the Surroundings Temperature 43
3.1.1 Sky Temperature 44
3.1.2 Ground Temperature 45
3.1.3 View Factors 45
3.1.4 Results 45
3.2 Adjusting the Roof-Measured Wind Speed to the South Wall at NIST 47
3.2.1 Power Law Adjustment 47
3.2.2 Building Effects 50
3.3 Predicting the Backside Thermal Resistance of the Module 54
3.3.1 Measurement of NOCT 55
3.3.2 Thermal Modeling of Module at NOCT Conditions 56

3.3.2.1 Calculating the Cell Absorbed Radiation 58
3.3.2.2 Calculating the Cover Absorbed Radiation 58
3.3.2.3 Calculating Radiative Heat Transfer 58
3.3.2.4 Calculating Convective Heat Transfer from the Module to Ambient Air 59
3.3.2.5 Backside Emissivity 61
3.3.3 Results 62
3.4 Investigating Differences between Modeled and Measured NOCTs 63
3.4.1 Analysis of NOCTs Reported on Manufacturers Datasheets 63
3.4.2 Comparison of Correction Factor Charts 64
3.4.3 Differences between Insulated and Uninsulated Modeled Correction Factor Charts 67
3.4.4 Differences between Modeled and Standard Correction Factor Charts 69
3.4.5 Suggested Changes to Improve Accuracy of NOCT Measurement 70
3.4.5.1 Report Testing Conditions with NOCT: Eliminate Correction Factor Charts 71
3.4.5.2 Provide Multiple Correction Factor Charts 72
3.5 Summary 72
4. Annual System Performance Validation 75
4.1 Steady State Energy Balance Model for Rack Mounted Modules 76
4.1.1 Absorbed Radiation 76
4.1.2 Power Output 76
4.1.3 Convective Heat Transfer 76
4.1.4 Radiative Heat Transfer 76
4.1.5 Interior Thermal Resistances 77
4.2 Additional Cell Temperature Models 77
4.2.1 Duffie and Beckman 77
4.2.2 Skoplaki et al. 78
4.2.3 King (Sandia) 79
4.3 Rack Mounted Modules Located at Sandia National Laboratories 80
4.3.1 Dataset Specific Adjustments 80
4.3.1.1 Adjustment of Wind Speed with Respect to Differences between Measurement and Module Heights 80

4.3.1.2 Consideration of Adjacent Buildings 81
4.3.1.3 Module Versus Array Dimensions 82
4.4 Rack Mounted Modules Located at NREL 83
4.4.1 Dataset Specific Adjustments 84
4.4.1.1 Adjustment of Wind Speed with Respect to Differences between Measurement and Module Heights 84
4.4.1.2 Module Versus Array Dimensions 84
4.4.1.3 Cover Properties 85
4.5 Filtering Described Datasets 85
4.5.1 Procedure 85
4.5.2 Shading 91
4.5.3 Cosine Effect on Pyranometer at NIST 92
4.5.4 Maximum Power Point Tracking Error in NREL Dataset 92
4.5.4.1 Data Inconsistencies 93
4.5.4.2 Comparative Results of Filtering Methods 96
4.6 Results 97
4.7 Sensitivity Study 100
4.7.1 Cover Properties 100
4.7.2 Dimensioning 105
4.7.3 Backside Properties 106
4.7.4 Weather Inputs 106
4.7.5 Module Mounting and Surroundings 109
4.7.6 Modifications to Steady State Energy Balance Model Based on Sensitivity Study 110
4.8 The Effect of Adjusting Wind Speed with Respect to Difference between Measurement and Module Heights 111
4.9 Effect of Inaccurate NOCT Measurements on the Duffie and Beckman Cell Temperature Model 112
4.10 Summary 115
5. Development of Model for Roof and Wall Mounted Modules 117
5.1 Integrated Mounting Configuration 119
5.2 Flush Mounting Configuration 119
5.3 Gap Mounting Configuration 120

5.3.1 Mounting Structures Are Parallel to the Ridge of the Roof 121
5.3.2 Mounting Structures Are Perpendicular to the Ridge of the Roof 123
5.3.3 Mounting Structures Do Not Significantly Impede the Flow of Air in Either Direction 125
5.4 Rack Mounting Configuration 126
5.5 Application to Building Mounted Modules 126
6. FORTRAN Implementation 127
6.1 New Parameters: Pre-Defined Options 127
6.1.1 Mounting Location 127
6.1.2 Mounting Configuration 127
6.1.3 Mounting Structure Orientation 128
6.1.4 Heat Transfer Dimensions 128
6.2 New Parameters: User-Defined Values 128
6.2.1 Module Dimensions 128
6.2.1.1 Length 128
6.2.1.2 Width 128
6.2.2 Gap Mounting Dimensions 129
6.2.2.1 Gap Spacing 129
6.2.3 Cover Properties 129
6.2.3.1 Cover Emissivity 129
6.3 Redundant Parameter 129
6.3.1 Area 129
6.4 New Input 129
6.4.1 Wind Direction 129
6.4.2 Attic Temperature 130
6.4.3 Indoor Temperature 130
6.5 Pre-Set Assumptions that Users Could Potentially Define 130
6.5.1 Sky Temperature 130
6.5.2 Ground Temperature 131
7. Conclusions and Recommendations 133
7.1 Conclusions 133
7.2 Recommendations for Future Work 136

References **139**
Appendix A: Module Properties **142**
Appendix B: Monthly Simulation Results (Sections 2.8 and 2.9) **145**
B.1: Mono-Si 145
B.2: Poly-Si 150
Appendix C: Adjusting Rooftop Wind Speed Measurements **151**
Appendix D: Free Convection Calculations (Nellis and Klein, 2009) **155**
Appendix E: Filtering Datasets **157**
Appendix F: Module Temperature and Performance Code (EES) **160**
Appendix G: NOCT Prediction Code (EES) **169**
Appendix H: Adaptable Model for TRNSYS (FORTRAN) 176

List of Figures

Figure 1.1: Typical layers of construction of a photovoltaic module. 2

Figure 1.2: Typical current-voltage and power-voltage curves of a PV module. Reproduced from Duffie and Beckman (2008). 5

Figure 1.3: Current-voltage plot showing temperature effects on a typical PV module. 6

Figure 2.1: Diagram of insulated mono-Si mounted in window recess at NIST. Arrows designate the various modes of energy transfer in and out of the module. Diagram is not to scale. 12

Figure 2.2: Heat transfer coefficients calculated for the mono-Si module from correlations in Table 2.2. The surface temperature is maintained at 300K while the ambient temperature is varied. Properties of air are calculated at the film temperature..... 18

Figure 2.3: Heat transfer coefficients calculated for the mono-Si module from correlations in Table 2.3. The cell and ambient temperature are set to 298K and 278K, respectively. Properties of air are calculated at the film temperature. 20

Figure 2.4: Cross sectional view of module divided by 2 lines per material. This structure will be referred to as a {2,2,2,2} nodal model. Drawing is not to scale. The location of the temperature measurement by NIST is also shown..... 23

Figure 2.5: Temperature prediction for June 4 applying Forced Convection Eq. (4) and Free Convection Eq. (3). Temperature predictions are calculated using both instantaneous and moving averaged wind speeds. 31

Figure 2.6: RMSEs and MBEs of temperature prediction and MBEs of power prediction for transient and steady state models. Each model was simulated with a {1,1,1,1} nodal structure and five minute input data. Forced convection correlation Equation (4) and free convection correlation Equation (1) were used for each case..... 36

Figure 2.7: RMSEs and MBEs of temperature prediction and MBEs of power prediction for {1,1,1,1} steady state model applying either hourly or five minute data. Forced convection correlation Equation (4) and free convection correlation Equation (1) were used for each case. 37

Figure 2.8: RMSEs and MBEs of temperature prediction and MBEs of power prediction for either {1,1,1,1} transient model applying five minute data or {1,1,1,1} steady state model applying hourly data. Forced convection correlation Equation (4) and free convection correlation Equation (1) were used for each case. 39

Figure 2.9: Schematic of temperatures and internal thermal resistances used in a steady state energy balance model of the module. Schematic is not to scale. 41

Figure 3.1: The difference between the energy prediction of the insulated mono-Si module caused by varying the method to predict the sky temperature and the energy prediction found using PIR measurements is displayed. The difference is made into a percentage by normalizing by the measured energy. 46

Figure 3.2: The difference between the energy prediction of the insulated mono-Si module caused by varying the method to adjust the rooftop wind measurements and the energy prediction found using the wind measurements at the module is displayed. The difference is made into a percentage by normalizing with the measured energy. 49

Figure 3.3: Schematic of steps taken to find the wind speed at the south wall module location at NIST using the measured roof wind speed. Schematic is not to scale. 52

Figure 3.4: The difference between the energy prediction of the insulated mono-Si module caused by varying the method to adjust the rooftop wind measurements and the energy prediction found using the wind measurements at the module is displayed. The difference is made into a percentage by normalizing by the measured energy. 54

Figure 3.5: Schematic of steady state energy balance on module at NOCT testing conditions. 57

Figure 3.6: Dotplot of NOCTs for the mono-Si modules approved by the CEC..... 64

Figure 3.7: Dotplot of NOCTs for the poly-Si modules approved by the CEC..... 64

Figure 3.8: Correction factor chart in ASTM and IEC standards. 65

Figure 3.9: Correction factor chart of insulated mono-Si module calculated by NOCT model 65

Figure 3.10: Correction factor chart of uninsulated mono-Si module calculated by NOCT model. 66

Figure 3.11: Correction factor chart in ASTM and IEC Standards. 70

Figure 3.12: Correction factor chart of unisulated mono-Si module calculated by NOCT model. 70

Figure 4.1: Flow chart to evaluate quality of input data and model. 91

Figure 4.2: I-V curve for Sanyo module at NREL also comparing calculated and measured maximum power points. 94

Figure 4.3: Schematic showing the differences used to find points with maximum power point tracking errors. 96

Figure 4.4: Energy prediction errors for the Sanyo array found by applying the 5-parameter model with measured backside temperatures, absorbed radiation calculated using the HDKR model and 15 minute input data. 97

Figure 4.5: Annual energy prediction error for each module previously described. The datasets for each module were filtered as described in Section 4.5 and then integrated into hourly datasets. 99

Figure 4.6: Sensitivity study on cover thickness..... 101

Figure 4.7: Sensitivity study on thermal conductivity 102

Figure 4.8: Sensitivity study on uniform module temperature. 103

Figure 4.9: Sensitivity study on cover emissivity. 104

Figure 4.10: Sensitivity study on module backside emissivity. 106

Figure 4.11: Sensitivity study on wind speed. 107

Figure 4.12: Sensitivity study on ground temperature. 108

Figure 4.13: Sensitivity study on sky temperature. 109

Figure 4.14: Sensitivity study on view factors 110

Figure 4.15: Sensitivity study accounting for lumped steady state energy balance model and location specific atmospheric pressure. 111

Figure 4.16: Annual energy prediction error for the modified steady state energy balance. Wind speed is not adjusted for measurement height. 112

Figure 4.17: Annual energy prediction error for the modified steady state energy balance. The Duffie and Beckman model applies NOCTs (Table 4.3) predicted by the NOCT model in Chapter 3. 115

Figure 5.1: Example of an integrated mounting configuration (Philadelphia Solar, 2009). 119

Figure 5.2: Example of flush mountings configurations (NIST, 2006). 120

Figure 5.3: Example of mounting structure oriented parallel to ridge of roof (South Ayrshire Council, 2010). 122

Figure 5.4: Example of mounting structure oriented perpendicular to ridge of roof (Green-Trust.Org, 2007). 124

Figure 5.5: Example of mounting structure that does not significantly impede the flow of air in either direction (Comfort Zone Mechanical Air, Inc., 2010). 125

Figure 5.6: An example of a rack mounting configuration (U.S. Environmental Protection Agency, 2010). 126

Figure C.1: Measured wind speed at the module versus rooftop wind speed adjusted to the height of the module using the power law for the month of December. A maximum surface roughness length of 10000 was used. 151

Figure C.2: Measured wind speed at the module versus rooftop wind speed adjusted to the height of the module using the procedure detailed in Section 3.2.2. The leeward correlation was used for all wind directions. 152

Figure C.3: Aerial photograph of NIST campus near photovoltaic modules. Leeward and windward directions are shown, along with obstructions in the windward direction. 152

Figure C.4: View of modules on south wall of NIST and building to the east of the modules..... 153

Figure C.5: Aerial view of Sandia site..... 153

Figure C.6: The five modules on the top of the structure are the HIT array at NREL (Marion, 2009). 154

Figure E.1: Plot of r vs. x (Figure 4.3) for points rejected by maximum power point tracking filter. 159

List of Tables

Table 2.1: Relevant meteorological measurements included in NIST datasets and associated instrumentation information. 10

Table 2.2: Free convection correlations. The characteristic length used in Grashof number calculations is the height of the vertically mounted module. 18

Table 2.3: Forced convection correlations. The characteristic length used to calculate the Reynolds number is the horizontal width of the vertical module for each correlation except the Sparrow correlation, which uses the Equation (2.10). 19

Table 2.4: RMSE errors for transient simulations of the insulated mono-Si module assuming various nodal structures. The values in the table are relative to the most complex structure, the {12,12,12,12} structure. 29

Table 2.5: Combinations of datasets and model types 32

Table 3.1: NOCT values reported by NIST and calculated NOCT values. 62

Table 4.1: Values of the mounting coefficient for various PV array mounting situations (Skoplaki et al., 2008). 79

Table 4.2: Empirically determined coefficients used to predict module back surface temperature as a function of irradiance, ambient temperature, and wind speed. Wind speed was measured at the standard height of 10 meters (King et al., 2004). 79

Table 4.3: Comparison of NOCT values used by the Skoplaki, Duffie and Beckman, and steady state energy balance temperature models. 113

Table A.1: Measured mono-Si performance and physical data (Boyd, 2010) 142

Table A.2: Material properties of the components of the mono-Si module (Davis et al. 2001) 142

Table A.3: Measured poly-Si performance and physical data (Boyd, 2010) 143

Table A.4: Properties of ETFE cover of poly-Si module (Brandup et al., 2005) 143

Table A.5: Mono-Si (Sandia) performance and physical data 143

Table A.6: HIT (NREL) performance and physical data 144

Table C.1: Values of surface roughness length for various types of terrain (Manwell et al., 2002). 151

Table E.1: Monthly energy prediction errors for NIST mono-Si BIPV with different filtering criteria applied to input data (Section 4.5.2). One filter rejects time periods with large zenith angles while the other filter does not. 157

Table E.2: HIT data rejected by I-V curve filter. 158

Nomenclature

A_i	Anisotropy Index (-) (HDKR model)
c	Specific Thermal Capacitance (J/kg-K)
C	Thermal Capacitance (J/K)
cf	NOCT correction factor (-)
D_h	Hydraulic Diameter (m)
e	Surface Roughness (-)
F	View Factor (-)
f_{fd}	Friction Factor for Fully Developed Flow (-)
f_{HDKR}	Modulating Factor (-) (HDKR model)
g	Gravity Constant (m/s^2)
Gr	Grashof Number (-)
G_b	Beam Normal Irradiance (W/m^2)
G_d	Diffuse Irradiance (W/m^2)
G_{bd}	Total Horizontal Irradiance (W/m^2)
h	Heat Transfer Coefficient (W/m^2-K)
k	Thermal Conductivity (W/m-K)
L	Length (m)
Nu	Nusselt Number (-)
P	Power (W)
Pr	Prandtl Number (-)
Q	Absorbed Radiation of the Module Cover (W/m^2)
$\dot{q}$	Rate of Energy Transfer per Unit Area (W/m^2)
R	Thermal Resistance per Unit Area (K/W)
Ra	Rayleigh Number (-)
Re	Reynolds Number (-)
S	Absorbed Radiation of the Photovoltaic Cell (W/m^2)
t	Time (s)
T	Temperature (K)
th	Thickness (m)
u	Wind Speed (m/s)
u_∞	Free Stream Wind Speed (m/s)

W	Width (m)
z	Wind Speed Measurement Height (m)
z_0	Surface Roughness Length for Wind Speed Adjustment (-)

Acronyms

ASTM	American Society for Testing and Materials
BIPV	Building Integrated Photovoltaics
FORTRAN	Formula Translation
HDKR	Hay, Davies, Klucher and Reindl Radiation Model (Duffie and Beckman, 2006)
HIT	Heterojunction with Intrinsic Thin Layer
IEC	International Electrotechnical Commission
MBE	Mean Bias Error
Mono-Si	Monocrystalline Silicon
MPPT	Maximum Power Point Tracker
NIST	National Institute of Technology and Standards
NREL	National Renewable Energy Laboratory
NOCT	Nominal Operating Cell Temperature
NTE	Nominal Terrestrial Environment (POA irradiance = 800 Wm^{-2}, Ambient Temperature = 20°C, Wind Speed = 1 ms^{-1})
PIR	Precision Infrared Radiometer
POA	Plane of Array
PV	Photovoltaics
RMSE	Root Mean Square Error
SAM	System Advisor Model
TMY	Typical Meteorological Year

Greek Letters

α	Absorptance (-) / Wind Speed Adjustment Exponent (-)
α_{Imp}	Maximum Power Current Temperature Coefficient (A/°C)
β	Slope of Module (°)
β_{Voc}	Open-circuit Voltage Temperature Coefficient (V/°C)
ΔT	Temperature Difference
ε	Long-wave Emissivity (-)
ρ	Density (kg/m^3)
ρ_g	Ground Reflectivity (-)
σ	Stefan-Boltzmann Constant (W/m^{2}K^4)
τ	Transmittance (-)
ω_m	Mounting Coefficient (-) (Skoplaki et. al, 2008)

Subscripts

amb	Ambient Conditions
b	Backside of Module
c	Cover of Module
conv	Convection
dp	Dew Point
in	Indoor Conditions
lam	Laminar
meas	Measured
mp	Maximum Power
oc	Open Circuit
out	Outdoor Conditions
rad	Radiative
ref	Reference Conditions
sc	Short Circuit
surr	Surroundings
T	Tilted
turb	Turbulent

1. Introduction

1.1 Project Purpose

Many research efforts have focused on the development of models that are able to predict photovoltaic (PV) module performance for any climatic condition. These models typically require the temperature of the photovoltaic component of the module, known as the cell, as an input. It is well documented that the cell temperature affects module performance, so accurately characterizing the cell's operating temperature is critical to achieving accurate estimates of system performance.

Photovoltaic modules are installed in a variety of locations and in a variety of mounting configurations. The mounting configuration affects the module performance due to two separate mechanisms: (1) incident radiation (primary) and (2) cell temperature (secondary). The purpose of this project is to develop and validate a model of a photovoltaic module capable of accurately predicting the cell temperature while adapting to various mounting configurations, mounting locations, and climates. Additionally, the model should only require readily available data from the module manufacturer, mounting information, and climatic information such that simulations can be quickly and economically completed. The end goal is to enable existing PV performance models to more accurately predict the in-situ performance of photovoltaic systems.

1.2 Photovoltaics

1.2.1 Technology

A photovoltaic cell is a solid state semiconductor device that converts a portion of incident radiation into electricity. Areas in the semiconductor are "doped" such that free

electrons created by the absorption of radiation flow from an area doped with excess electrons to an area doped with a deficiency of electrons. Similar to the performance of semiconductors in other applications, the efficiency of a photovoltaic cell decreases as the temperature of the cell increases. Additional information is readily available as photovoltaics are covered extensively in literature. Duffie and Beckman (2006) also present a list of relevant literature that may provide a good starting point.

1.2.2 Composition

The cell is the building block of a photovoltaic module, and the main function of the additional module materials is to provide structural support and shield the cell from adverse weather conditions. Specifically, the module materials should be electrically insulating, prevent moisture ingress, and resist weathering.

A typical module construction is shown below in Figure 1.1. Covers of photovoltaic modules are usually composed of high-transmittance glass that allows a high percentage incident radiation to pass through to the cell while also providing structural support to the module. Encapsulant materials are typically very thin and are used to surround and protect the cell and module circuitry. Backsheets are often composed of thin, laminated polymer materials.

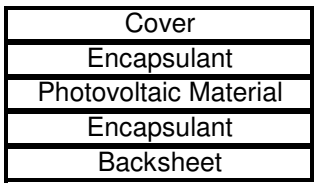

Figure 1.1: Typical layers of construction of a photovoltaic module.

For some modules the cover is a thin polymer material. In this case, the backsheet is often a more substantial material (glass, for example) in order to provide structural support.

1.2.3 Application

Photovoltaics are implemented on both large and small scales. For example, homeowners and businesses often purchase modules to partially offset their electrical load. Some electrical utilities have also built large photovoltaic power plants. These plants can have capacities of over 1 megawatt and cover hundreds of acres (PV Resources, 2010). In each of these cases, an accurate prediction of the performance of the photovoltaics is necessary to determine the financial feasibility of the project. Predicting the performance of a potential site requires both a performance model and historical weather data. Typical Meteorological Year (TMY) datasets provide relevant weather data in hourly increments and are typically used for predictive modeling. Many options are available for performance models.

Additionally, photovoltaic power plants may utilize performance models as a diagnostic tool to compare predictions of power generated to the actual electrical power generated. Consistent over-prediction of power by a model often signifies that module maintenance is required. Since measured performance data exists for these arrays, the performance model can be more empirical and apply shorter time steps that allow the potential for greater accuracy.

1.3 Performance

The performance of an operating module is a function of the module characteristics, incident radiation, cell temperature, and the load connected to the module. The limits of the range of possible operating conditions are the short circuit (*sc*) case and the open circuit case (*oc*), respectively. Neither of these operating conditions generates power. Intermediate operating conditions do generate power and consequently are of the most interest. Figure 1.2 shows typical current – voltage (I-V) and power - voltage curves for a photovoltaic module. As the applied load drives the module away from short circuit conditions, power production increases until the load is such that the module is at the maximum power point. Ideally a module would always produce maximum power, but in many applications it is constrained by the characteristics of the load. Most modules that are designed to supply power to the electrical grid, however, are equipped with maximum power point trackers (MPPT) that force the module into this condition.

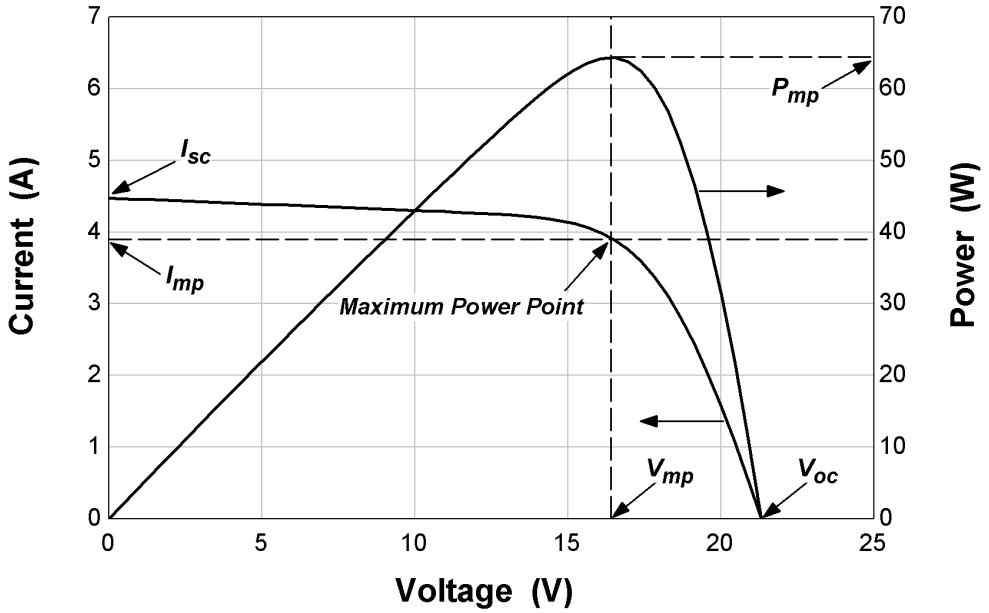

Figure 1.2: Typical current-voltage and power-voltage curves of a PV module. Reproduced from Duffie and Beckman (2008).

The effect of temperature can be shown observed on an I-V curve as shown in Figure 1.3. Note that the open circuit voltage and maximum power are affected by varying temperature while the short circuit current is relatively stable.

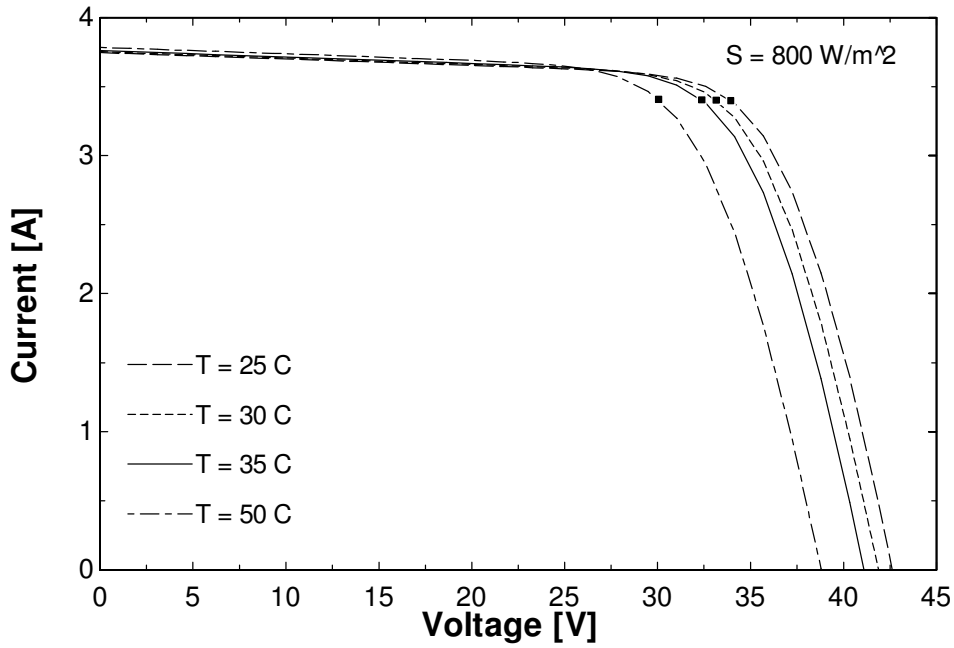

Figure 1.3: Current-voltage plot showing temperature effects on a typical PV module.

1.3.1 Performance Models

Performance models are required to determine the I-V curve of any given module at any irradiance and cell temperature conditions. Boyd (2010) details existing performance models and designates the five parameter model (DeSoto et al, 2006) as a model that is both accurate and can be solved only using data available from the manufacturers. Since this model is consistent with the goals of this project it is used to simulate module performance results throughout the remainder of this report. The cell temperature models evaluated in this report are used to provide a cell temperature input to the five parameter model.

1.3.2 Cell Temperature Models

Many cell temperature models are available in literature. Details of a sampling of these models are included below. These models can be generally grouped into three categories: empirical models, semi-empirical models, and theoretical models. Skoplaki and Palyvos

(2009) list additional cell temperature models that are not included in the following sections.

1.3.2.1 Empirical Models

Empirical models are developed purely from experimental data. Empirical models have the possibility to be very accurate since they are developed from actual data and do not need to make assumptions. The downside is the fact that, since the model requires measured data, it is difficult to predict the performance of a module before installation. King et al. (2004) have developed an empirical model for three mounting types that is dependent on irradiance, wind speed, and ambient temperature. This model is further detailed in Chapter 4. Shresta et. al (2009) have developed a cell temperature model for the interior modules in a gap mounted rooftop array.

1.3.2.2 Theoretical Models

Theoretical models apply established heat transfer correlations to predict the temperature of the module. As opposed to empirical models, theoretical models do not require measured performance. Fuentes (1984) developed an extensive transient model that is adaptable to different mounting using equations manipulating the reported Nominal Operating Cell Temperature (NOCT). Jones and Underwood (2001) developed a transient model for a rack mounted module, while Davis et al. (2001) developed a transient model for a building integrated module. Duffie and Beckman (2008) presented a simplified steady state model that adapts to the mounting of the module using the reported NOCT. This model is also further detailed in Chapter 4.

1.3.2.3 Semi-Empirical Models

Semi-empirical models are defined as theoretical models that are slightly modified by information from experimental data. For example, Del Cueto (2000) empirically calculates coefficients to improve a theoretical steady state model. Krauter et al. (2008) developed a semi-empirical transient model. Skoplaki et al. (2008) developed a simplified steady state model and modified the temperature for mounting conditions based on an empirical mounting coefficient. This model is also further detailed in Chapter 4.

1.4 Research Motivation

The stated goal to develop a model that only requires readily available data from the module manufacturer, mounting information, and climatic information necessitates the use of a theoretical model. The following work focuses on developing and validating a mounting-adaptable theoretical cell temperature model. This process explores the consequences of simplifying assumptions found in many cell temperature models. The final model is simulated along with the King et al. (2004), Duffie and Beckman (2008), and Skoplaki et al. (2008) models in order to understand model accuracy, robustness, and flexibility under a range of mounting conditions and modules. This research is to support the Solar Advisory Model (SAM) developed and modified at the National Renewable Energy Laboratory (NREL). SAM (NREL, 2010) is a free software tool available for examining the costs, financing, and performances of various solar system technologies.

2. Development of Energy Balance Model

This chapter will focus the development of a cell temperature model from an energy balance on a PV module. First, the module and corresponding experimental datasets will be discussed. Then, the energy balance model will be defined and simulations results used to specify model structure, correlations, and input data type will be presented. Finally, another module will be evaluated to verify the results.

2.1 NIST Experimental Site and Datasets

Ideally, the development and validation of a model to predict PV cell temperature are facilitated with the most accurate and descriptive experimental data available. This validation data offers the opportunity to minimize the number of assumptions and correlations applied to the model. The NIST "Round 2" datasets (Dougherty et al. 2004) contained more useful measurements than other available datasets, such as the wind speed directly at the module (as opposed to being measured at a nearby weather station), and the surroundings temperature experienced by the module. The experimental set-up for the Round 2 data was originally characterized by Fanney and Dougherty (2001). The experimental set-up includes a test bed of different modules vertically inserted into five adjacent windows on the south wall of a building at NIST in Gaithersburg, MD. This type of mounting is often referred to as building integrated photovoltaics, or BIPV. Relevant meteorological measurements included in the NIST datasets are shown in Table 2.1. All measurements listed are instantaneous values. Relevant performance data such as backside temperature (instantaneous) and power (instantaneous and time-averaged) were also provided in five minute intervals.

Table 2.1: Relevant meteorological measurements included in NIST datasets and associated instrumentation information.

Measurement	Instrument	Location
Beam Normal Irradiance (G_{bn})	Pyrheliometer	Rooftop Tracking
Diffuse Horizontal Irradiance (G_d)	Shaded Disk w/ Thermopile-Based Pyranometer	
Global Horizontal Irradiance (G)	Thermopile-Based Pyranometer	Rooftop Fixed
Plane of Array Global Irradiance (G_T)		Plane-of-Array Fixed
Ambient Temperature (T_{amb})	Sheated Type-T Thermocouple	Rooftop
Wind Speed (u)	Ultrasonic Wind Sensor	Plane-of-Array Fixed
Infrared Radiation Measurements $\left(q''_{PIR}\right)$	Precision Infrared Radiometer	Plane-of-Array Fixed

From the Round 2 modules, a mono-silicon (mono-Si) module was chosen for use in initial model validation efforts for several reasons. First, the thermal characteristics of the mono-Si module are readily available (Davis et al. 2001). Second, mono-Si measured outputs are more consistently available, especially for cloudy days characterized by low radiation; the outputs of other Round 2 modules were often unavailable during these time periods. Finally, the 5-parameter module performance model (De Soto et al. 2006) has been shown to be accurate for the mono-Si module (Boyd, 2010). Module performance data and thermal characteristics are shown in Appendix A.

One downside of the Round 2 set-up is that the vertical mounting of the module complicates calculations of absorbed radiation that are necessary to predict the cell temperature of the module. Due to its mounting orientation, the module will experience high incidence angles, particularly during the summer. Since summer months are characterized by the largest values of irradiance and ambient temperature, however, the simulation of these months is important in the validation effort for a cell temperature

model. The high incidence angles on the module increase the uncertainties in determining the absorbed radiation. This uncertainty increase will then propagate to calculations requiring absorbed radiation as an input. Additionally, the vertical mounting of the modules causes a large mismatch of incidence angles between the module and the measurement devices. This mismatch may create uncertainties in irradiance calculations because the module may be receiving irradiance at a significantly lower incidence angle than the horizontal pyranometer and shaded pyranometer. For example, when the incidence angle with respect to the module is low (and therefore power calculations become most important), the incidence angle with respect to the pyranometers is likely high and irradiance measurements become more uncertain (Myers et al., 2002). Because of the impact of these issues, techniques to reduce the uncertainty in absorbed radiation calculations become important and are addressed in subsequent sections.

Early morning shading on the mono-Si module occurs from October through March due to the orientation and location of the module; consequently, a uniform starting period for data each day is chosen beginning at 9:30 A.M. In addition, the depth of the module recessed into its frame opening is also noted to cause shadows at early and late hours (Dougherty et al. 2004); therefore, data after 4:00 P.M. are omitted.

2.2 Energy Balance Model

A model to predict the cell temperature of a PV module can be developed by applying the law of conservation of energy to the module. In the broadest sense, this law can be explained by Equation (2.1). PV modules, regardless of mounting, will typically have multiple modes of energy output but only one source of energy input: absorbed radiation.

Figure 2.1 shows the different modes of energy transfer for the Round 2 mono-Si module at NIST. For this system, a more specific energy balance can be defined by Equation (2.2). Note that in both Figure 2.1 and Equation (2.1) "in" and "out" refer to "indoor" and "outdoor", respectively. The following sections will discuss the energy inputs and outputs of the energy balance. Then different methods of accounting for the temperature gradient and thermal capacity of the module materials will be discussed.

$$\text{Energy In - Energy Out = Energy Stored} \tag{2.1}$$

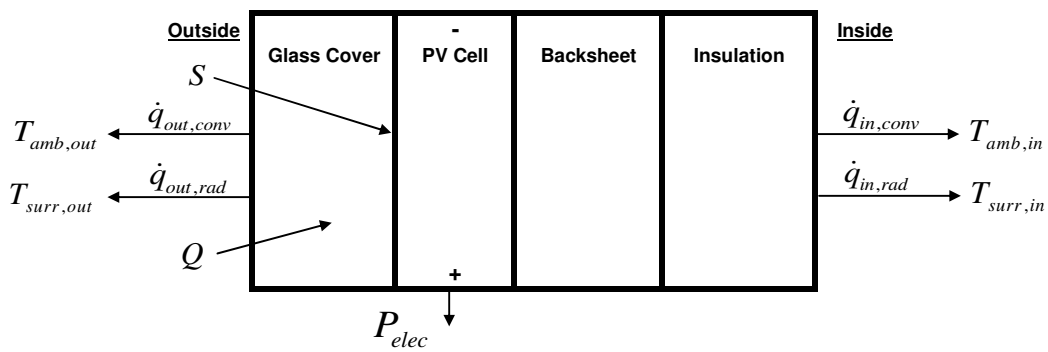

Figure 2.1: Diagram of insulated mono-Si mounted in window recess at NIST. Arrows designate the various modes of energy transfer in and out of the module. Diagram is not to scale.

An energy balance on Figure 2.1 is defined by Equation (2.2),

$$S + Q - (\dot{q}_{out,conv} + \dot{q}_{out,rad} + \dot{q}_{in,conv} + \dot{q}_{in,rad} + P_{elec}) = C \cdot \frac{dT}{dt} \tag{2.2}$$

where S is the radiation absorbed by the cell, Q is the radiation absorbed by the cover, $\dot{q}_{out,conv}$ is the convective heat transfer to the ambient air, $\dot{q}_{out,rad}$ is the radiative heat transfer from the cover to the surroundings, $\dot{q}_{in,conv}$ is the convective heat transfer to the indoor air, $\dot{q}_{in,rad}$ is the radiative heat transfer from the insulation to the indoor

surroundings, P_{elec} is the electrical power produced by the module, C is the thermal capacitance of the module, T is the temperature of the module, and t is time.

2.3 Energy Inputs

2.3.1 Cell Absorbed Radiation

The amount of absorbed radiation by the cell (S) is the dominant mode of energy input. For a simulation with no measured performance data, this value can be predicted using the Hay, Davies, Klucher, and Reindl (HDKR) model (Duffie and Beckman, 2006). The HDKR model uses measured beam, diffuse, and total horizontal irradiance to calculate the total irradiance on a tilted surface. Then tau-alpha values are used to calculate the amount of the incident radiation that is absorbed. However if measurements of the irradiance on a tilted surface are available, the absorbed radiation can then be corrected by the total measured POA (plane of array) irradiance, as shown in Equation (2.3) and described by Boyd (2008).

$$\frac{S_{HDKR,corrected}}{S_{HDKR,calculated}} = \frac{G_{T,measured}}{G_{T,HDKR}} \tag{2.3}$$

The negative effect of the vertical mounting on uncertainties in the absorbed radiation calculations was noted in Section 2.1. When performance data (current, voltage, power) are known, a more consistent method to calculate absorbed radiation can be developed. By using measured performance data, absorbed radiation can be “back-calculated” from the power and cell temperature measurements.

The five parameter model typically uses absorbed radiation and estimated cell temperature to predict the module power output. If instead the module power output and

cell temperature are measured, then the absorbed radiation can be calculated. This method necessarily assumes that the fidelity of the five parameter model in describing the data is high. Five minute time-averaged power and an average of consecutive cell temperatures (beginning and end of the five minute period) were used to calculate the absorbed radiation for the NIST datasets. Note, the modeling efforts of this study focus on cell temperature modeling and not performance modeling, which allows the absorbed radiation to be backed-out without damaging the integrity of the model validation process.

2.3.2 Cover Absorbed Radiation

The function of the cover is to protect the cell from the environment, and in some cases to provide support for the module. Unfortunately, the cover will also reflect and absorb incident radiation. This absorbed radiation (Q) is a secondary mode of energy input.

In order to calculate the radiation absorbed by the cover, the absorptance of the cover for ground-reflected, diffuse, and beam radiation is needed. First, the transmittance of glass at the incidence angles corresponding to each type of radiation needs to be found by considering the absorption losses, as shown in Equation (2.4) (Duffie and Beckman, 2006),

$$\tau_a = e^{\left(\frac{-KL}{\cos(\theta)}\right)} \tag{2.4}$$

where K is the extinction coefficient, L is the thickness, and θ is the refraction angle. The refraction angle is dependent on the angle of incidence for each source of radiation.

Then, the transmittance is used to find the absorptance for each type of incident radiation by applying Equation (2.5) (Duffie and Beckman, 2006). Note that this equation applies a simplification that assumes the cover has zero reflectivity.

$$\alpha \cong 1 - \tau_a \tag{2.5}$$

Once the absorptance is found for each component of the incident radiation, it is inserted into Equation (2.6) to estimate the magnitude of radiation absorbed by the cover. Equation (2.6) is adapted from Duffie and Beckman's (2006) HDKR model for a PV cell's absorbed radiation.

$$Q_{HDKR} = \left(G_b + G_d \cdot A_i\right) \cdot R_b \cdot \alpha_b + G_d \cdot \left(1 - A_i\right) \cdot \left(\frac{1+\mathrm{Cos}(\beta)}{2}\right) \cdot \left(1 + f_{HDKR} \cdot \left(sin(\beta/2)\right)^3\right) \cdot \alpha_d + G_{bd} \cdot \rho_g \cdot \left(\frac{1-\mathrm{Cos}(\beta)}{2}\right) \cdot \alpha_g \tag{2.6}$$

Similar to the cell's absorbed radiation calculations, the cover's absorbed radiation calculations are affected by the uncertainties caused by the vertical mounting. Using the method shown in Equation (2.3), the absorbed radiation in the cover can be corrected by applying Equation (2.7).

$$\frac{S_{backed-out}}{S_{HDKR,calculated}} = \frac{Q_{corrected}}{Q_{HDKR}} \tag{2.7}$$

2.4 Energy Outputs

2.4.1 Power Output

Power (P_{elec}) is the most important output of any useful PV module. While the efficiency of most operating modules is below 20%, the module power needs to be accounted for as an output in the energy balance. The five parameter model can be applied with absorbed

radiation and cell temperature as inputs to calculate the power production of a module. Since cell temperature is an input to the model predicting power and power is an input to the model predicting temperature, solving the energy balance becomes an iterative process.

2.4.2 Convective Heat Transfer

An operating PV module will exchange thermal energy with the surrounding ambient air through convection. Free convection occurs when the module is at a higher temperature than the ambient air. In this process, air adjacent to the module becomes heated and therefore buoyant compared to the air at the ambient temperature. This buoyancy difference creates air flow that enhances heat transfer between the module and the air. Forced convection also occurs when the module is at a higher temperature than the ambient air, but additionally requires an existing air flow to transfer energy from the module to the ambient air. Typically this "existing air flow" will be a result of the wind, although some manufacturers provide modules with fans attached to reduce the module temperature. Since both modes of convective heat transfer will occur simultaneously when the module temperature is higher than the ambient air temperature and wind is present, a technique is required to calculate the combined heat transfer from the module to the ambient air. The following subsections detail the different existing convection correlations and combination correlations that will be evaluated for the mono-Si module.

Correlations for both free and forced convection typically provide values for the average Nusselt number $\left(\overline{Nu}\right)$ at various environmental conditions. The Nusselt number can be entered into Equation (2.8) to calculate the average heat transfer coefficient $\left(\overline{h}\right)$. The

characteristic length $\left(L_{char}\right)$ in Equation (2.8) is dependent on the direction of air flow across the surface experiencing convection.

$$\bar{h} = \frac{\overline{Nu} \cdot k}{L_{char}} \tag{2.8}$$

Finally, the average heat transfer coefficient can be entered in Equation (2.9) to calculate the heat transfer per unit area from the module to the ambient air. Since the NIST datasets provide measurements of both the outdoor and indoor ambient temperature that the cover and backside of the module respectively experience, the average heat transfer coefficient is the only unknown quantity remaining to complete the convective heat transfer calculation.

$$\dot{q}_{conv} = \bar{h}\left(T_{cover} - T_{ambient}\right) \tag{2.9}$$

2.4.2.1 Free Convection

The free convection correlations evaluated for the vertically mounted mono-Si module are shown in Table 2.2, and the associated heat transfer coefficients are plotted in Figure 2.2. This plot shows the three correlations evaluated generate significantly different heat transfer coefficients. Subsection 2.8.5.2 will focus on selecting the most appropriate correlation for the vertically mounted module.

Table 2.2: Free convection correlations. The characteristic length used in Grashof number calculations is the height of the vertically mounted module.

Source and Reference	Free Convection Correlation	Conditions	Eq #
Churchill and Chu Incropera et al. (2006)	$\overline{Nu} = \left(0.825 + \frac{0.387 \cdot Ra^{1/6}}{\left(1+\left(0.492/\Pr\right)^{9/16}\right)^{8/27}}\right)^2$	Uniform Surface Temp Laminar and Turbulent Flow	1
Ostrach (Davis et al. 2001)	$\overline{Nu} = 0.476 \cdot Gr^{\frac{1}{4}}$	Uniform Surface Temp Laminar Flow	2
Integral Solution (Davis et al. 2001)	$\overline{Nu} = 0.667 \cdot \left(\frac{\Pr^2}{0.952+\Pr}\right) \cdot Gr^{1/4}$	Uniform Surface Temp Laminar Flow	3

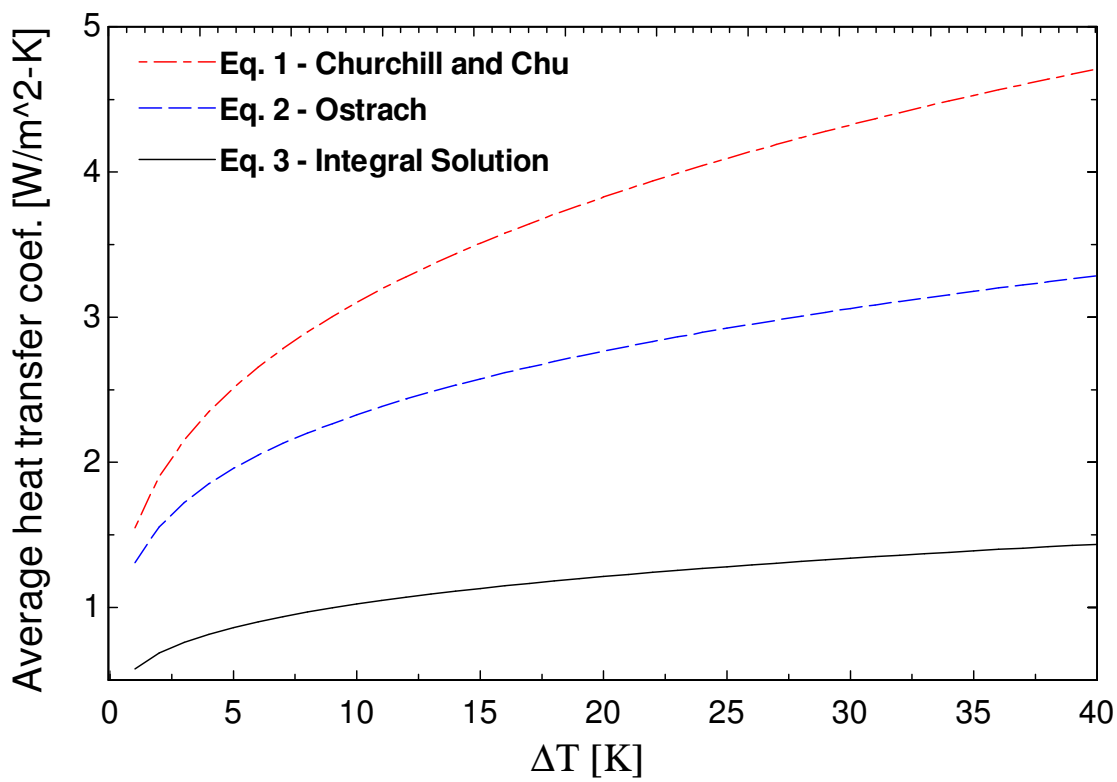

Figure 2.2: Heat transfer coefficients calculated for the mono-Si module from correlations in Table 2.2. The surface temperature is maintained at 300K while the ambient temperature is varied. Properties of air are calculated at the film temperature.

2.4.2.2 Forced Convection

The forced convection correlations evaluated for the vertically mounted mono-Si module are shown in Table 2.3, and the associated heat transfer coefficients are plotted in Figure 2.3. Similar to free convection, the four correlations evaluated generate significantly

different heat transfer coefficients. The difference is more evident between the turbulent and laminar correlations, which is expected. Section 2.8.5.2 details the process of selecting the most appropriate forced convection correlation.

Table 2.3: Forced convection correlations. The characteristic length used to calculate the Reynolds number is the horizontal width of the vertical module for each correlation except the Sparrow correlation, which uses the Equation (2.10).

Source and Reference	Forced Convection Correlation	Conditions	Eq #
Integral Solution (Davis et al. 2001)	$\overline{Nu} = 0.664 \cdot \mathrm{Re}^{\frac{1}{2}} \cdot \mathrm{Pr}^{\frac{1}{3}}$	Laminar Flow Uniform Surface Temp. $\mathrm{Pr} > 0.6$	1
Sparrow (Davis et al. 2001)	$\overline{Nu} = 0.86 \cdot \mathrm{Re}_c^{\frac{1}{2}} \cdot \mathrm{Pr}^{\frac{1}{3}}$	Laminar Flow Uniform Surface Temp. $20{,}000 < \mathrm{Re}_c < 90{,}000$	2
NuBelt (Eicker 2003)	$\overline{Nu} = \dfrac{0.037 \cdot \mathrm{Re}^{0.8} \cdot \mathrm{Pr}}{1 + 2.443 \cdot \mathrm{Re}^{-0.1} \cdot \left(\mathrm{Pr}^{2/3} - 1\right)}$	Turbulent Flow Uniform Surface Temp.	3
Schlichting (Incropera et al. 2006)	$\overline{Nu} = 0.037 \cdot \mathrm{Re}^{\frac{4}{5}} \cdot \mathrm{Pr}^{\frac{1}{3}}$	Uniform Surface Temp. Tripped Boundary Layer $0.6 < \mathrm{Pr} < 60$ $\mathrm{Re} < 10^8$	4

$$L_{char} = \frac{4 \cdot Area}{Perimeter} \tag{2.10}$$

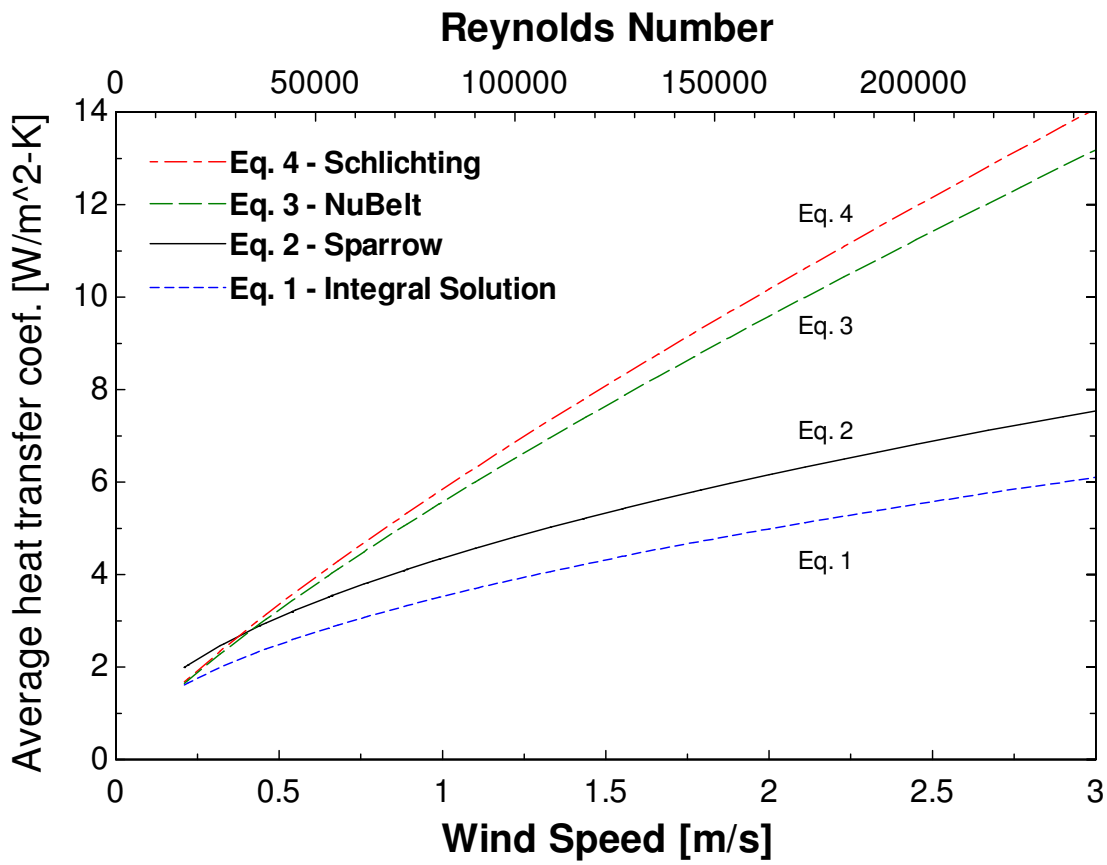

Figure 2.3: Heat transfer coefficients calculated for the mono-Si module from correlations in Table 2.3. The cell and ambient temperature are set to 298K and 278K, respectively. Properties of air are calculated at the film temperature.

2.4.2.3 Combining Free and Forced Convection Coefficients

A correlation is required to calculate the combined free and forced heat transfer coefficient from the module to the ambient air. Equations (2.11) (Eicker, 2003) and (2.12) (Duffie and Beckman, 2006) are evaluated in Section 2.8.5.1.

$$\bar{h}_{total} = \sqrt[3]{\left(\bar{h}_{forced}{}^{3} + \bar{h}_{free}{}^{3}\right)} \tag{2.11}$$

$$\bar{h}_{total} = \max(\bar{h}_{forced}, \bar{h}_{free}) \tag{2.12}$$

2.4.3 Radiative Heat Transfer

One of the benefits of the NIST datasets is the inclusion of precision infrared radiometer (PIR) measurements. The vertical outdoor PIR at NIST experiences, or "sees", a hemisphere of various objects at different temperatures including the sky temperature, ground temperature, and adjacent building temperatures. The proportion of radiation emitted from the PIR to each temperature to the total radiation emitted from the PIR is called the view factor. The sum of the view factors between the module and each temperature source it experiences, therefore, should add to one. The PIR measurement $\left(q''_{PIR}\right)$ can be adjusted with Equation (2.13) to provide the temperature of the surroundings the PIR experiences with a view factor of one. This measurement simplifies radiative heat transfer calculations, as the temperature and view factors for each temperature source do not need to be determined. In the same manner, the vertical indoor PIR provides an indoor surroundings temperature.

$$T_{surr} = \left(\frac{q''_{PIR}}{\sigma} \right)^{1/4} \tag{2.13}$$

Once the surroundings temperature is known, only the emissivity (ε) of the cover is required. Since the emissivity of mono-Si module cover is known, the radiative heat transfer per unit area is easily calculated with Equation (2.14).

$$\dot{q}_{radiative} = \varepsilon_{cover} \sigma \left(T_{cover}^4 - T_{surroundings}^4 \right) \tag{2.14}$$

2.5 Consideration of Spatial Temperature Gradients

The previous sections have defined each of the energy inputs and outputs shown in Figure 2.1. Before the equations predicting heat transfer and absorbed radiation can be calculated along with the energy balance in Equation (2.2), the temperature structure of the module needs to be determined.

As Figure 2.1 shows, the thermal energy inputs and outputs are assumed to occur only at the cover and backside and not the sides of the module. The energy inputs, absorbed radiation, are considered constant on a per unit area basis. Therefore, the temperature of the cover surface and backside surface is considered uniform with respect to the module's height and width. Then, it is assumed that, at any given thickness, the corresponding material is characterized by uniform temperature with respect to the module's height and width. These assumptions lead to the simplification that the temperature of the module only varies with respect to the thickness of the module.

Next, the temperature difference, with respect to the thickness of the module, needs to be analyzed. The module can be treated as one uniform temperature entity or divided into separate pieces called nodes that are characterized by constant temperature. An example of the module divided into nodes can be seen in Figure 2.4.

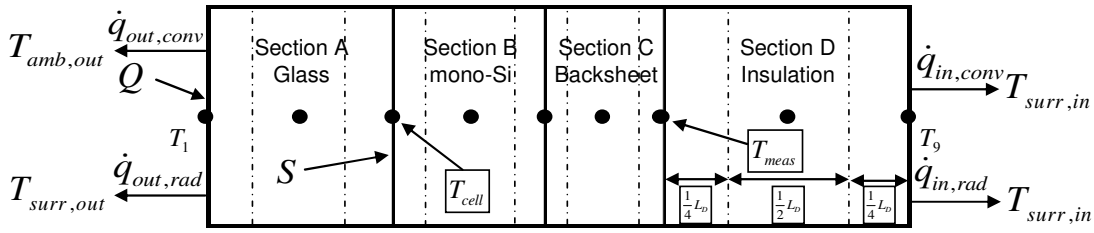

Figure 2.4: Cross sectional view of module divided by 2 lines per material. This structure will be referred to as a {2,2,2,2} nodal model. Drawing is not to scale. The location of the temperature measurement by NIST is also shown.

Figure 2.4 shows each layer of material that comprises the PV module divided by two vertical lines, which delineate three areas. The first and last areas for each material layer are the same width, while the interior areas of each section are twice as large as the outer areas. This difference in area allows a constant distance between the nodes of a given layer. An energy balance can then be written for each node. A naming convention is established that indicates the number of nodes for each material layer in the module starting with the glass, as indicated in the Figure 2.4. For example, {2,2,2,2} indicates that two nodes are used in each of the four material layers.

A nodal structure requires that the locations of the absorbed radiation inputs are logically specified. For future nodal models, the absorbed radiation of the cover will be applied to the node on the interface between the cover and surroundings, and the absorbed radiation of the cell will be applied to the node on the interface between the cover and cell. This node will also be considered the cell temperature. Also if a nodal structure is adopted, an energy balance is required for each node, as opposed to the uniform temperature case that required one energy balance for the entire module.

If the module is assumed to be at a uniform temperature, Equation (2.2) defines an energy balance on the module. For an arbitrary {N,N,N,N} nodal model, however, five different equations are required to define an energy balance for the entire module:

(1) An energy balance on the node located on the interface between the cover and surroundings, node 1, is defined by Equation (2.15).

$$Q-\left(\dot{q}_{out,conv}+\dot{q}_{out,rad}\right)+\frac{T_2-T_1}{R_A/N}=\rho c\frac{th_A}{2N}\frac{dT_1}{dtime} \tag{2.15}$$

(2) An energy balance on the node located on the interface between the insulation and indoor environment (for node 4*N*+1) is defined by Equation (2.16).

$$-\left(\dot{q}_{in,conv}+\dot{q}_{in,rad}\right)-\frac{T_{4N+1}-T_{4N}}{R_D/N}=\rho_D c_D\frac{th_D}{2N}\frac{dT_{4N+1}}{dtime} \tag{2.16}$$

(3) An energy balance on the node located on the interface between the cover and cell (for node *N*+1) is defined by Equation (2.17).

$$S+\frac{T_{N+2}-T_{N+1}}{R_B/N}-\frac{T_{N+1}-T_N}{R_A/N}=\left(\rho_A c_A\frac{th_A}{2N}+\rho_B c_B\frac{th_B}{2N}\right)\frac{dT_{N+1}}{dtime} \tag{2.17}$$

(4) An energy balance for the two remaining nodes located on material interfaces (for nodes (i) = 2*N*+1 and 3*N*+1) is defined by Equation (2.18).

$$\frac{T_{i+1}-T_i}{R_{i+1}/N}-\frac{T_i-T_{i-1}}{R_{i-1}/N}=\left(\rho_{i-1}c_{i-1}\frac{th_{i-1}}{2N}+\rho_{i+1}c_{i+1}\frac{th_{i+1}}{2N}\right)\frac{dT_i}{dtime} \tag{2.18}$$

(5) An energy balance for the remaining internal nodes (i) is defined by Equation (2.19).

$$\frac{T_{i+1}-T_i}{R_i/N}-\frac{T_i-T_{i-1}}{R_i/N}=\rho_i c_i \frac{th_i}{N}\frac{dT_i}{dtime} \tag{2.19}$$

In the previous equations, R_i represents the thermal resistance to conduction per unit area between opposite ends of a given material (i). This thermal resistance can be calculated by Equation (2.20).

$$R_i=\frac{th_i}{k_i} \tag{2.20}$$

At this point, there is either one differential equation (uniform temperature case) or a set of coupled differential equations (nodal structure) that define the transient energy balance on the module. If the initial temperature(s) are known, then the temperature(s) at any time can then be found for by integrating Equation (2.21) or a set of similar equations over time.

$$T_i=T_{i,previous}+\int_0^{timestep}\frac{dT_i}{dtime}dtime \tag{2.21}$$

2.6 Consideration of Thermal Capacitance

The energy balances discussed in the previous section contain a stored energy term that attempts to account for the energy needed to change the temperature of the mass of material analyzed. This term complicates the energy balance in a few ways. First, it requires material property information such as density and heat capacity that would otherwise be unneeded. Additionally, the inclusion of a transient term increases the computational effort required to solve for the module temperature. Finally, most “real world” simulations will be completed with TMY data that are provided in hourly

increments, and an hour interval between input data is too long to account for transient effects. For these reasons, eliminating the transient terms would be helpful if it can be justified.

The thermal time constant of the module is a primary indicator of the importance of the transient term in the energy balance equations. There are several ways to calculate the time constant. One way is to observe the time-temperature dependence of the module. The time constant is the period required for the difference between the cell temperature and the final temperature to reach 37% of the difference between the initial and final temperatures after a step change to new conditions. The time constant can also be estimated by finding the product of the thermal capacity of the module and the thermal resistance of the module to the surroundings. Time constants calculated by both techniques were in the range between 500 and 1000 seconds. Since the NIST datasets provide data in five minute, or 300 second, intervals, the calculated range of time constants suggests that transient effects will be significant.

2.7 Determining an Appropriate Nodal Structure

At this point, all of the inputs required to solve the transient, nodal, energy balance model have been discussed. The next step is to determine the simplest nodal structure that will be capable of providing accurate results. As Section 2.5 explains, a nodal structure is necessary to account for temperature differences throughout the thickness of the module. Therefore, nodes are only needed where significant temperature gradients exist with respect to the thickness of the module. A Biot number analysis can help to determine if significant temperature gradients will exist.

The Biot number is the ratio of the thermal resistance between opposite ends of the material (internal resistance) considered to be at uniform temperature and the thermal resistance between the material and its surroundings (external resistance), as shown in Equation (2.22). If the Biot number is small (approximately 0.1 for this study), then the internal resistance can be considered negligible and the temperature of the material in question can legitimately be considered uniform. The internal thermal resistance per unit area is calculated by Equation (2.20). The external thermal resistance is approximated as the parallel combination of the outdoor convective, outdoor radiative, indoor convective, and indoor radiative thermal resistances. The convective resistance per unit area is defined by Equation (2.23). It is important to note that the choice of free, forced, and combination correlations (Section 2.4.2) does not have a significant effect on this analysis. The radiative resistance per unit area is defined by Equation (2.24).

$$Biot = \frac{R_{internal}}{R_{external}} \tag{2.22}$$

$$R_{convective} = \frac{1}{\bar{h}_{convective}} \tag{2.23}$$

$$R_{radiative} = \frac{1}{\varepsilon_{cover}\sigma\left(T_{material}^2 + T_{surr}^2\right)\left(T_{material} + T_{surr}\right)} \tag{2.24}$$

A sample of Biot numbers for layers comprising the insulated mono-Si module were calculated at various environmental conditions. This sample showed that Biot number of the insulated module is typically around 10, and therefore the temperature of the module can not be assumed to be constant. This result is logical, since the Biot number compares

thermal resistances, and the function of the insulation is to provide thermal resistance. Therefore the insulation is characterized by a large thermal gradient that must be accounted for with a separate node.

Accepting that the insulation requires at least one node, another Biot number analysis can be completed on the remaining module materials. In this case (referred to as the "uninsulated" module) the external resistance must include the resistance of the insulation. A similar sample of Biot numbers for the uninsulated module produced values lower than 0.1. This finding suggests that the temperature of the uninsulated module can be assumed to be uniform.

A brief analysis was completed using the previously defined energy balance equations to determine the number of nodes required to define the insulation. The cell temperature was predicted using the transient energy balance model with each nodal structure listed in Table 2.4. While accuracy with respect to the measured values is the final goal of this project, the objective of this analysis was to determine the nodal structure at which the temperature profile is equal to the temperature profile predicted by the most complex nodal structure (the {12, 12, 12, 12} structure). Therefore, the results show the difference between the root mean square error (RMSE), shown in Equation (2.25), of the temperature prediction for the model applying the nodal structure listed and the model applying the {12,12,12,12}, or baseline, nodal structure. The results show that the Biot number analysis was correct in predicting that the temperature can not be considered uniform for the insulated mono-Si module, as a large difference in errors occurs between the lumped and {12,12,12,12} structures. The small difference between the remaining

structures and the {12,12,12,12} structure suggest that a {1,1,1,1} structure sufficiently accounts for the temperature gradient throughout the thickness of the module. It is important to note that these results are not sensitive to the choice of free, forced, and combination correlations (Section 2.4.2). Based on these results, the {1,1,1,1} structure will be evaluated in the following sections.

Table 2.4: RMSE errors for transient simulations of the insulated mono-Si module assuming various nodal structures. The values in the table are relative to the most complex structure, the {12,12,12,12} structure.

Nodal Structure	RMSE Temperature (Value - Baseline) [K]
Lumped	17.1
{1,1,1,1}	-0.1
{2,2,2,2}	0
{4,4,4,4}	0
Baseline: {12,12,12,12}	

2.8 Specifying the Model Structure, Correlations, and Input Data Type

The previous section defined the nodal structure required to sufficiently account for the thermal gradients throughout the thickness of the material. Now, the following questions remain about the transient, nodal, energy balance model:

(1) What are best free convection, forced convection, and convection coefficient combination correlations (Section 2.4.2)?

(2) The time constant of the mono-Si module was calculated in Section 2.6, and was found to be significant with respect to the five minute intervals of the input data. Is it possible, however, that over the course of a long-term simulation, these transient effects will cancel and a steady state model can be implemented?

(3) Typical Meteorological Year (TMY) data, which are typically used in simulations by designers, are available in hourly increments. Does the model lose precision when the five minute data are integrated into hourly datasets?

These questions will be addressed by comparing results of long-term simulations. In this case, "long-term" refers monthly simulations. June, October, and December were simulated to account for seasonal variations in input data. The following subsections discuss modifications the long-term simulation procedure followed to answer these questions.

2.8.1 Wind Speed Input

The wind speed measurement provided by NIST is an instantaneous measurement taken every five minutes from an ultrasonic wind sensor at the same location and plane of array (POA) as the module. A simulation was completed applying the {1,1,1,1} transient model, using five minute data from June 4 and varying the method used to input wind speed. In one case the instantaneous wind speed was used, in the other an hourly moving average wind speed. The hourly moving average wind speed was calculated by averaging 30 minutes of wind speeds before and after the data point considered. Data points before the first 30 minutes at the beginning or end of the day used the first or last hour average, respectively. As Figure 2.5 shows, using instantaneous wind speed as an input to predict temperature results in a predicted temperatures that do not closely follow the measured module temperature. It is apparent that the instantaneous wind speed value is not representative of the average wind speed over the five minutes, as consecutive five minute wind measurements often differ by over 100%. This discrepancy causes the

calculated five minute heat transfer coefficient to be incorrect, which results in a difference between the slopes of the predicted and measured temperatures during many simulation times.

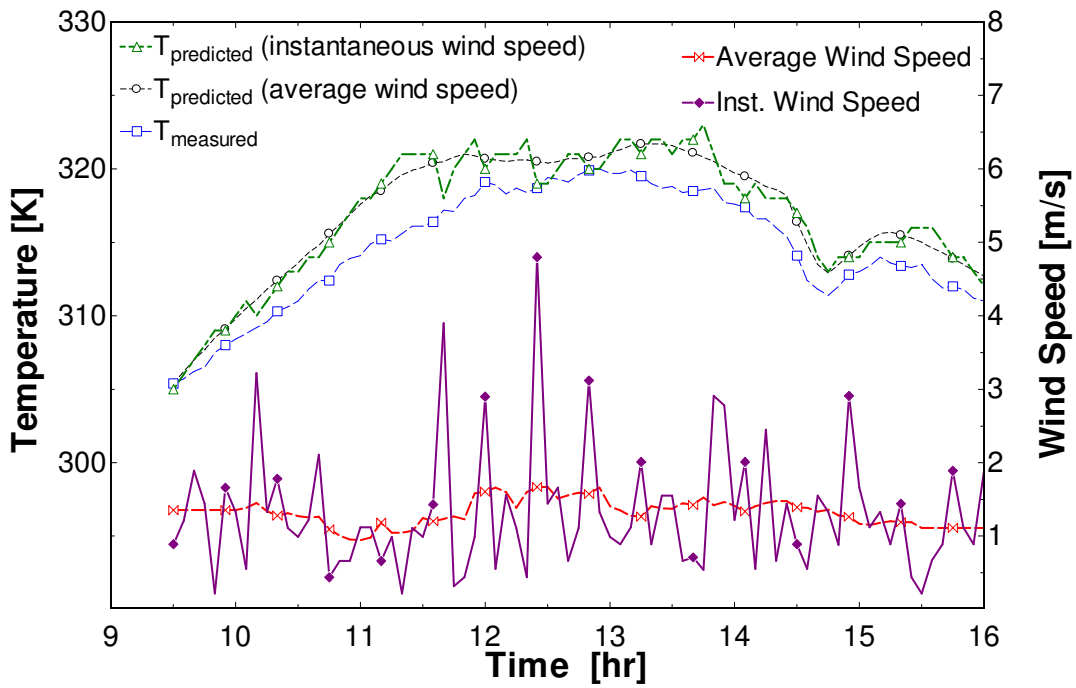

Figure 2.5: Temperature prediction for June 4 applying Forced Convection Eq. (4) and Free Convection Eq. (3). Temperature predictions are calculated using both instantaneous and moving averaged wind speeds.

2.8.2 Hourly Data

Hourly data sets were compiled using the existing NIST data. Values in the hourly datasets were calculated as the average of all five minute data points available within the respective hour. Values were centered on the start of an hour. For example, a set corresponding to 10:00 was compiled from data starting at 9:30 and ending at 10:30. The last data point available (due to shading) is 16:00, so only data from 15:30 to 16:00 filled the final set.

2.8.3 Long-term Simulation Procedure

To answer the questions posed at the start of this section, both five minute and hourly data as well as transient and steady state {1,1,1,1} energy balance models were evaluated. Four combinations of these options exist and are listed in Table 2.5. Regardless of the dataset, each simulation calculated the module temperature at the same five minute intervals that the original data were supplied. Therefore, times where five minute data were not available were not simulated in hourly simulations order to maintain consistency with the input data. The input data for each time step for simulations applying hourly sets were found by linearly interpolating the data from the two hours surrounding the time. For example, input data for 10:20 were found by interpolating between the data centered at 10:00 and 11:00. Data between 9:30 and 10:00 were linearly extrapolated using the 10:00 and 11:00 data sets.

Table 2.5: Combinations of datasets and model types

Combination #	Dataset	Transient
1	Hourly	Yes
2	Hourly	No
3	5-minute	Yes
4	5-minute	No

Finally, for each combination listed in Table 2.5, all possible combinations of free convection correlations, forced convection correlations, and convection coefficient combination correlations was evaluated. Following this procedure, 24 simulations were run for each combination listed in Table 2.5.

2.8.4 Statistical Analysis

The following long-term simulations generate two important predicted values that can be compared to measured data: temperature and power. The goal of a cell temperature model is to predict cell temperature. Therefore, both the mean bias error (MBE), shown in Equation (2.25), and root mean square error (RMSE), shown in Equation (2.26), were calculated with respect to predicted temperature. As previously noted, however, in most cases the cell temperature is only important as an input to a performance model. Theoretically, the model with the lowest errors in temperature prediction could have higher power prediction errors than other models due to the time of day that the model is inaccurate. For example, the model may predict temperatures accurately during low incident irradiance and power production, resulting in low temperature prediction errors; however if the model over predicts temperature during high irradiance periods, the power prediction statistics will be dominated by this error. For these reasons, the MBE of predicted power is calculated and considered the most important criteria in selecting the most accurate model.

$$RMSE = \sqrt{\frac{1}{n}\sum_{i=1}^{n}\left(y_{model} - y_{meas}\right)^2} \tag{2.25}$$

$$MBE = \frac{1}{n}\sum_{i=1}^{n}\left(y_{model} - y_{meas}\right) \tag{2.26}$$

where y_{model} and y_{meas} designate the modeled and measured values, respectively, of a given quantity.

2.8.5 Results

2.8.5.1 Combining Free and Forced Convection Coefficients

Two methods for combining free and forced convection were discussed in the Section 2.4.2.3. Predicted temperatures for June were simulated by applying the combinations of free and forced convection correlations while using both mixed convection approaches. The results showed that Equation (2.11) was more accurate than Equation (2.12) for each combination of the free and forced correlations. Therefore only Equation (2.11) was used to combine free and forced convection coefficients for the remainder of this study.

Both of these combinations of correlations calculate similar values of the combined heat transfer coefficient when one mode of heat transfer is dominant. The difference between the correlations appears when the heat transfer coefficients calculated for both modes of convection are approximately equal. Therefore, it can be understood that Equation (2.11) was found to be more accurate, as the total heat transfer coefficient is likely greater than the heat transfer coefficient calculated from either mode.

These results also indicated that the most appropriate forced convection correlation was turbulent. Therefore, only Equation (2) in Table 2.3 is evaluated as a check for laminar flow in the following subsections since it consistently provides a larger heat transfer coefficient than Equation (1).

2.8.5.2 Free and Forced Convection Coefficients

A plot of the MBE of predicted power, and plots of the MBE and RMSE of predicted temperature for each combination listed in Table 2.5 and each month simulated are shown in Appendix B. Each plot contains a bar for each of the possible combinations of

free and forced convection correlations. Simulations applying turbulent forced convection correlation Equations (3) and (4) (Table 2.3) consistently produced the lowest errors for power and temperature for each month and for each model combination. These results show that the forced flow across the module is better represented as turbulent, even if the velocity is low enough to suggest laminar flow. Since the difference between the turbulent equations appears negligible (Table 2.3 and Appendix B), Equation (4) will be used in future simulations. The results also show that the turbulent free convection correlation Equation (1) (Table 2.2) is the most accurate. These findings are logical since wind, even at low velocities, is typically considered turbulent.

2.8.5.3 Transient and Steady State Models

Figure 2.6 compares results of transient and steady state models (the stored energy term is neglected for a steady state model) simulated with a {1,1,1,1} nodal structure and five minute data. Forced convection correlation Equation (4) and free convection correlation Equation (1) were used for each case shown in the figure. It shows that while transient models have lower RMSEs of predicted temperature, the MBEs of predicted temperature and power for both transient and steady state models are nearly equal. These results show that the increased variability introduced by the steady state models tends to average out over time. This finding is logical, as the time constant of the back-insulated BIPV mono-Si module is significant (Section 2.6). This time constant is causing a lag (due to thermal capacitance) between the time when the energy inputs and outputs change and the time that the module reaches steady state temperature. By definition, the steady state model will not account for this lag. Therefore, during a cloudless day, the steady state model will over predict temperature during the morning when incident radiation is

constantly increasing and under predict temperature during the afternoon when the incident radiation is constantly decreasing. This study found that, for the mono-Si module evaluated, these errors tend to cancel over the course of a month.

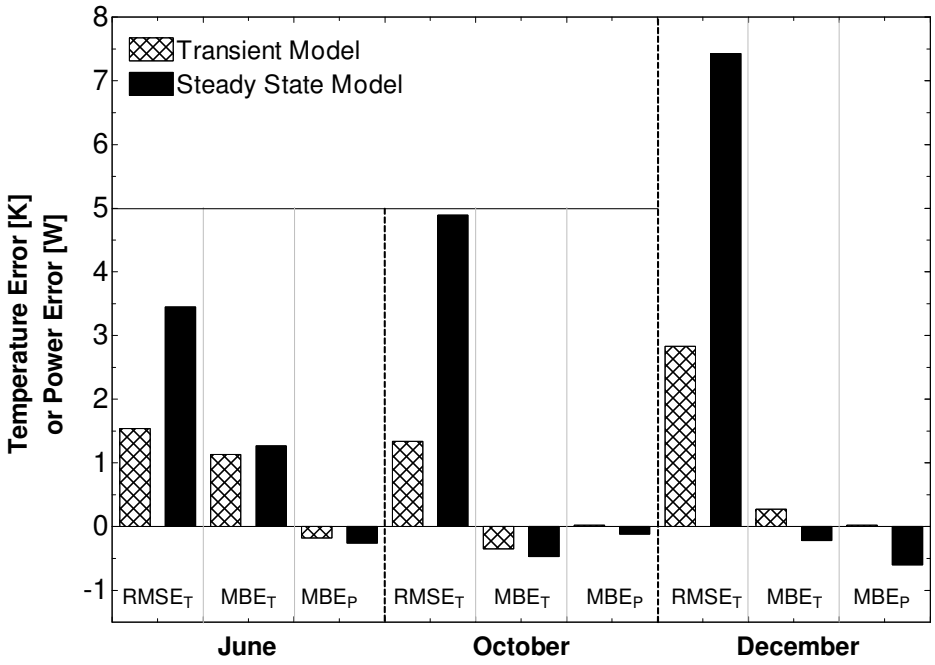

Figure 2.6: RMSEs and MBEs of temperature prediction and MBEs of power prediction for transient and steady state models. Each model was simulated with a {1,1,1,1} nodal structure and five minute input data. Forced convection correlation Equation (4) and free convection correlation Equation (1) were used for each case.

This result is likely to be true for any module experiencing "symmetric" weather. If for some reason a module experienced asymmetric weather (mounted at an azimuth angle other than 0°, shaded during morning or afternoon, etc.), further analysis should be completed to ensure unbiased results.

2.8.5.4 Five Minute and Hourly Datasets

Figure 2.7 compares results of {1,1,1,1} steady state models applying hourly and five minute data. Forced convection correlation Equation (4) and free convection correlation Equation (1) were used for each case shown in the figure. It shows that the simulations

applying hourly data actually tend to be more accurate. Using less discrete input data certainly causes a decrease in precision, so the error introduced by the hourly data is likely canceling out another error in the model. The MBEs of predicted temperature and power, however, suggest that the difference between models applying hourly and five minute input data is not significant, at least in the case of the mono-Si module.

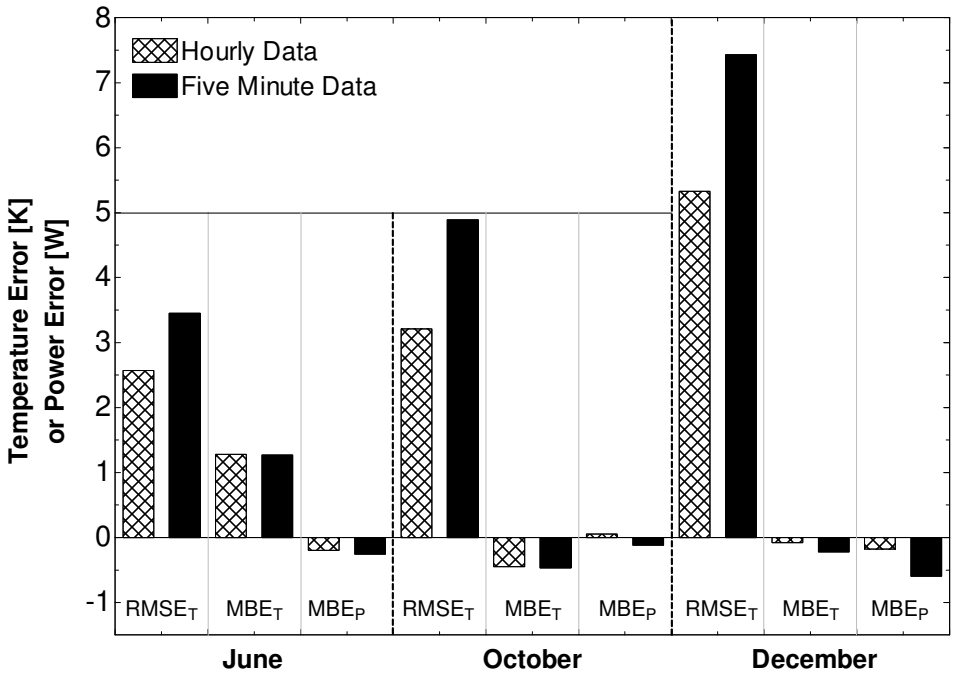

Figure 2.7: RMSEs and MBEs of temperature prediction and MBEs of power prediction for {1,1,1,1} steady state model applying either hourly or five minute data. Forced convection correlation Equation (4) and free convection correlation Equation (1) were used for each case.

2.9 Verification of Results

The previous subsections concluded forced free convection correlation Equation (4), free convection correlation Equation (1), and free and forced convection combination correlation Equation (2.11) were the most accurate correlations to model the mono-Si module. It was also found that a steady state model and hourly data could be applied with negligible increase in MBEs of both predicted power and predicted temperature. In

order to verify these conclusions, the long-term simulation procedure described in Section 2.8 was repeated for the poly-Si module with an ETFE cover that was also included in the Round 2 experiments at NIST. Only the {1,1,1,1} transient model applying five minute data and the steady state model applying hourly data were evaluated, as these combinations model structure and input data are considered the most and least descriptive, respectively, of the four combinations listed in Table 2.5.

2.9.1 Poly-Si Module Performance Data and Material Properties

The poly-Si module was also custom-fabricated. A 0.05 mm thick piece of ETFE was used for the cover. The ETFE was backed by the cell, an opaque backsheet, a 6 mm piece of glass for structural support, and insulation. The backsheet, glass, and insulation are equal in size and properties to the backsheet, glass, and insulation components used in the mono-Si module. ETFE properties are listed in Appendix A. The emissivity of ETFE could not be found and was assumed to be equal to 0.84. Poly-Si module performance data are listed in Appendix A.

2.9.2 Long-term Simulation Results

The poly-Si module was simulated for June, October, and December using both a five minute transient and hourly steady state model. These results can be found in Appendix B and show that, similar to the mono-Si results, turbulent forced convection correlation Equations (3) and (4) (Table 2.3) and turbulent free convection correlation Equation (1) (Table 2.2) consistently produce the lowest errors for power and temperature for each month and for each model combination simulated. These results are additional evidence

that these correlations best describe the heat transfer coefficients of a module located outdoors.

Figure 2.8 compares the results of the {1,1,1,1} transient model applying five minute data and the {1,1,1,1} steady state model applying hourly data. These results show that decreasing the complexity of the model and input data to a steady state model applying hourly data causes negligible change to MBEs of power and temperature prediction. Since this conclusion was also reached for the mono-Si module, the remaining chapters will focus solely on the steady state model.

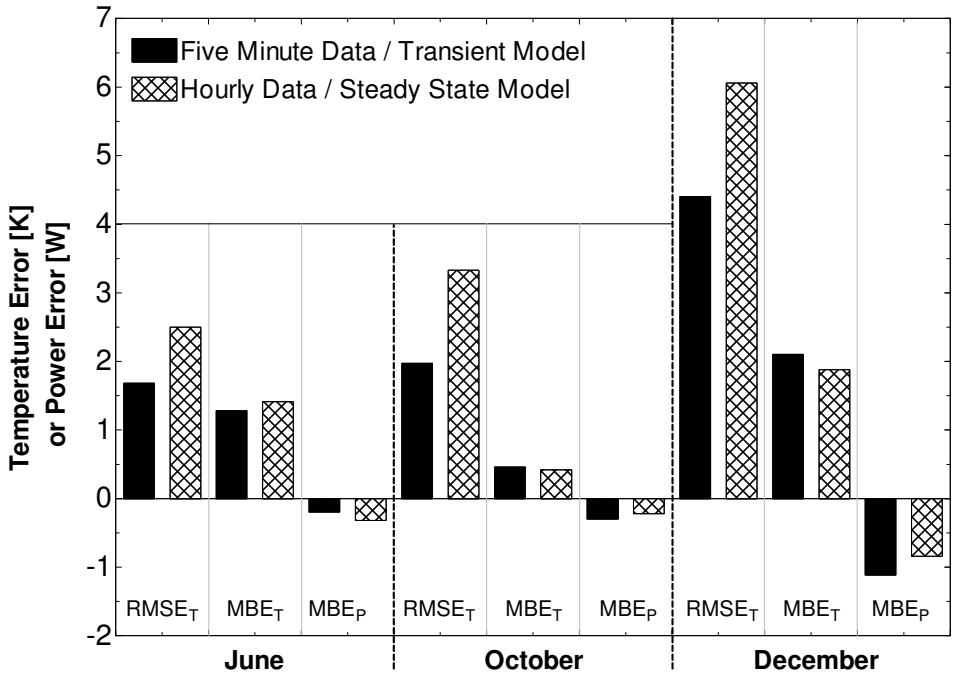

Figure 2.8: RMSEs and MBEs of temperature prediction and MBEs of power prediction for either {1,1,1,1} transient model applying five minute data or {1,1,1,1} steady state model applying hourly data. Forced convection correlation Equation (4) and free convection correlation Equation (1) were used for each case.

2.9.3 Emissivity of ETFE cover

Figure 2.8 shows that both of the models studied over predict the temperature of the poly-Si module. This over prediction may be due to the fact that the correct value of cover thermal emissivity is unknown. Upon further inspection, the value of 0.84 that was used in the calculations appears to be low. An additional poly-Si simulation was completed with an upper limit emissivity of one (rather than 0.84) and the results showed lower MBE of predicted temperature and pressure. Therefore, the emissivity of the poly-Si cover will be approximated as one for the remainder of this study.

2.10 Summary

At this point, all of the energy inputs and outputs of the energy balance model can be calculated. It was also shown that hourly datasets could be used with minimal loss of accuracy. Simulation results suggest that the transient term in the energy balance model can be neglected with minimal loss in the accuracy of long term energy and temperature predictions. These findings result in the {1,1,1,1} transient model being replaced by a steady state model. The steady state model does not account for the thermal capacitance of the materials in the module; consequently the nodal structure is no longer required.

The steady state energy balance only requires three temperatures: (1) the temperature at the interface between the cover and the outside, (2) the cell temperature (assumed to be the temperature at the interface of the cell and cover) and (3) the temperature at the interface between the backside and indoors. The thermal resistances between the cell and the cover and backside (R_1 and R_2, respectively), are also required to calculate the conductive heat transfer. A schematic of the temperatures and the internal thermal

resistances is shown in Figure 2.9. The steady state simulations completed in Section 2.8.5 use this effective thermal resistance network while calculating additional interior temperatures.

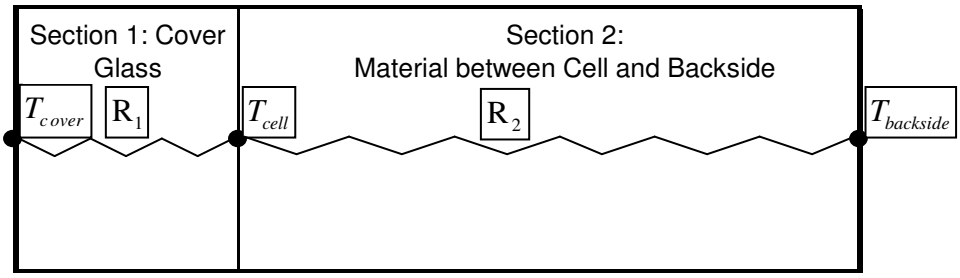

Figure 2.9: Schematic of temperatures and internal thermal resistances used in a steady state energy balance model of the module. Schematic is not to scale.

The currently defined steady state, nodal energy balance applying hourly data can be used to accurately predict the temperature of the mono-Si module with the unusually descriptive NIST input data. Most, specifically TMY, datasets, do not include PIR or nearby wind speed measurements, which were included in the NIST dataset. Additionally, most module datasheets do not include enough information to determine the internal thermal resistances of the module. The next chapter will focus on determining the importance of these pieces of information and estimating the value of each piece.

3. Reducing Model Inputs to Available TMY Data

Chapter 2 detailed the development of a temperature prediction model based on an energy balance of an operating PV module. With minimal increases in monthly bias errors, the model was reduced to a steady state model requiring hourly input data. The input datasets used to develop the model, however, were atypically descriptive; containing measurements such as the temperature of the surroundings, the wind speed measured directly at the module, and a complete characterization of module materials and dimensions. In most practical modeling situations, these measurements will not be available. This chapter explores techniques to estimate this information from readily available sources.

Section 2.8.4 discussed different statistics to determine the most accurate model. It was judged that the mean bias error of power prediction is the most important statistic as it determines the final error in total energy prediction. Simulation results showed that models with low mean bias errors of power prediction typically exhibited low errors with respect to temperature prediction. Therefore, for the remaining simulations, the total energy calculated over the simulated time period is the quantity of interest.

3.1 Estimating the Surroundings Temperature

The equation defining the radiative heat transfer from the module to the surroundings is described in Section 2.4.3. In this section, performance data were evaluated using the surroundings temperature as measured by a precision infrared radiometer (PIR). These measurements will, generally, not be available for most installations; therefore, the surroundings temperature must be estimated. Section 2.4.3 also noted that the

surroundings temperature measured by the PIR is actually a composite of the temperatures of the objects that the module "sees". These objects can be generally grouped as either the sky or the ground, each with a uniform temperature. The view factors (*F*) between the module and these objects also affect the PIR measurement and must be estimated. Once these values are known, Equation (3.1) defines the radiative heat transfer from the cover to its surroundings.

$$\dot{q}_{radiative} = \varepsilon F_{sky} \sigma Area \left(T_{cover}{}^{4} - T_{sky}{}^{4} \right) + \varepsilon F_{ground} \sigma Area \cdot \left(T_{cover}{}^{4} - T_{ground}{}^{4} \right) \tag{3.1}$$

3.1.1 Sky Temperature

Duffie and Beckman (2006) provide two correlations to find sky temperature. Equation (3.2) (Swinbank and Roy, 1963) only requires an ambient temperature input, while Equation (3.3) (Berdahl and Martin, 1984) requires ambient temperature and the dew point. Since the NIST dataset does not include dew point measurements, data were retrieved from Weather Underground (2010) archives of measurements taken in Washington, D.C.

$$T_{sky} = 0.0522 T_{amb}^{1.5} \tag{3.2}$$

$$T_{sky} = T_{amb} \left(0.711 + 0.0056 T_{dp} + 0.000073 T_{dp} + 0.013 \cos(15t) \right)^{\frac{1}{4}} \tag{3.3}$$

In Equation (3.3) the sky and ambient temperatures are in Kelvin, the dew point is in degrees Celsius, and *t* is the hour from midnight.

3.1.2 Ground Temperature

The ground temperature is more difficult to estimate due to effects associated with incident radiation, convective and radiative heat transfer, and thermal capacitance considerations. Therefore, the ground temperature is estimated to be equal to the ambient air temperature.

3.1.3 View Factors

The view factor between the module cover and the sky is calculated by Equation (3.4) which approximates the cover tilted relative to an infinite plane. Then the view factor between the cover and ground is calculated by Equation (3.5).

$$F_{cover-to-sky} = \frac{1+\cos(\beta)}{2} \tag{3.4}$$

$$F_{backside-to-ground} = 1 - F_{cover-to-sky} \tag{3.5}$$

3.1.4 Results

Figure 3.1 shows simulation results of the insulated mono-Si module using the steady state model applying hourly data and varying the equation used to calculate radiative heat transfer. Both proposed correlations for sky temperature were used, as well as a constant adjustment assuming the sky temperature is equal to 20°C below the ambient temperature. The results are displayed as the difference in monthly energy predictions between the model applying the different methods to calculate the sky temperature and the baseline model detailed in Chapter 2. The difference is made into a percentage by normalizing by the measured energy, as shown in Equation (3.6). As Figure 3.1 shows, both of the proposed correlations are more consistent with the baseline than setting the

sky temperature equal to 20°C below the ambient temperature. Since the proposed correlations show similar results, the Berdahl and Martin Equation will be used for the remainder of the report, as its inclusion of the dew point creates the flexibility to predict different sky temperatures at the same ambient temperature. This flexibility is important because the sky temperature is dependent on the amount of cloud cover.

$$\frac{\text{Total Energy Predicted}_{\text{Altered Model}} - \text{Total Energy Predicted}_{\text{Baseline Model}}}{\text{Total Energy Measured}} \times 100\% \qquad (3.6)$$

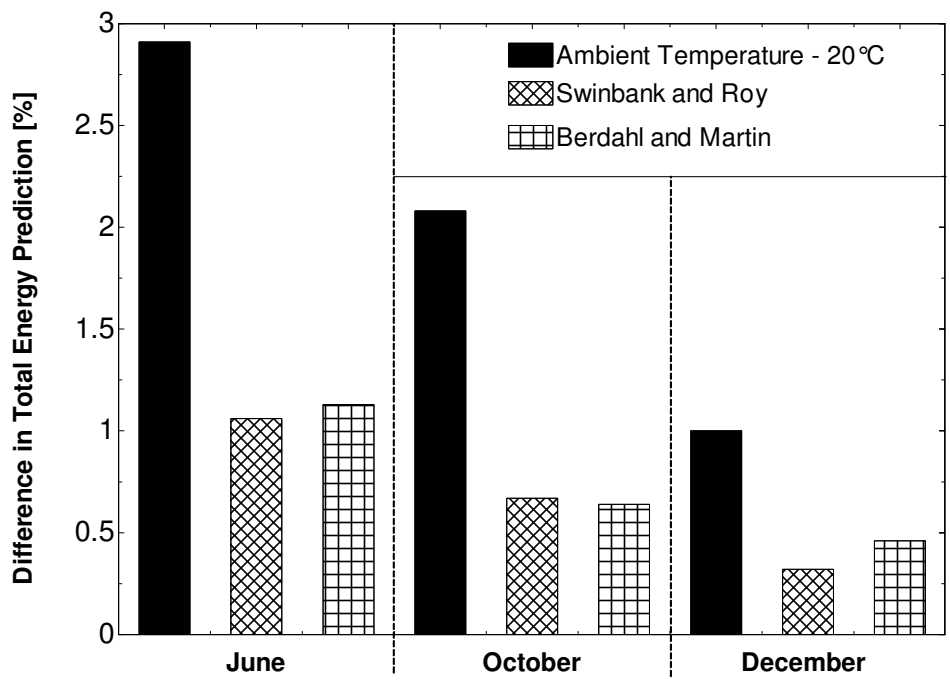

Figure 3.1: The difference between the energy prediction of the insulated mono-Si module caused by varying the method to predict the sky temperature and the energy prediction found using PIR measurements is displayed. The difference is made into a percentage by normalizing by the measured energy.

3.2 Adjusting the Roof-Measured Wind Speed to the South Wall at NIST

The wind speed is required to calculate the forced convection from the module to the ambient air. Simulations in Chapter 2 were completed with the wind speed measured at the module. In most modeling situations, the wind speed at the exact location of the module will likely be unknown. The following section evaluates methods to adjust the wind speed measured on the rooftop of the building where modules are mounted. This study should be an indicator of both the importance and difficult of adjusting wind speeds for building integrated modules.

3.2.1 Power Law Adjustment

In order to adjust the wind speed from the rooftop to the wall, an assumption of the dependence of wind speed with respect to height is required. One approach to create this vertical velocity profile uses the power law profile, shown in Equation (3.7). This equation relates the ratio of calculated velocity and measured (or reference) velocity to the ratio of the height at the calculated velocity and height at the measured (ref) velocity raised to a value of α. Manwell et al. (2002) determine α using Equation (3.8). The value z_0 represents the terrain's surface roughness length. These values are shown in Table C.1 in Appendix C and vary from 0.01 for very smooth landscapes to 3,000 for centers of cities with tall buildings. A maximum value of z_0 = 10,000 is valid in Equation (3.8). The roughness length for the NIST campus is estimated at 175 because the campus contains a few buildings and scattered trees and hedges. This length results in a value of $\alpha = 0.536$.

$$\frac{u(z)}{u(z_{ref})} = \left(\frac{z}{z_{ref}}\right)^{\alpha} \tag{3.7}$$

$$\alpha = 0.096\log(z_0) + 0.016(\log(z_0))^2 + 0.24 \tag{3.8}$$

The rooftop wind measurements at NIST were collected at an elevation approximately 68 feet above the ground. The wind measurements taken near the building-integrated modules are at an elevation approximately 28 feet above the ground.

Figure 3.2 shows simulation results of the insulated mono-Si module using the steady state model applying hourly data and adjusting the rooftop wind measurements using Equations (3.7) and (3.8). As expected, the simulation directly applying rooftop measurements exhibited the greatest difference from the baseline simulation using the measured wind speed at the wall. Adjusting the rooftop wind speed using the power law and setting z_0 = 175 in Equation (3.8) reduces the difference between the altered model and the baseline for each month. Despite this reduction, the difference remains greater than 7% for October and December. Since the differences are caused by over estimating the wind speed, larger values of z_0 are evaluated to further decrease the estimated wind speed. First, a value of z_0 = 1500 is applied, which describes a suburban terrain. As expected, the differences in energy prediction resulting from this roughness level were less than the differences resulting from the smaller roughness level; however, the difference still remains greater than 7% for October and December. Finally, a maximum z_0 value of 10,000 is applied. Results produced by this z_0 value are similar to prior simulation results using z_0 = 1500, and large differences between modeled and baseline energy predictions remain.

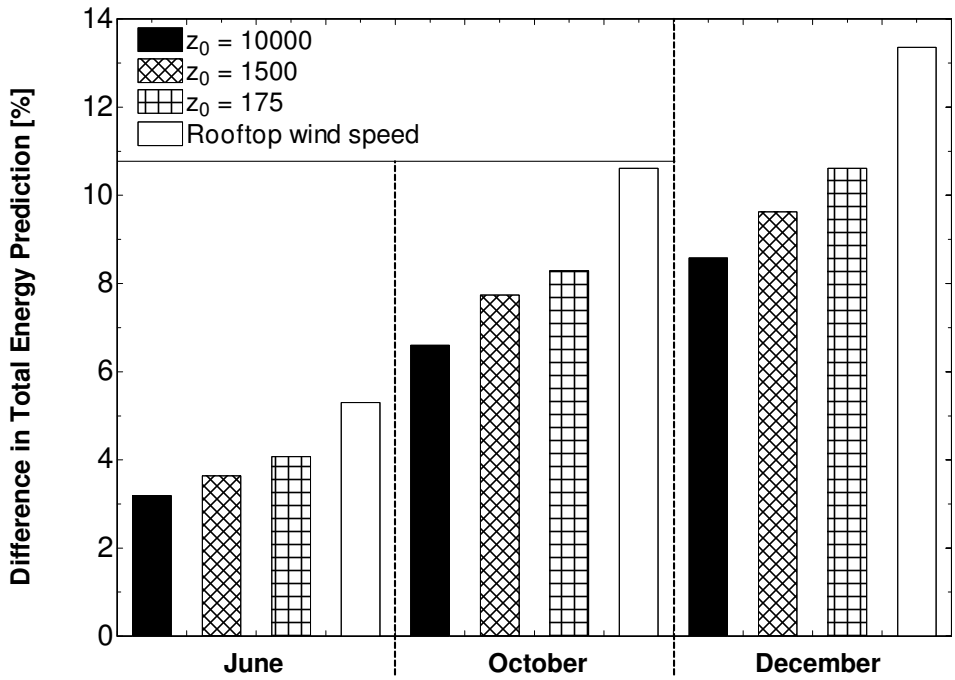

Figure 3.2: The difference between the energy prediction of the insulated mono-Si module caused by varying the method to adjust the rooftop wind measurements and the energy prediction found using the wind measurements at the module is displayed. The difference is made into a percentage by normalizing with the measured energy.

The differences between simulations applying a power law adjustment to the rooftop wind speed and simulations applying the wind speed measured at the wall are due to the power law's inability to adjust the roof wind speeds to the wind speeds that are measured at the module. Figure C.1 in Appendix C shows that the adjusted roof speed measurements are consistently larger than the measured wind speeds at the wall, even when the maximum roughness level is used. This fact suggests that the difference between the roof and wall wind speeds is not exclusively dependent on the vertical distance between the two locations. Therefore it is likely that the building itself is altering the wind speeds near its walls. Correlations which calculate wind speeds near building walls exist in literature and may help to improve results.

3.2.2 Building Effects

Emmel et al. (2006) lists three correlations (Ito et al. (1976), Sharples (1984), and Loveday and Taki (1996)) that attempt to adjust free speed wind measurements to local wind measurements taken at a vertical wall of a building. Sharples conducted his experiments on an 18 story high rise, which makes his results difficult to apply to low rise buildings such as the NIST building in question. Therefore Sharlpes' work is not further investigated. Ito et al. conducted their experiments on a six story building. While this building is more representative of the NIST building than the building in the Sharlpes study, information such as building height and experimental measurement heights are withheld. Therefore the work of Ito et al. is not further investigated. The Loveday and Taki experiment contains the best combination of adequate information and representative building size; therefore, it is used in the following analysis.

Loveday and Taki conducted their experiments on a 28 meter tall, eight story building. Unobstructed wind measurements were taken 11 meters above the roof. Wind speeds were measured one meter away from the wall on the sixth floor, at a height of approximately 19.25 meters. Loveday and Taki found that the wind speed near the wall was dependent on the wind direction. Therefore two equations were developed to calculate wind speed at the wall. One equation was characterized by windward conditions, while the other was defined by leeward conditions. Windward conditions are defined by a wind direction between 0 and ±90 degrees from the outward orientated normal vector of the wall, while leeward conditions include all other wind directions. Loveday and Taki's equations for calculating wind speed at the wall are shown in Equations (3.9) and (3.10).

$$u_{wall,windward} = 0.58u_{roof} - 0.5 \tag{3.9}$$

$$u_{wall,leeward} = 0.157u_{roof} - 0.027 \tag{3.10}$$

These equations can be adapted to the conditions at NIST to predict the wall wind speeds from the roof wind measurements. Since roof and wall measurement heights are different between NIST and the Loveday and Taki experiment, NIST measurements must be adjusted. Figure 3.3 details the adjustment procedure. First, NIST's roof wind speed is adjusted to the height of Loveday and Taki's roof measurements using the power law, Equation (3.7), with a roughness length of 175. Then Loveday and Taki's equations are applied to adjust the roof wind speed to the wall measurement height. Finally, the power law is applied with a roughness length of 175 to adjust the wind speed from Loveday and Taki's wall measurement height to NIST's wall measurement height.

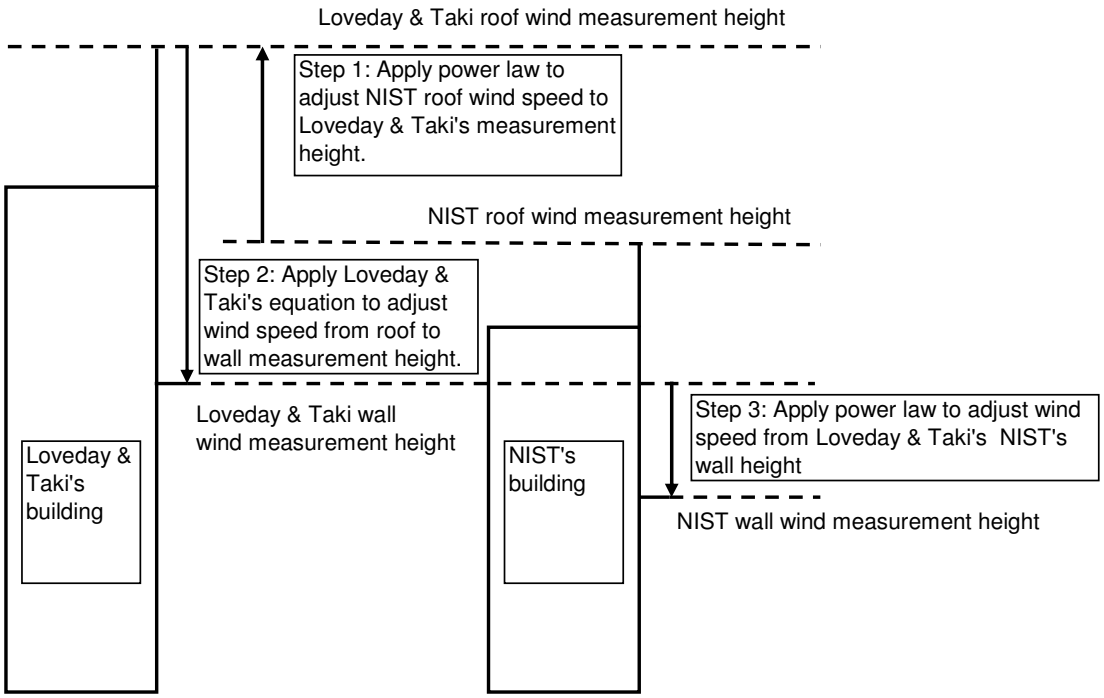

Figure 3.3: Schematic of steps taken to find the wind speed at the south wall module location at NIST using the measured roof wind speed. Schematic is not to scale.

Figure 3.4 shows simulation results of the insulated mono-Si module using the steady state model applying hourly data and adjusting the rooftop wind measurements using the procedure detailed in Figure 3.3. Unfortunately, wind direction measurements are not available after October 14th in the NIST dataset, so the simulation was run once assuming all wind was in a windward direction and once assuming a leeward orientation. The results show differences between the leeward Loveday and Taki correlation and the baseline model are reduced to less than 1%, which this reduction is a vast improvement from the power law correlations. A plot of predicted wall speed versus measured wall speed is shown in Figure C.2 in Appendix C. Note that, as expected from the performance results, Loveday and Taki's correlation does a better job of predicting wind speed than the power law.

Loveday and Taki's windward correlation, however, does not show an improvement from the power law. This contrast between prediction differences produced by leeward and windward is interesting. Wind direction measurements available from NIST before October 14th, 2002 show a steady mix of both leeward and windward winds. Therefore a predominately leeward wind direction is not the explanation. The advantage of the leeward correlation may be explained by closer inspection of the NIST site. Figure C.3 in Appendix C shows an aerial photograph of the NIST campus around the modules. The photograph shows that the windward directions are all somewhat obstructed, especially in the south and east. An east-facing photograph taken underneath the modules is shown in Figure C.4 in Appendix C and displays the relative height of the building to the east of the module location. These obstacles may create a leeward effect for the modules regardless of the free stream wind direction.

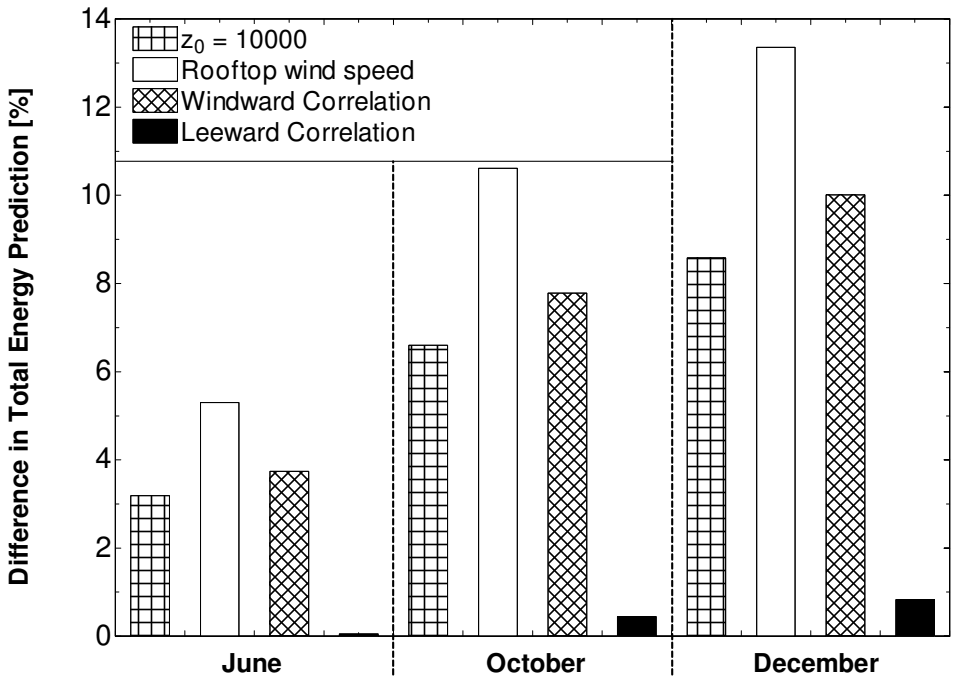

Figure 3.4: The difference between the energy prediction of the insulated mono-Si module caused by varying the method to adjust the rooftop wind measurements and the energy prediction found using the wind measurements at the module is displayed. The difference is made into a percentage by normalizing by the measured energy.

3.3 Predicting the Backside Thermal Resistance of the Module

Figure 2.9 shows a schematic of the temperatures and internal thermal resistances used in the steady state energy balance model of the mono-Si module. The internal thermal resistances are easily calculated with Equation (2.20) for the insulated mono-Si module since the module's materials and dimensions are known. While most module datasheets provide enough information to calculate the thermal resistance of the module's cover, information on the materials composing the module's backside is typically not provided. Therefore, a method must be developed to predict this resistance. The following sections will detail a procedure that uses the nominal operating cell temperature (NOCT) to estimate the backside thermal resistance of a module.

3.3.1 Measurement of NOCT

Module datasheets typically provide a NOCT that determines the cell temperature at a specified set of conditions. ASTM (2008) and IEC (2005) both provide standards for NOCT measurement under the following conditions:

- The module is not connected to a load (or operating as on open circuit).
- The acceptable range of wind speeds during the measurements is between 0.25 m-s^{-1} and 1.75 m-s^{-1} and the acceptable range of ambient temperatures is between 5°C and 35°C.
- The cell temperature and the ambient temperature are measured at various plane-of-array (POA) irradiances on a sunny day. Then regression analysis is used to report the difference between the cell temperature and ambient temperature at a POA irradiance of 800 W-m^{-2}. The uncorrected NOCT is then found by adding 20°C and is then corrected from actual test conditions to the reporting conditions of 1 m-s^{-1} and 20°C using the correction factor table provided in the standard, Figure 3.8.

The reporting conditions (including the POA irradiance of 800 W-m^{-2}) are referred to as the nominal terrestrial environment (NTE).

The IEC standard provides more detail regarding the mounting of the module:

- The IEC standard prescribes the tilt angle of the module to be 45° ±5°. The ASTM standard only calls for the module to be "normal to the sun within ±5° at solar noon", which allows for varying tilt angles depending on location and time of year. This

difference will only affect the relative amounts of beam, diffuse, and ground reflected irradiance for each testing standard since the POA irradiance is specified for both.

- Both standards also call for planar surfaces to be extended around modules designed to be mounted in arrays. ASTM calls for the module to be "tested in the interior of a subarray", while IEC states that the module be "mounted within a planar surface that extends at least 0.6 meters beyond the module in all directions. The surfaces are designed to simulate the thermal boundary conditions of modules installed in arrays. For the NIST modules that are individually mounted, this instruction seems to somewhat contradict the goal of characterizing a module as it is to be mounted. Therefore, the following analysis does not consider a potential planar bordering that may contribute to a slightly higher temperature measurement during field measurements.

Since there are no other significant differences between the standards (the correction factor plot for IEC is also indistinguishable from the ASTM plot); both should provide nearly the same temperature for the NIST modules.

3.3.2 Thermal Modeling of Module at NOCT Conditions

In order to use of the NOCT to predict the backside thermal resistance, the conditions described in Section 3.3.1 must be modeled. Equations (3.11), (3.12), and (3.13) define an energy balance for each temperature node in the steady state energy balance model, shown in Figure 3.5.

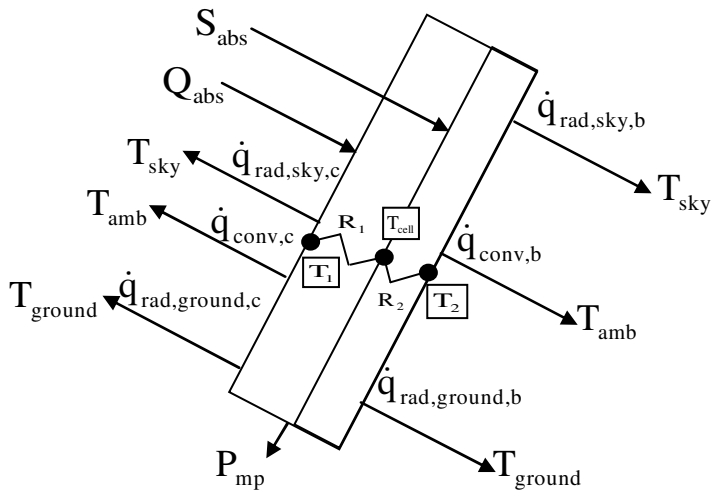

Figure 3.5: Schematic of steady state energy balance on module at NOCT testing conditions.

$$\underbrace{S_{NOCT}}_{\substack{\text{Absorbed}\\\text{Radiation:}\\\text{Cell}}} - \underbrace{\frac{T_{cell,NOCT}-T_1}{R_1}}_{\substack{\text{Conductive heat transfer}\\\text{from cell to cover}}} - \underbrace{\frac{T_{cell,NOCT}-T_2}{R_2}}_{\substack{\text{Conductive heat transfer}\\\text{from cell to backside}}} = 0 \tag{3.11}$$

$$\underbrace{\frac{T_{cell,NOCT}-T_1}{R_1}}_{\substack{\text{Conductive heat}\\\text{transfer from}\\\text{cell to cover}}} + \underbrace{Q_{abs}}_{\substack{\text{Absorbed}\\\text{Radiation:}\\\text{Cover}}} \underbrace{-\varepsilon_c F_{c\text{-}s}\sigma\left(T_1^4-T_{sky}^4\right)}_{\substack{\text{Radiation heat transfer}\\\text{from cover to sky:}\\\dot{q}_{rad,sky,c}}} \underbrace{-\varepsilon_c F_{c\text{-}g}\sigma\left(T_1^4-T_{ground}^4\right)}_{\substack{\text{Radiation heat transfer from}\\\text{cover to ground:}\\\dot{q}_{rad,ground,c}}} \underbrace{-\bar{h}_c\left(T_1-T_{amb}\right)}_{\substack{\text{Convective heat}\\\text{transfer from cover}\\\text{to ambient air:}\\\dot{q}_{conv,c}}} = 0 \tag{3.12}$$

$$\underbrace{\frac{T_{cell,NOCT}-T_2}{R_2}}_{\substack{\text{Conductive heat transfer}\\\text{from cell to backside}}} \underbrace{-\varepsilon_b F_{b\text{-}s}\sigma\left(T_2^4-T_{sky}^4\right)}_{\substack{\text{Radiation heat transfer from}\\\text{backside to sky:}\\\dot{q}_{rad,sky,b}}} \underbrace{-\varepsilon_b F_{b\text{-}g}\sigma\left(T_2^4-T_{ground}^4\right)}_{\substack{\text{Radiation heat transfer from}\\\text{backside to ground:}\\\dot{q}_{rad,ground,b}}} \underbrace{-\bar{h}_b\left(T_1-T_{amb}\right)}_{\substack{\text{Convective heat transfer}\\\text{from backside to ambient air:}\\\dot{q}_{conv,b}}} = 0 \tag{3.13}$$

There are three equations and three unknowns when the material properties of the module are known and the cell temperature is the value of interest. If the cell temperature is known, however, then a different value can be solved. The following sections describe calculations and assumptions that allow the thermal resistance (R_2) of the material on the backside of the cell to be calculated when the cell temperature is known.

3.3.2.1 Calculating the Cell Absorbed Radiation

The absorbed radiation of the cell at NOCT conditions needs to be calculated using the HDKR model, detailed in Section 2.3.1. The NOCT testing standard does not provide enough information to complete the radiation calculation using the HDKR model, so additional assumptions are required. First, the slope of the module at NOCT is required. Since the ASTM standard allows for a variety of slopes, the IEC standard of 45° is used. The latitude of the testing location and the date of the test are also unknown, so an incidence angle of 0° is assumed. Since the POA irradiance is specified, additional information on either the beam normal, diffuse, total horizontal irradiance is required to completely characterize the incident radiation. If the hourly clearness index is assumed to be the maximum value of one, then according to the Erbs, et. al correlation (Duffie and Beckman, 2006) the ratio of hourly diffuse irradiance to hourly total horizontal irradiance is approximately 0.15. Finally, the solar reflectance of the ground is required. Since the NOCT guidelines state that the test be performed in a location with low values of ground solar reflectance, a value of 0.1 is assumed.

3.3.2.2 Calculating the Cover Absorbed Radiation

The HDKR model is also used to calculate the absorbed radiation of the cover as detailed in Section 2.3.2, specifically Equation (2.6). Assumptions made in the previous section about irradiance and ground solar reflectance are applied in this section.

3.3.2.3 Calculating Radiative Heat Transfer

The module radiates to both the sky and the ground. View factors are determined by Equations (3.4) and (3.5). The sky temperature is estimated using ambient temperature measurements in Equation (3.2), and the ground temperature is estimated to be equal to

ambient air temperature. To complete the calculations the emissivity of the cover is known.

3.3.2.4 Calculating Convective Heat Transfer from the Module to Ambient Air

Equation (3.14) (Nellis and Klein 2008) calculates the free convection from a plate mounded at an arbitrary slope (β). Each of the three functions listed in Equation (3.14) are dependent on a gravity vector (g) which is dependent upon β.

$$\overline{\mathrm{Nu}}_{\mathrm{free}} = \mathrm{MAX}\left[\overline{\mathrm{Nu}}_{\mathrm{v}}, \overline{\mathrm{Nu}}_{\mathrm{uf}}, \overline{\mathrm{Nu}}_{\mathrm{df}}\right] \tag{3.14}$$

The subscripts used in Equation (3.14) refer to the following situations:

- *v*: Calculate $\overline{\mathrm{Nu}}$ as if plate is vertical (free convection Equation (1) in Table 2.2) with $g = g\sin(\beta)$.

- *uf*: Calculate $\overline{\mathrm{Nu}}$ as if plate is horizontal upward facing (Appendix D) with $g = g\,\mathrm{MAX}\left[0, \cos(\beta)\right]$.

- *df*: Calculate $\overline{\mathrm{Nu}}$ as if plate is horizontal downward facing (Appendix D) with $g = g\,\mathrm{MAX}\left[0, -\cos(\beta)\right]$.

Both NOCT standards state that the wind direction during the test should be predominately from the north or south, while the module should be mounted normal to the sun at solar noon. These conditions create a situation where the wind is neither normal nor parallel to the module; therefore, calculating the forced convection coefficient between the cover and wind is more complicated. Many equations dealing with forced

convection at various orientations can be found in literature; however, none are exact matches to the mounting of a photovoltaic module for NOCT testing. Sparrow et al. (1979) report heat transfer coefficients for various angles of plate inclinations. The results of Sparrow et al. were found for laminar flow, however, and did not clearly specify if free convection was included in the equations. Test et al. (1981) present measurements taken from an outdoor experiment and report that the calculated heat transfer coefficients are higher than those given by theory and wind tunnel tests. They attribute these differences to the turbulence of the wind. Because their measurements were taken at a wind speed high enough to neglect free convection, their results may not be accurate at the low wind speeds that characterize NOCT testing. Sharples and Charlesworth (1997) present equations derived from field measurements of heat transfer from a 1.81 by 0.89 meter plate mounted on the roof of a single story house with a roof pitch of 35°. Equations are provided as a function of wind direction at 45 degree increments. While Sharples and Charlesworth's experimental set up resembles the NOCT arrangement closely, forced and free convection are not presented separately, which causes the convection coefficient to have a dependence on temperature that is not included in the equations. Sharples and Charlesworth's results compare within 10% to Test's results at a wind speed of 1 ms^{-1}.

The discussion presented above suggests that an equation for forced convection that does not include free convection is needed to represent NOCT conditions. The previous discussion suggests that the flow of wind over a plate is turbulent, so forced convection Equation (4) in Table 2.3 (applied in the steady state energy balance model for forced convection induced by parallel flow) is used to calculate the turbulent forced convection

coefficient. It should be noted that while Sparrow's correlation shows some increase in laminar heat transfer with respect to plate inclination because the thermal boundary layer is compressed, the increased area and turbulent flow associated with NOCT measurements should reduce this effect.

Finally, the characteristic length used to determine the Reynolds number needs to be evaluated. The steady state energy balance model developed in Chapter 2 assumes that the air flow across the module is parallel to the ground, so the width of the module is used as the characteristic length. This assumption is understandable because the wind speed was measured parallel to the module and the NIST modules are nearly square (1.2 meters by 1 meter). For more rectangular modules, choosing either the width or length of module is more significant. For example, a module evaluated in Chapter 4 is 1.56 by 0.8 meters wide, and the heat transfer coefficient calculated by using the width is 15% larger than the heat transfer coefficient calculated using length. However, using the characteristic length defined by Equation (2.10) instead of module width only increases the heat transfer coefficient by 8%. Therefore, this equation will be used to calculate the characteristic length.

The total convection heat transfer coefficient resulting from both free and forced convection is then calculated by Equation (2.11).

3.3.2.5 Backside Emissivity

The backside of the module will radiate to both the sky and the ground. The ground that the backside of the module radiates to is on the north side of the module. This orientation shades the ground from incident radiation, which should force the ground temperature to

be closer to ambient and make the assumption that ground temperature is equal to ambient temperature more accurate. The emissivity of the backside of the mono-Si module at NIST is listed in Appendix A. Typically the material composition of the backside is unknown; for these cases, the long-wave emissivity is set to 0.7.

3.3.3 Results

NIST provided the NOCT and module material properties for the mono-Si technology as both an insulated and un-insulated module, which allows the calculation of the backside thermal resistance using the NOCT model described earlier this section for both cases. The backside thermal resistance of the insulated module is known to be 2.88 KW^{-1}, but using the procedure detailed above it is calculated to be 0.216 KW^{-1}. Since this difference is significant, using the NOCT model to predict the NOCT with the known backside resistance provides insight into the discrepancy. These results are found in Table 3.1 and show that NOCTs predicted by the model do not match the NOCTs measured by NIST. The EES (Klein, 2010) code used for these calculations is included in Appendix G.

Table 3.1: NOCT values reported by NIST and calculated NOCT values.

	Nominal Operating Cell Temperature (NOCT) °C			
	mono-Si		poly-Si	
	Insulated	Un-insulated	Insulated	Un-insulated
NIST Values	66.9	43.7	62.4	39.5
Steady State Calculations	77.3	50.2	69.6	49
Difference (NIST - S.S.)	-10.4	-6.5	-7.2	-9.5

3.4 Investigating Differences between Modeled and Measured NOCTs

The results in Table 3.1 suggest that an error exists in either the modeled or the reported NOCTs. Simulation results in Chapter 2, however, show that the steady state model is typically more accurate than these results. Additionally, the NOCT model should be as accurate in this scenario since the NOCT test is designed to give a steady state temperature, thereby making the observed increase in RMSE of temperature prediction between the steady state and transient model negligible. Acknowledging that some error is present in the NOCT model, the remainder of this chapter will focus on inaccuracies in the NOCT measurement procedure.

3.4.1 Analysis of NOCTs Reported on Manufacturers Datasheets

A study for California Energy Commission (CEC) tabulates a list of modules (Beckman, 2009) and corresponding module properties, including NOCT. Figure 3.6 and Figure 3.7 show the reported NOCTs for each of the approved mono-Si and poly-Si modules, respectively. Note that none of the measured values for either technology are as low as the corresponding measured values from NIST, which suggests that the NIST values may be too low. Furthermore, Muller (2010) suggests that modules of a given technology and packaging components should be characterized by similar NOCTs. From this information, one could hypothesize that the procedure to measure the NOCT, detailed briefly in Section 3.3.1, may lead to variability between tests and ultimately inaccuracies. While Muller (2010) evaluates possible procedural causes of uncertainties, the remainder of this chapter will focus on possible uncertainties introduced by the correction of cell temperature from testing to NTE conditions using the standard correction factor chart.

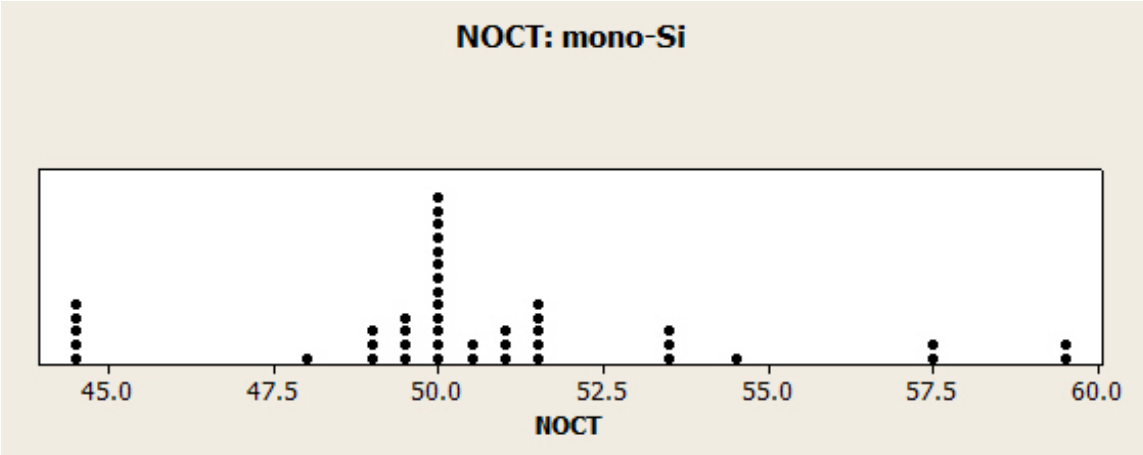

Figure 3.6: Dotplot of NOCTs for the mono-Si modules approved by the CEC.

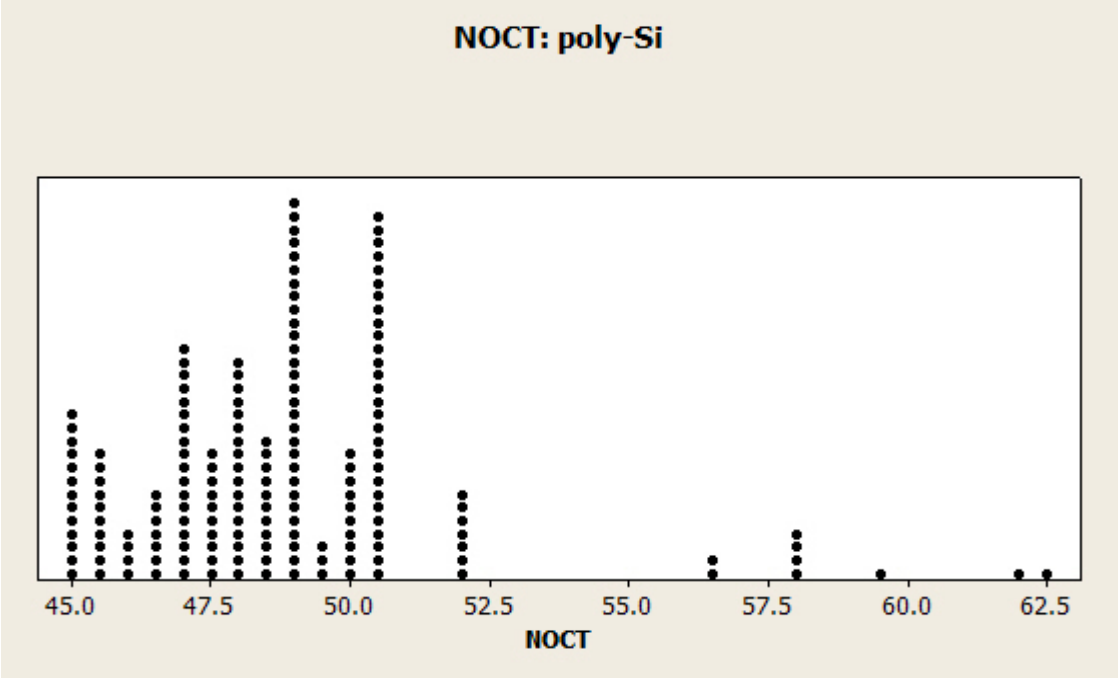

Figure 3.7: Dotplot of NOCTs for the poly-Si modules approved by the CEC.

3.4.2 Comparison of Correction Factor Charts

As Section 3.3.1 details, a correction factor chart is used to adjust the measured NOCT from conditions at the testing environment to conditions at the NTE. The correction factor chart provided by ASTM and IEC is shown in Figure 3.8. A correction factor chart for the insulated mono-Si module can be created, however, by using the NOCT model

described in the previous section and known module material properties. First, NTE conditions are imposed to find the NOCT. Then the cell temperature is found at a variety of wind speeds and ambient temperatures. Finally, Equation (3.15) is applied to find the correction factor at each combination of wind speed and ambient temperature. A plot of correction factors over the range of acceptable wind speeds and ambient temperatures during testing is shown in Figure 3.9.

$$cf = (NOCT - T_{amb})_{NTE} - (T_{cell} - T_{amb})_{\text{non-NTE test conditions}} \tag{3.15}$$

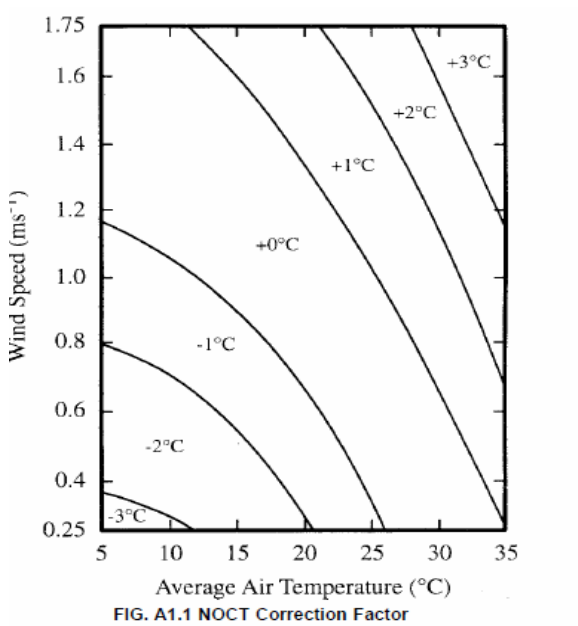

Figure 3.8: Correction factor chart in ASTM and IEC standards.

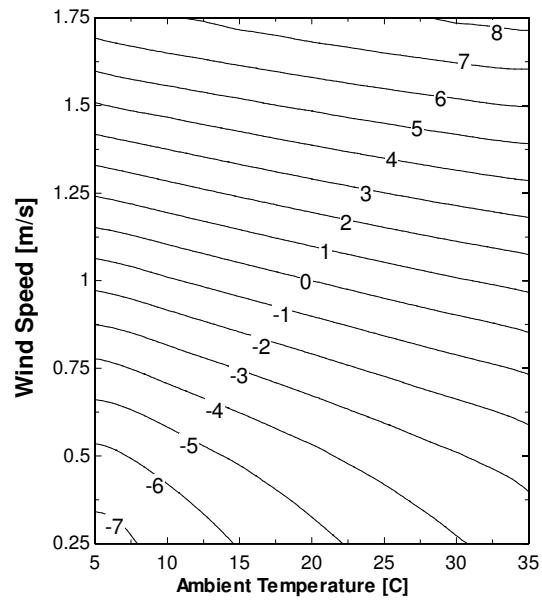

Figure 3.9: Correction factor chart of insulated mono-Si module calculated by NOCT model

A comparison of the correction factor plots shows up to a 5°C difference between the NOCT corrections interpolated from Figure 3.8 and Figure 3.9. This difference is significant and likely contributes to the large differences between modeled and predicted NOCTs shown in Table 3.1. It should be noted that Figure 3.9 was developed for an insulated module. The modeled correction factor chart for the uninsulated mono-Si module is shown in Figure 3.10, and is different than both Figure 3.8 and Figure 3.9. Since both NOCT standards (IEC and ASTM) only supply one correction factor chart, these findings raise two questions:

(1) Why are the modeled correction factor charts different?

(2) Why are both of the modeled correction factor charts different than Figure 3.8?

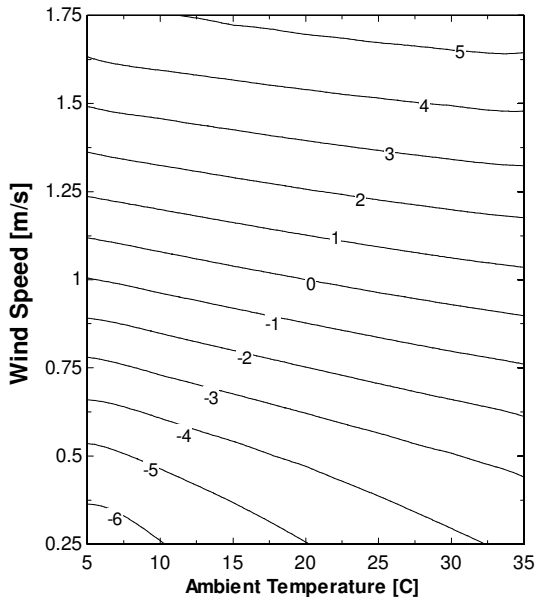

Figure 3.10: Correction factor chart of uninsulated mono-Si module calculated by NOCT model.

3.4.3 Differences between Insulated and Uninsulated Modeled Correction Factor Charts

Application of heat transfer principles helps to explain the differences between the insulated and uninsulated correction factor charts. First, it is important to note that the varying wind speed and, to a lesser degree, ambient temperature affect the heat transfer coefficient (*h*) from the surface of the module to the environment. Now, one can assume that there are two modules with identical cover areas absorbing equal solar radiation (q'''): one uninsulated module and one insulated module. The environmental conditions are an arbitrary "condition 1", which is restricted by the acceptable NOCT testing conditions. Neglecting radiation, Equations (3.16) and (3.17) describe steady state energy balances on the uninsulated and insulated modules, respectively.

$$q''=2h_1 \cdot \Delta T_{uninsulated,1} \tag{3.16}$$

$$q''=h_1 \cdot \Delta T_{insulated,1} \tag{3.17}$$

The heat transfer coefficient in Equation (3.16) is doubled because each side of the uninsulated module experiences roughly the same heat transfer coefficient, while only the front side of the insulated module experiences significant heat transfer. Next, solving for $\Delta T_{insulated,1}$ yields Equation (3.18).

$$\Delta T_{insulated,1}=2\Delta T_{uninsulated,1} \tag{3.18}$$

Now suppose that the wind speed were altered such that Equation (3.19) were true. This new arbitrary environmental condition, again restricted by wind speeds within the

acceptable range for NOCT testing, is labeled in the following equations as "condition 2".

$$h_2 = a \cdot h_1 \tag{3.19}$$

Then, Equations (3.20) and (3.21) are also true.

$$\Delta T_{insulated,2} = 2\Delta T_{uninsulated,2} \tag{3.20}$$

$$\Delta T_{unins,1} = a \cdot \Delta T_{unins,2} \quad \text{and} \quad \Delta T_{ins,1} = a \cdot \Delta T_{ins,2} \tag{3.21}$$

Finally, the difference between temperature gradients for each module is calculated by subtracting Equation (3.20) from Equation (3.18) and is shown in Equation (3.22).

$$\left(\Delta T_{ins,1} - \Delta T_{ins,2}\right) = 2\left(\Delta T_{uninsulated,1} - \Delta T_{uninsulated,2}\right) \tag{3.22}$$

If "condition 1" is assumed to represent NTE conditions, then Equation (3.22) can be rewritten as Equation (3.23). This equation shows that the correction factor of insulated modules should be twice the correction factor of the uninsulated module at the two heat transfer coefficients. This difference explains why the correction factor chart for the insulated modules is more sensitive to wind speed and, to a lesser degree, ambient temperature than the insulated module: under non-NTE conditions ("condition 2"), the difference between the cell and ambient temperatures for both modules at NTE conditions is divided by *a*, as shown by Equation (3.21), but at both conditions the temperature difference for the insulated module is twice as large as the temperature difference for the uninsulated module, as shown by Equations (3.20) and (3.18).

Therefore, at an arbitrary testing condition, the magnitude of the correction factor for the insulated module is greater than the correction factor for the uninsulated module , which is observed when comparing Figure 3.9 and Figure 3.9.

$$\text{Correction factor}_{\text{insulated module}} = 2 \cdot \text{Correction factor}_{\text{uninsulated module}} \tag{3.23}$$

3.4.4 Differences between Modeled and Standard Correction Factor Charts

Since both of the modeled correction factor charts are different than the standard correction factor chart, it is worth attempting to recreate the standard chart. One possibility is that the standard chart assumes laminar forced convection over the module, so another correction factor plot can be developed using the NOCT model and forced convection Equation (1) in Table 2.3 and is shown in Figure 3.12. This plot shows that when laminar forced convection is applied, the correction factor chart produced by the NOCT model is similar to the chart provided by ASTM and IEC (Figure 3.11). This finding suggests that the ASTM plot was created with a laminar heat transfer coefficient. Simulation results in Chapter 2, however, showed that turbulent forced convection correlations more accurately predicted the module temperature when applied to the steady state model. It may be appropriate, given these results, to use Figure 3.10 as the correction factor chart for testing open rack modules outdoors.

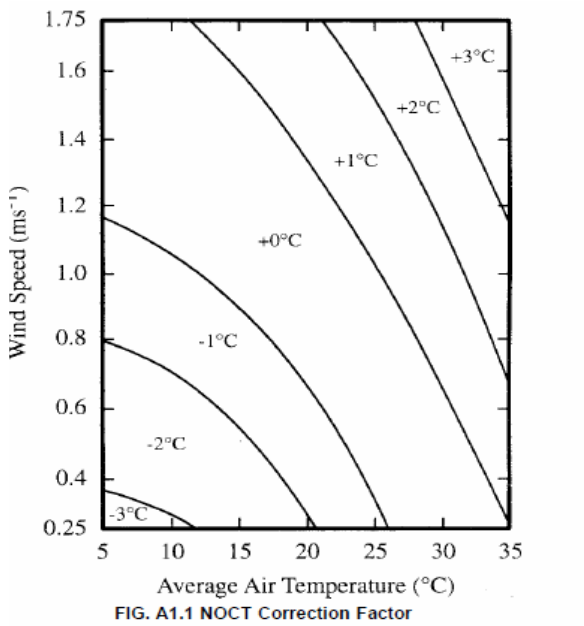

Figure 3.11: Correction factor chart in ASTM and IEC Standards.

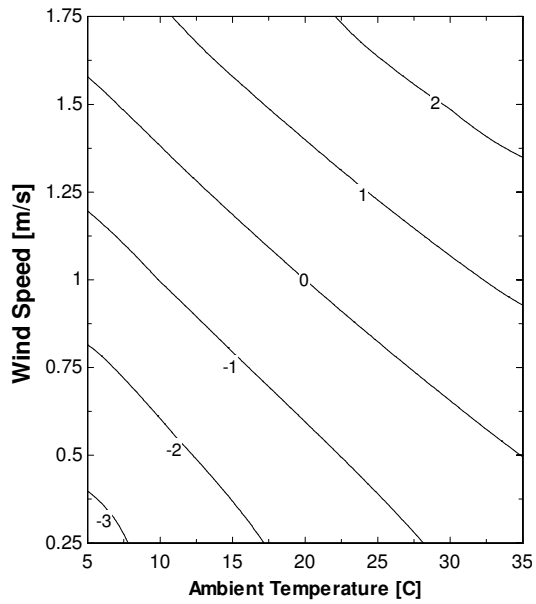

Figure 3.12: Correction factor chart of unisulated mono-Si module calculated by NOCT model.

3.4.5 Suggested Changes to Improve Accuracy of NOCT Measurement

The previous sections have shown that the correction factor chart is highly dependent on both the mounting of the module in question (insulated or uninsulated) and the thermal model chosen to characterize the testing environment (turbulent or laminar). It seems likely that the correction factor chart in the standard is designed for uninsulated modules experiencing laminar flow. These conditions are not exclusive to all modules that are tested for NOCT, especially insulated modules (modules mounted flush to a building wall or roof can be considered insulated). With this fact in mind, the following changes are suggested to make NOCT tests more accurate and more adaptable to a variety of modules and thermal models.

3.4.5.1 Report Testing Conditions with NOCT: Eliminate Correction Factor Charts

The NOCT is designed to provide the user information that can ultimately be used to predict the module temperature. A module will certainly experience different environmental conditions throughout its lifetime. An accurate thermal model must accommodate for this range of conditions, so the information obtained from the NOCT is typically manipulated such that it can be used to predict module temperature at these conditions. Therefore, the NTE conditions at which the NOCT is reported are arbitrary in the sense that a manipulation from NTE to simulation conditions is always required.

If the NTE conditions are indeed arbitrary, then one may question the benefit of requiring the cell temperature be reported at NTE. As detailed earlier, a correction factor is applied to adjust temperature measurements to NTE conditions. From a qualitative perspective, this procedure takes an exact temperature measurement and adds uncertainty to it via the correction factor. When using a thermal model applying the NOCT, however, it is highly likely that using the NOCT found by applying a correction factor will produce an incorrect temperature at original testing conditions. Therefore, this procedure has failed to accurately predict the temperature at the only conditions where it should be absolutely correct.

A more accurate procedure would be to report the measured cell temperature at the measured testing conditions (wind speed and ambient temperature). Then the cell temperature would at least be guaranteed to be correct at one condition (within experimental uncertainty), and the modeler would have the option of choosing inputs to a thermal model. This scenario will likely introduce inconsistencies in testing conditions

between different modules, but reporting the conditions on the manufacturer's data sheet would be an easy fix to this problem.

3.4.5.2 Provide Multiple Correction Factor Charts

The previous sections detailed the differences in correction factor charts caused by the mounting of the module and the testing conditions assumed. Multiple correction factor charts could be supplied in the standards that would allow the tester to choose the chart the best represents the testing conditions. This approach would allow more accurate estimates of NOCT at NTE conditions. It would also create, however, a more complicated standard, and the new correction factor charts would have to be agreed upon.

3.5 Summary

This chapter evaluated a correlation to predict the sky temperature, which is useful for typical datasets that do not include PIR measurements of surroundings temperature. Wind speed adjustment methods were also evaluated to allow the wind speeds measured on the rooftop to be used in simulations. The most accurate method was highly specific to the NIST building; however, and is likely not applicable to other BIPV environments. Finally, a steady state energy balance of the module at NOCT conditions was developed in order to predict the backside thermal resistance of the module, but predicted results did not match measured results. An investigation of the NOCT measurement standard found that uncertainties in the correction factor chart may be responsible for the poor results. Finally, methods to improve the accuracy of the NOCT measurement standard were recommended.

At this point, simulations can be completed using standard datasets. The next chapter will focus on yearly simulations of the two BIPV modules already discussed as well as two open rack modules located at Sandia National Laboratories and NREL, respectively.

4. Annual System Performance Validation

Chapter 2 focused on developing and validating the steady state energy balance model. Chapter 3 focused on techniques to reduce the required model inputs to the data available in TMY datasets and manufacturer datasheets. The simulations in Chapter 2 were completed with performance and weather data for BIPV modules located on the south wall of a NIST building in Gaithersburg, Maryland. These modules were integral to the initial development and validation of the steady energy balance model. It is important to assess whether the current model can be extended for different module mounting configurations and climates. A common mounting arrangement not yet considered is a latitude-sloped rack mounted module.

This chapter considers adaptations to the model required to apply the steady state energy balance model to rack mounted modules. Then three cell temperature models that are commonly cited in literature are defined. Next, two additional datasets providing weather and performance measurements for open rack modules in separate locations are described. A data filtering process is presented that allows consistent filtering between datasets for quality control. Finally, yearly performance simulations of these modules, along with the two BIPV modules from NIST, are included to show the performance of the steady state energy balance model over a long-term simulation period for various mounting configurations and locations. The performance simulations of these modules are also completed using the three other cell temperature models. Additionally, a sensitivity study is completed for the steady state energy balance model.

4.1 Steady State Energy Balance Model for Rack Mounted Modules

The steady state energy balance for a rack mounted module differs from the energy balance for the BIPV module because the backside of the module is exposed to and exchanges energy with the ambient environment. Fortunately, a model for a rack mounted module is easily developed using existing correlations discussed for the BIPV and NOCT models in Chapters 2and 3, respectively.

4.1.1 Absorbed Radiation

For the rack mounted module, the radiation absorbed by the cell is calculated using the HDKR method detailed in Section 2.3.1. Note that since the POA irradiance is not provided in TMY datasets, the absorbed radiation is not corrected using Equation (2.3). The radiation absorbed by the cover is also calculated using the HDKR method as described in Section 2.3.2 and is not corrected.

4.1.2 Power Output

The power produced by the module is calculated with the five parameter model as described in Section 2.4.1.

4.1.3 Convective Heat Transfer

The correlations used to calculate the convective heat transfer for the NOCT model in Section 3.3.2 are applied to the rack mounted model.

4.1.4 Radiative Heat Transfer

The correlations presented in Section 3.1 are applied to the rack mounted model. Specifically, the sky temperature is calculated using Equation (3.3), the ground temperature is assumed to be equal to the ambient temperature, and the view factors are

calculated using Equations (3.4) and (3.5). The backside emissivity of the module is typically unknown and therefore is assumed to be 0.7.

4.1.5 Interior Thermal Resistances

The material properties of a module's cover are typically known; therefore, the thermal resistance between the front of the module and the cell is calculated using Equation (2.20). The backside resistance, however, is still required. Although the NOCT method discussed in Chapter 3 did not accurately predict the backside thermal resistances for the NIST modules, it is used to calculate the backside thermal resistances for the rack mounted modules presented in the next section. The NOCT method is considered accurate for these new modules because their NOCTs appear reasonable in relation to Figure 3.6 and Figure 3.7.

4.2 Additional Cell Temperature Models

The steady state energy balance model has been validated in the previous chapters, and its performance is evaluated in the Section 4.6 using yearly, hourly datasets. At this point, it is important to introduce other cell temperature models often cited in literature that can be used for comparison purposes to the steady state energy balance model.

4.2.1 Duffie and Beckman

The Duffie and Beckman (2006) model shown in Equation (4.1) is evaluated, with minor alterations to conform to available data. Equation (4.1) requires POA irradiance, the transmittance-absorptance product of the cover, the module efficiency. The altered model shown in Equation (4.2) applies absorbed radiation values and the power output of the module. Equation (4.2) is used in subsequent simulations. These changes are

intended to make the model more adaptable to various operating conditions, as the absorption and efficiency are no longer constants. This model requests the wind speed at the module height (u).

$$\frac{T_{cell} - T_{amb}}{T_{NOCT} - T_{amb,NOCT}} = \frac{G_T}{G_{NOCT}} \frac{9.5}{5.7 + 3.8u} \left[1 - \frac{\eta_{cell}}{(\tau\alpha)} \right] \tag{4.1}$$

$$\frac{T_{cell} - T_{amb}}{T_{NOCT} - T_{amb,NOCT}} = \left(\frac{9.5}{5.7 + 3.8u} \right) \cdot \left(\frac{S - P_{mp}}{S_{NOCT}} \right) \tag{4.2}$$

4.2.2 Skoplaki et al.

The Skoplaki et al. (2008) model is shown in Equation (4.3) where ω_m is the mounting coefficient. Values of the mounting coefficient for various mounting configurations are shown in Table 4.1. The Skoplaki et al. model requires the wind speed at the free stream height of 10 meters above the ground (u_∞).

$$T_{cell} = T_{amb} + \omega_m \left(\frac{0.32}{8.91 + 2u_\infty} \right) G_T \tag{4.3}$$

Table 4.1: Values of the mounting coefficient for various PV array mounting situations (Skoplaki et al., 2008).

PV array mounting type	ω_m
Free standing	1.0
Flat roof	1.2
Sloped roof	1.8 (1.0-2.7)
Façade integrated	2.4 (2.2-2.6)

4.2.3 King (Sandia)

The cell temperature model implemented in the Sandia performance model (King et al. 2004), is shown in Equations (4.4) and (4.5). This model also requires the wind speed at the free stream height.

$$T_1 = G_T \cdot exp\left(a + b \cdot u_\infty\right) + T_{amb} \tag{4.4}$$

$$T_{cell} = T_1 + \left(\frac{G_T}{G_{T,ref}}\right)\Delta_T \tag{4.5}$$

Inputs a, b, and ΔT are mounting-dependent values and given in Table 4.2.

Table 4.2: Empirically determined coefficients used to predict module back surface temperature as a function of irradiance, ambient temperature, and wind speed. Wind speed was measured at the standard height of 10 meters (King et al., 2004).

Module Type	Mount	a	b	ΔT (°C)
Glass/cell/glass	Open rack	-3.47	-0.0594	3
Glass/cell/glass	Close roof mount	-2.98	-0.0471	1
Glass/cell/polymer sheet	Open rack	-3.56	-0.0750	3
Glass/cell/polymer sheet	Insulated back	-2.81	-0.0455	0
Polymer/thin-film/steel	Open rack	-3.58	-0.1130	3
22X Linear Concentrator	Tracker	-3.23	-0.1300	13

4.3 Rack Mounted Modules Located at Sandia National Laboratories

Sandia supplied one year of data for five mono-Si modules that were connected in series and rack mounted in a side-by-side arrangement at a fixed slope (slope=latitude=35°). Each individual module is 1.56 meters long and 0.8 meters wide (1.24 m^2), which makes the entire array area 6.221 m^2. The distance between modules is approximately 1 meter. Weather and performance data were collected for the one year period from April 1, 2007 to March 31, 2008. Module performance and physical data are shown in Table A.5 in Appendix A. Relevant data measured at the site include DC voltage and current, irradiance (global horizontal, diffuse horizontal, and direct beam), air temperature, wind speed, wind direction, dew point temperature, and backside temperature. Instantaneous module performance and weather data are provided in two minute intervals.

4.3.1 Dataset Specific Adjustments

There are many differences in the experimental set-up between the Sandia and NIST modules that were used for validation purposes in Chapter 2. It is important to identify these differences and their possible effects before modeling efforts are initiated.

4.3.1.1 Adjustment of Wind Speed with Respect to Differences between Measurement and Module Heights

One major difference between sites is the location of the wind speed measurement. The BIPV data collected at NIST included measured wind speed at both the south wall near the modules as well as on the roof of the building. The wind speeds measured at the wall provided an accurate value for initial evaluation of heat transfer models. The roof wind speeds were then used to calculate the wall wind speeds. Simulations completed in Section 3.2 with these calculated wall wind speeds showed that the building and

surrounding landscape have a significant effect on adjusting wind speeds to various locations, and miscalculation of the wall wind speeds caused large errors in predicted module energy production. Therefore it is important to identify and correct any differences between the measured wind speed site and the module site.

At the Sandia installation, the wind speed was measured approximately 550 feet to the east of the modules at an elevation of 30 feet above the ground. Therefore, the wind speed input to the steady state energy balance and the Duffie and Beckman models is adjusted for this slight difference in heights by using Equations (3.7) and (3.8). The wind speed inputs to the Skoplaki and King models do not require adjustment. From the surface descriptions corresponding to given z_0 values (Table C.1 in Appendix C), the Sandia location is best described by values between 250 and 1500. Based on experience, z_0 = is set to 250 for this location. A sensitivity study later in this chapter evaluates this range of values.

4.3.1.2 Consideration of Adjacent Buildings

An aerial view of the array location at Sandia (Figure C.5 in Appendix C) shows a few buildings directly north of the modules while there are no obstructions in any direction from the wind tower, which suggests that winds from the north may slow near the modules and measured wind velocities may need to be further adjusted. The building is approximately 2 meters north of three of the modules. The building is approximately 3 meters wide (east to west), 6.5 meters long (north to south), and 3 meters tall. According to Wegley et al. (1980), there will be a decrease in wind speed along with an increase in turbulence downstream of the building. Since the projected area of the building into the

wind is relatively small, the increase in turbulence is assumed to offset the decrease in velocity. This assumption follows logic similar to that used to apply the same heat transfer coefficient to the windward and leeward side of the module. It should be noted that, at some size, the projected area of the obstruction will be large enough to cause considerable decreases in wind speed on the leeward side of the obstruction (similar to the south wall at NIST as described in Section 3.2). Currently, this size is unknown and further research may prove beneficial in this area. It is certain that wind speed is a significant contributor to heat transfer from a module; therefore, the accuracy of thermal models (especially for building integrated photovoltaics) is dependent on the accuracy of predicted wind speeds.

4.3.1.3 Module Versus Array Dimensions

Another difference is the area covered by the modules. The total module area for the NIST study was 1.2 m^2 while the Sandia modules cover 6.22 m^2. Shrestha et al. (2009) show that modules on the downstream ends of closely spaced, gap mounted rooftop arrays do not receive the same cooling effect from the wind, which is consistent with heat transfer theory. The five modules in this study are spaced by 1 meter, which is greater than the width of a module. It is likely that the turbulence associated with the wind, combined with the spacing, negates the thermal boundary layer buildup associated with decreasing heat transfer coefficients. It is also important to note that if the effect of combined module area on heat transfer is indeed noticeable, it will only occur during due east or west winds; therefore, it is assumed that each module experiences the same conditions. For this reason the steady state energy balance model is evaluated for one

module and is assumed to apply to all modules in the array. A sensitivity study later in this chapter evaluates the use of array dimensions in the heat transfer calculations.

4.4 Rack Mounted Modules Located at NREL

NREL supplied one year of data for four PV arrays to use for further evaluation of the steady state energy balance model. A HIT (Heterojunction with Intrinsic Thin Layer) Grid-Connected System was chosen to evaluate the cell temperature models for another rack mounted system because manufacturer's data were available for this array. The availability of data from the HIT technology was important for technology diversity since the other modules considered in this study included only mono-Si and poly-Si technologies. Module performance and physical data are shown in Table A.6 in Appendix A. The HIT array, shown in Figure C.6 in Appendix C, consists of five rack mounted modules mounted at a fixed slope equal to the latitude (40°) and connected in series with a resultant maximum power point voltage of 279 volts at STC. The mounting description provided by NREL also detailed possible shading of the array during the final hour of the day. Each module is 1.32 meters by 0.89 meters. The spacing between the modules is approximately 2 inches, so the overall array dimensions are approximated as 1.32 meters by 4.46 meters. Relevant data measured at the site include DC voltage and current, irradiance (global horizontal, diffuse horizontal, direct beam, and global plane of array (POA)), air temperature, wind speed, wind direction, relative humidity, and module backside temperature. The data were collected for the year 2008. The backside temperature of the array was measured from one module. Measurements of these quantities were taken every five seconds and compiled into 15 minute time-averaged

values. Quality assurance flags for irradiance, air temperature, and snow cover were included by NREL.

4.4.1 Dataset Specific Adjustments

4.4.1.1 Adjustment of Wind Speed with Respect to Differences between Measurement and Module Heights

The wind speed is measured at a location coincident with the installation of the array and therefore does not need to be adjusted for height or obstructions for the steady state energy balance and Duffie and Beckman models. However, the measured wind speed needs to be adjusted to the free stream wind speed for the King et al. and Skoplaki et al. models by using Equations (3.7) and (3.8). Similar to the adjustment for Sandia, z_0 = is set to 250 for this location, and a sensitivity study later in this chapter evaluates this range of values.

4.4.1.2 Module Versus Array Dimensions

The HIT modules comprising the NREL array are spaced by approximately two inches. Arguments about the effect of a larger thermal boundary layer, similar to those for the Sandia module, are also important for this array. With a spacing of this distance, it is more likely that the effect of a larger thermal boundary on heat transfer will occur under most wind conditions. Similar to the Sandia module, the magnitude of this effect and the wind conditions that may cause it are, unfortunately, unknown. For this reason the steady state energy balance model is evaluated for one HIT module and is assumed to apply to all modules in the array

4.4.1.3 Cover Properties

Cover properties were not included in the manufacturer's datasheet, although it was specified that the cover was glass. Cover properties are needed for both the 5-parameter performance model and the steady state energy balance thermal model. In the performance model, cover properties (thickness, extinction coefficient, and refractive index) help determine the amount of incident radiation that is absorbed by the photovoltaic cell. In the thermal model, cover properties (thickness, emissivity, and thermal conductivity) are needed to determine the thermal characteristics of the module. Therefore, it was assumed that the cover was identical to the cover for the Sandia module.

4.5 Filtering Described Datasets

Oftentimes datasets contain data that may not be useful for evaluating the performance of a predictive model. Since the following sections of this chapter attempt to compare yearly simulation results between four different datasets, it is important to develop a consistent and logical filtering procedure that can be applied uniformly to all datasets for quality control.

4.5.1 Procedure

The following procedure describes a data filtering and model evaluation process that has been developed from experience in working with the NIST, NREL, and Sandia datasets. Part of this procedure defines intermediate values that are calculated during the simulation process; these values can be compared to experimentally measured values in order to (1): identify model errors and (2) identify suspicious data. It should be noted

that the criteria used when deciding that predicted and modeled values are significantly different is left to individual modelers, based on their modeling objectives and previous experiences. In any case, the following procedure is recommended to help in identifying serious errors in measured datasets and simulation code.

1. Sort by incidence angle: For some mounting conditions the sun will be behind the module during the early morning and later afternoon. In these cases, the module will not experience any direct beam irradiance, while irradiance measurements that are greater than zero will still be recorded. While a well written code could handle this situation during yearly simulations, it is easier to simply reject time periods with an incident radiation angles greater than 90°. The incidence angle is a function of solar time, module geometry, and geographical coordinates. There is little threat to the legitimacy of the modeling results in the case that these points are disregarded, as the module would produce minimal power during these times of day.

2. Module Shading: In some cases, a module will experience shading, which affects module performance, during some periods of the day. While ultimately it is important for models to account for this shading, shading complicates basic validation. The effects of even a small amount of shading can have significant effects on array performance. Therefore, unless accounting for shading is a modeling goal, data measured when any part of a module in an array was shaded should be rejected. It is more important that time periods affected by shading be rejected than times affected by negative incidence angles be rejected because the times affected by

shading could be characterized by enough irradiance to produce significant amounts of power.

There are two methods to identify time periods experiencing shading. The first method requires knowing the dimensions and distance of obstructions. Then geometry can be used to calculate times when shading of direct solar radiation will occur. The second option is to visually observe times when the module is shaded.

3. Incomplete Data: Oftentimes data are missing for a measurement during a time period. The value of the measurement is sometimes set to -999. Time periods including missing data for any relevant measurement should be rejected.

4. Quality Assurance Flags: Some data files may include quality assurance flags to designate certain periods that may contain suspect data. Usually these flags are developed by applying additional measurements that are not necessary in the thermal or performance models. For example, a dataset available from NREL includes a flag that identifies periods with potential snow cover on the module. This flag was developed using ground reflectance data. Ultimately the choice of flags used to filter the data is a combination of both the available flags and the preferences of the modeler. Implementation of data rejection based on snow flags, however, is highly recommended unless the objective of the model is to assess the effects of snow cover.

5. Consecutive Constant Values: Experience has shown that in some cases a string of consecutive constant values will be provided for the same measurement. For example, in the HIT dataset the cell temperature is reported as 0°C for many

consecutive points. Realistically, some number of consecutive measurements should not be equal. These values can often be confirmed as inaccurate by viewing the residuals for the time period in question.

6. Reasonable Cell Temperature: If the measured cell temperature is less than the ambient temperature (especially hours after sunrise), there is a likely error in one or both of the measurements.

7. Quality Assurance Calculations: The flow chart in Figure 4.1 shows the order that calculations should be evaluated in order to determine the usability of the weather and performance data. The flow chart assumes that beam normal, horizontal diffuse, total horizontal, and POA irradiance measurements are available. The ultimate goal is to determine if errors exist in the data or model. At the end of every possible path there is a suggestion detailing the best way to proceed.

   The first comparison is to calculate total horizontal irradiance using beam normal and diffuse radiation and compare the results to the measured total horizontal. While these values will typically not be equal, from observation the relative differences should be approximately 10% or less. A more appropriate threshold may be developed by accounting for uncertainties in the irradiance measurement devices. If the difference is significantly larger than this threshold value, then the inaccurate measurement needs to be determined by comparing the calculated (HDKR) and measured POA irradiance measurements.

The HDKR method requires beam normal, horizontal diffuse, and total horizontal irradiance measurements, but any two of the measurement can be used to calculate the third. Therefore, three different combinations of two of the measurement can be used calculate POA irradiance. If only one of the three measurements is inaccurate, then calculating the POA irradiance with the other two measurements should produce a value approximately equal to the measured POA irradiance. If none of the combinations used to calculate POA irradiance produce accurate results, then either multiple measurements are likely inaccurate and the data should be rejected, or the model used to predict POA irradiance is inaccurate. Further evaluation of the data should help to differentiate between these two possibilities. (It should be noted that it is possible that the measured POA irradiance and only one of the other irradiance measurements are incorrect, and therefore the process of testing combinations of the other three measurements could be repeated and comparable to power measurements. This procedure is not advisable, as it does not allow any assessment of the accuracy of measured and predicted power).

Assuming that an accurate method of either calculating the POA irradiance or total horizontal irradiance has been identified, the power can be calculating using the 5-parameter model with calculated absorbed radiation (HDKR) and measured temperature as inputs. Then some different scenarios are possible:

a) Predicted maximum power is approximately equal to measured maximum power. This result suggests the input data are accurate. If the predicted POA

irradiance is not equal to the measured irradiance, however, the measured value of POA irradiance may be inaccurate.

b) Predicted maximum power is not equal to measured maximum power. If the predicted POA irradiance is approximately equal to the measured (observations from filtering effort have shown that differences less than 40 Wm^{-2} are typical, although this value may differ depending on the site and instrumentation), then inaccuracies are likely in the maximum power measurements. If the predicted POA irradiance is not approximately equal to the measured, then the absorbed radiation can be corrected using Equation (2.3). If the predicted and measured maximum power are approximately equal after this correction, then inaccuracies were likely in the HDKR method (most likely due to an inaccurate ground reflectance value) and modeling efforts should be completed using corrected absorbed radiation. If the predicted and measured maximum power are not approximately equal after this correction, then inaccuracies are likely in both the maximum power and POA irradiance measurements.

c) The other possibility is that the 5-parameter model is inaccurate. Validation efforts have shown, however, that this model is accurate, at least for crystalline technologies, when correct inputs are supplied. Therefore, if there is a problem with the model, errors are more likely to occur consistently throughout a time period rather than randomly.

It is worth repeating that this procedure provides a logical framework to evaluate the quality of measured data and performance models. It is highly recommended that when differences are found between measured and predicted values, analysis is completed to determine the root cause of error, rather than simply rejecting the time period. Oftentimes the root cause is unexpected and may identify previously unknown sources of error (either in the input data or model implementation).

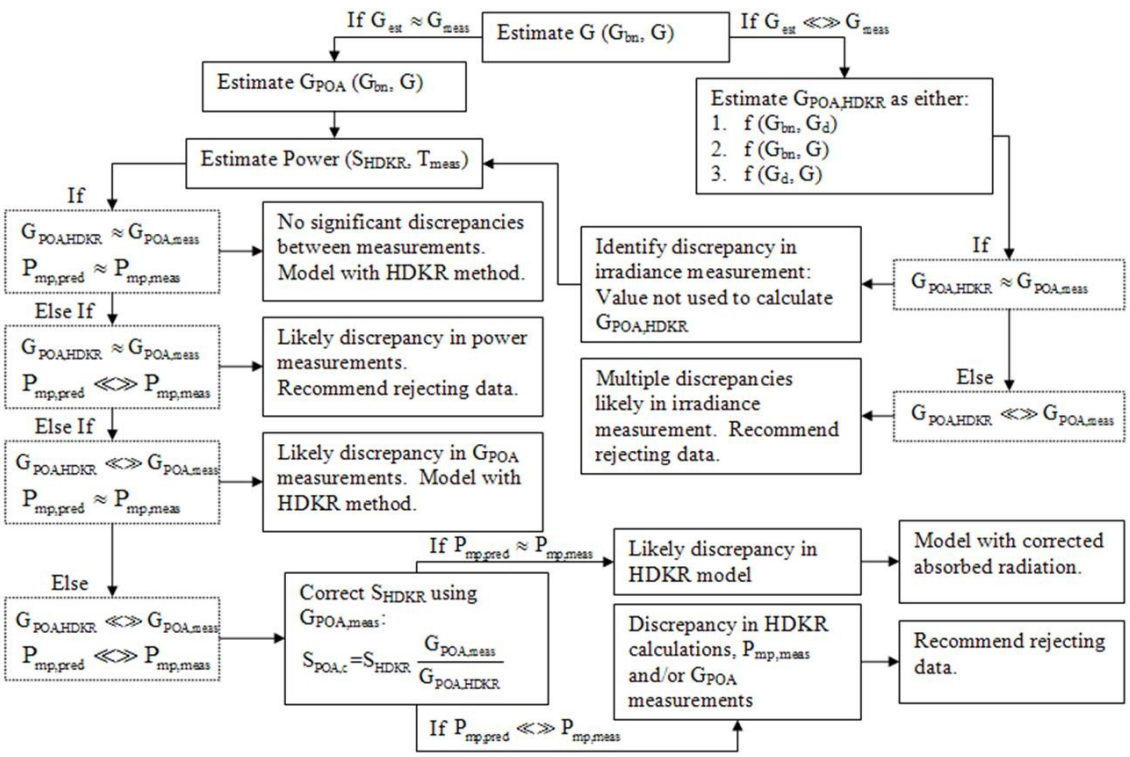

Figure 4.1: Flow chart to evaluate quality of input data and model.

4.5.2 Shading

Datasets for both the mono-Si and poly-Si modules were filtered for shading as recommended by NIST (Dougherty, 2010). The last hour of every day was removed from the HIT dataset because of shading concerns as recommended by NREL (Marion, 2009).

4.5.3 Cosine Effect on Pyranometer at NIST

As noted in Section 2.1, the vertical mounting of the modules causes a large mismatch of incidence angles between the module and the measurement devices. This mismatch may create uncertainties in irradiance calculations because the module may be receiving irradiance at a significantly lower incidence angle than the horizontal pyranometer and shaded pyranometer. In order to negate the impact of these uncertainties and focus on temperature and performance modeling errors, a filter was added to reject time periods that are characterized by zenith angles greater than 75° because larger angles were observed to exhibit higher uncertainties in the cosine response of pyranometers (Myers et al., 2002).

Monthly energy prediction errors (Equation (4.6)) were calculated with the 5-parameter and measured temperature for two datasets: one with the zenith angle filter and one without. As Table E.2Table E.2 in Appendix E shows, applying the zenith angle filter slightly reduces modeling errors in the winter months. This result is expected as the mismatch between incidence angles is highest during winter months for the datasets evaluated in this research. The zenith angle filter is applied in subsequent simulations.

$$\text{Energy Prediction Error} = \frac{\text{Total Energy Predicted}}{\text{Total Energy Measured}} \times 100\% \tag{4.6}$$

4.5.4 Maximum Power Point Tracking Error in NREL Dataset

Quality assurance calculations (detailed in Section 4.5.1) for the HIT dataset showed unusually large energy prediction errors for many days. For example, 33 days had errors

of over 20%. Further inspection of the data explains the most likely reason for these errors.

4.5.4.1 Data Inconsistencies

Data from March 15 were studied to explain the large energy prediction errors observed for that day. The DC power measurements for many time periods were unusually low considering the irradiance measurements were high – i.e. consistent with a clear, sunny day. During these periods, the measured voltage was higher and the measured current lower, compared to time periods experiencing similar irradiance measurements and expected power outputs. Figure 4.2 shows the calculated I-V curve, the calculated maximum power point, and the measured maximum power point for 12:28, March 15. While the measured maximum power point falls near the I-V curve (suggesting a fairly accurate absorbed radiation calculation and performance model), it is appreciably far from the calculated maximum power point. This variation suggests that an error existed in either locating the maximum power point by the tracker or the measurement of current and voltage at the point. Given that the AC power measurement is also low when the DC power is unusually low, it is likely the maximum power point tracker is the source of the errors.

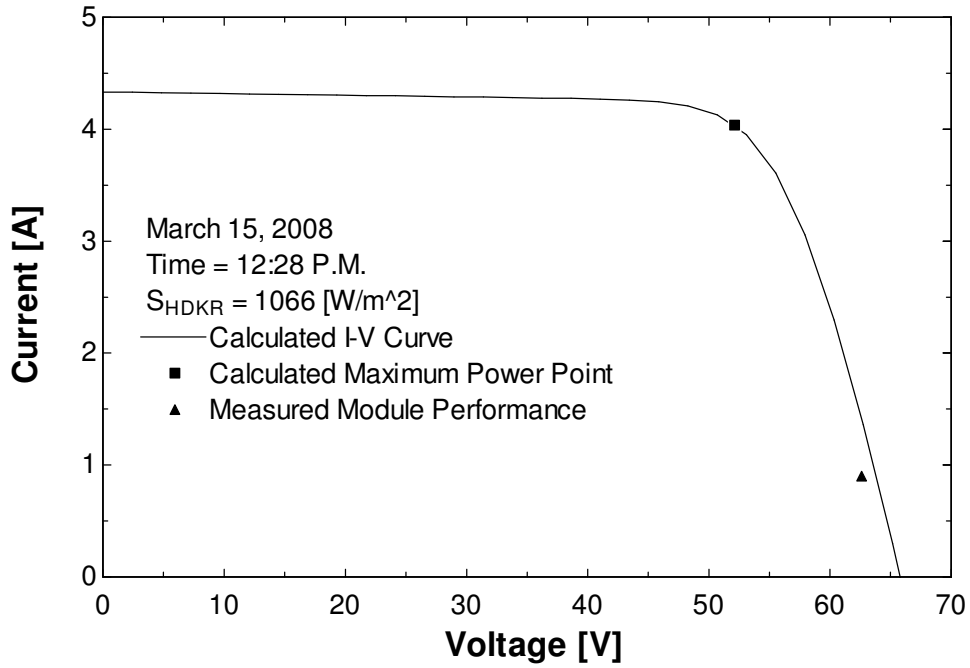

Figure 4.2: I-V curve for Sanyo module at NREL also comparing calculated and measured maximum power points.

At this point, it is necessary to develop a filter which will disregard time periods when the array was clearly not operating at the maximum power point. This filter must be developed carefully and logically, as deleting time periods that the model does not agree with could unfairly improve the model's results unless a strong case can be made for the deletion. Observations of suspicious data show that the measured voltage and current at maximum power tend to be near the steep linear portion of the I-V curve; in other words, the voltage is too high while the current is too low. The fact that the measured point is near the calculated curve suggests the current-voltage model is acceptable, and the problem is that the maximum power tracker is not functioning properly. The proposed filter compares the difference between the measured voltage and the calculated voltage at maximum power to the difference between the measured voltage and the voltage found from the calculated I-V curve at the measured current. If the measured voltage is much

closer to the I-V curve than it is to the calculated voltage, then the point will be rejected under the assumption that it corresponds to a maximum power point tracking error. The criterion for making this decision is as follows.

Figure 4.3 shows a schematic of the differences used to analyze the voltage and current measurements for each time period. These differences are used to calculate a ratio by applying Equation (4.7). If *r* is greater than 1.25, then the measured voltage is considered appreciably closer to a point on the I-V curve than the maximum power point, and the point was disregarded, as shown in Equation (4.9). Note that Equation (4.8) ensures that *y* has a minimum value of 1.6. This restriction ensures that if *x* is less than or equal to 2 volts, then the point will not be rejected.

$$r = \frac{x}{y} \tag{4.7}$$

$$y = \max\left[\mathrm{abs}\left(y_1\right), 1.6\right] \tag{4.8}$$

$$\text{disregard point if } r > 1.25 \tag{4.9}$$

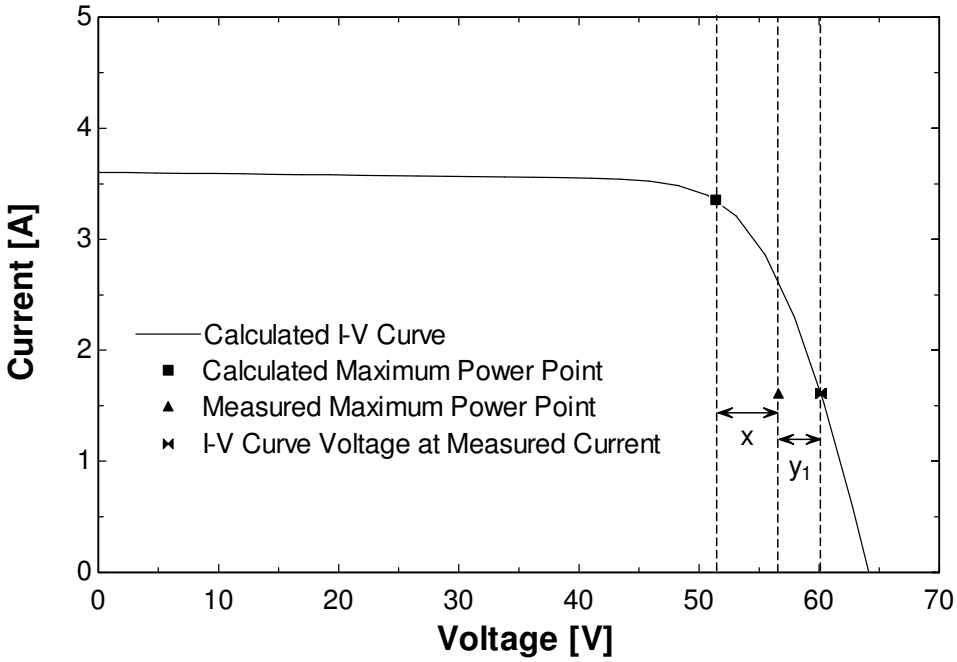

Figure 4.3: Schematic showing the differences used to find points with maximum power point tracking errors.

4.5.4.2 Comparative Results of Filtering Methods

The filtering method described in the previous section identified an additional 329 points to remove from the dataset. After this filter the dataset contained 12,473 points. The majority of these points occurred in January, February, and March. A complete listing of removed points is located in Table E.2 in Appendix E. A plot of *r* vs. *x* for the rejected points is also located in Figure E.1 in Appendix E and shows that while some rejected points are near the cutoff of 1.25, most are described by *r* values greater than 2. Simulation results found by applying the 5-parameter model with measured backside temperatures, absorbed radiation calculated using the HDKR model and 15 minute input data are shown in Figure 4.4. Results are included for the Basic and I-V Curve filtering methods described. Results for the three months suspected of faulty maximum power point tracking data show that combining the I-V Curve filter with the initial filter

significantly improves the results to expected values. For example, the prediction errors for January, February, and March are similar to the results for the remaining months when the I-V Curve filter is added. Based on these results, subsequent simulations were completed using the combination of both filters.

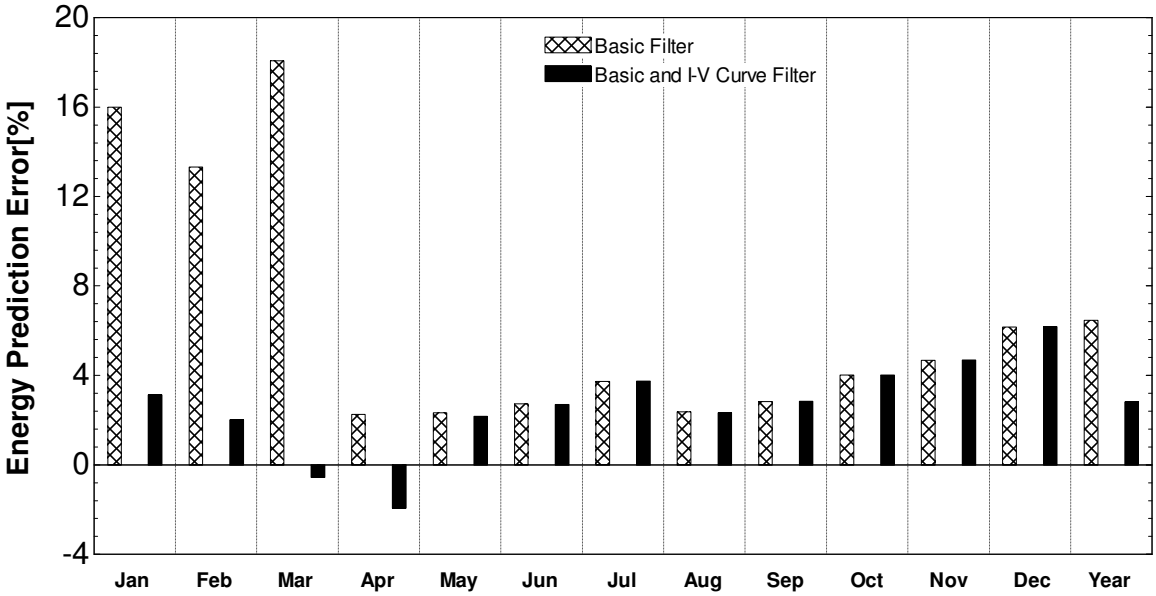

Figure 4.4: Energy prediction errors for the Sanyo array found by applying the 5-parameter model with measured backside temperatures, absorbed radiation calculated using the HDKR model and 15 minute input data.

4.6 Results

The annual simulation results for each module previously described in this report are shown in Figure 4.5. There are five simulation results for each module. Four results correspond to the steady state energy balance model described in Chapter 2 and earlier sections in this chapter and the three other cell temperature models presented. The last result applies the measured temperature in the five parameter model to predict module performance, which can be used to differentiate between the error created by the cell temperature model from the error inherent in the five parameter model. The Sandia and

NREL datasets provide backside temperature, which can be approximately 1°C lower than the cell temperature under high values of incident radiation. Therefore applying the backside temperature may results in a minor over prediction of power. Note that for all simulations, hourly input data (direct beam and horizontal diffuse) and calculated absorbed radiation (HDKR model) are applied. The wind speed adjustments described for each site are applied. The measured backside thermal resistance for the NIST modules is applied since the calculated values were shown to be inaccurate. Per the recommendations in Chapter 3, Equation (3.3) is applied to calculate the sky temperature for the rack mounted modules. Equation (3.2) is implemented for the NIST modules, because annual dew point data were not available. The EES (Klein, 2010) code used for these simulations and subsequent sensitivity studies is included in Appendix F.

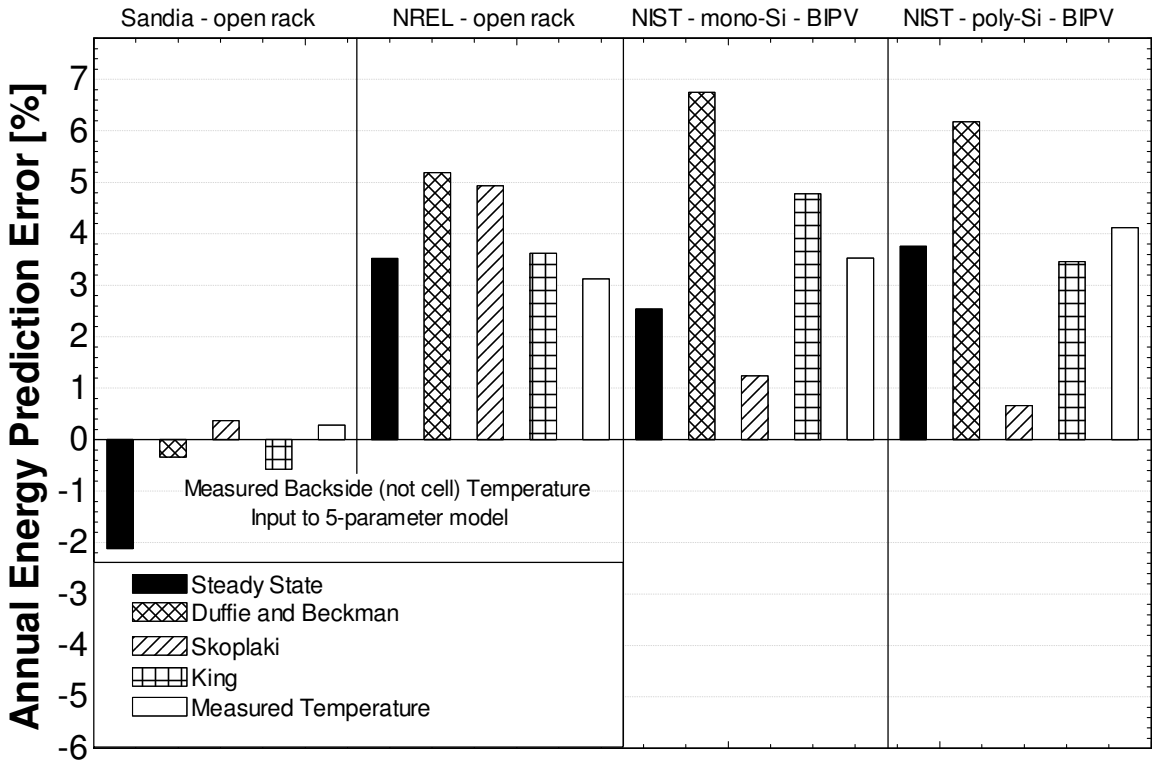

Figure 4.5: Annual energy prediction error for each module previously described. The datasets for each module were filtered as described in Section 4.5 and then integrated into hourly datasets.

A few important conclusions can be drawn from Figure 4.5. First for each combination of modules and cell temperature models, the energy prediction error is less than 7%. This error includes the effect of estimated absorbed radiation based on direct normal and horizontal diffuse measurements, which were documented by Sandia to have uncertainties of ±1% and ±7%, respectively. This ceiling suggests that, with the proper amount of information, a decent estimate of module performance can be made. When the results of the cell temperature models are compared to the results of the five parameter model applying measured temperature, the relative energy prediction error each combination of modules and cell temperature models is less than 3.5%.

The results of the racked mounted are especially interesting, as for both modules, the deviation between the cell temperature models is small. This consistency between models suggests that the cell temperature models will all produce similar results for all rack mounted modules. A comparison of results of the cell thermal models for both BIPV modules, however, shows large deviations between cell temperature models. The cause of this variation is explored in the following sections.

4.7 Sensitivity Study

At this point, a sensitivity study on the steady state energy balance model is beneficial because: (1) the results help determine the most important inputs to the model and (2) an analysis of possible values of module properties that are difficult to find (introducing possible uncertainties) help determine the range of acceptable values for these inputs. The results are displayed as the difference in annual energy predictions between the model adjusted by the sensitivity study and the baseline model used to produce the results in the previous sections. This difference is made into a percentage by normalizing by the measured energy, as detailed in Equation (3.6).

4.7.1 Cover Properties

Cover Thickness: This value may be provided by the manufacturer, although its absence from datasheets is not unusual. In each module studied to date, the cover material has been provided. The thickest glass cover encountered during this research was the 6 mm cover on the NIST mono-Si module. This cover also matches the thickest sheet of glass advertised in SolarPhire's (PPG Industries, Inc., 2008) brochure; for this reason 6 mm is set as the upper end of the range of possible cover thicknesses. The Sandia and NREL

modules have 3.2 mm glass covers, while the poly-Si module has a 0.05 mm ETFE cover. A minimum of 0.001 mm was set for the other end of the range to simulate a module without a cover.

The results of applying this range of cover thicknesses are shown in Figure 4.6 (each module is simulated for each of the two remaining cover options) and suggest that assuming an incorrect cover thickness can have a significant impact on the results of modules with non-traditional covers (thick glass or ETFE in this case). For example, assuming a 3.2 mm cover instead of a 6 mm cover for the mono-Si module leads to around a 2% difference in annual energy production. It should be noted, however, that these differences are affected by two separate functions of the cover: absorbing and reflecting incident radiation and elevating the cell temperature due to increased thermal resistance. Both of these effects combine to degrade the power produced. Evaluating a range of thermal conductivities helps determine which of these functions has the greatest impact on model predictions.

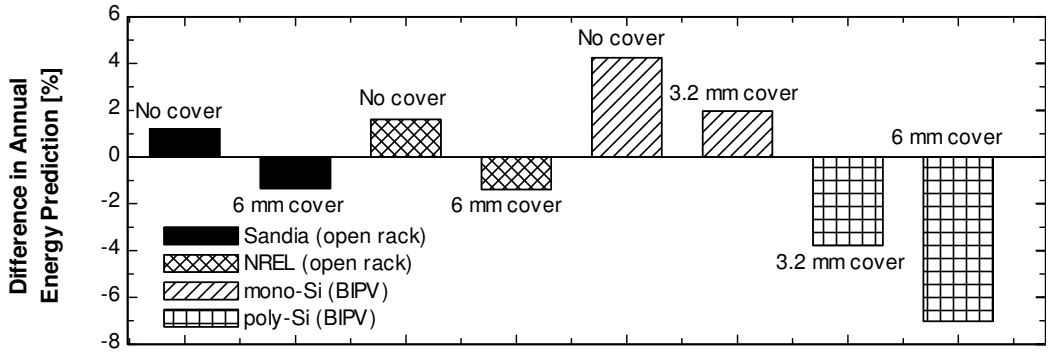

Figure 4.6: Sensitivity study on cover thickness.

<u>Cover Thermal Conductivity:</u> Assuming the cover material is known, thermal conductivity can be found from information provided by the the cover's manufacturer, or

from material property reference books. A sensitivity study was completed assuming a worst case scenario that the manufacturer of the glass is unknown and the latter technique is required to find the thermal conductivity. Bansal and Doremus (1986) provide thermal conductivity for a variety of glass compositions. Assuming that no information is available about the glass composition of the cover, a range of possible conductivities from 0.466 to 2.49 [W/m-K] can be developed from this information. Considering that the conductivity of the ETFE cover is 0.24 [W/m-K], however, this value will be set as the low value of the range.

The results of applying this range of thermal conductivities (with actual cover thicknesses) are shown in Figure 4.7 and do not show a significant impact in results, except in the case of the mono-Si module when the conductivity is decreased by a factor of five. This finding suggests that the thermal resistance of the cover is not significant because it is smaller than the resistance between the module and environmental conditions. For the mono-Si module with the low conductivity applied, the thermal resistance of the cover increases to a significant value, and therefore the impact on the results is greater.

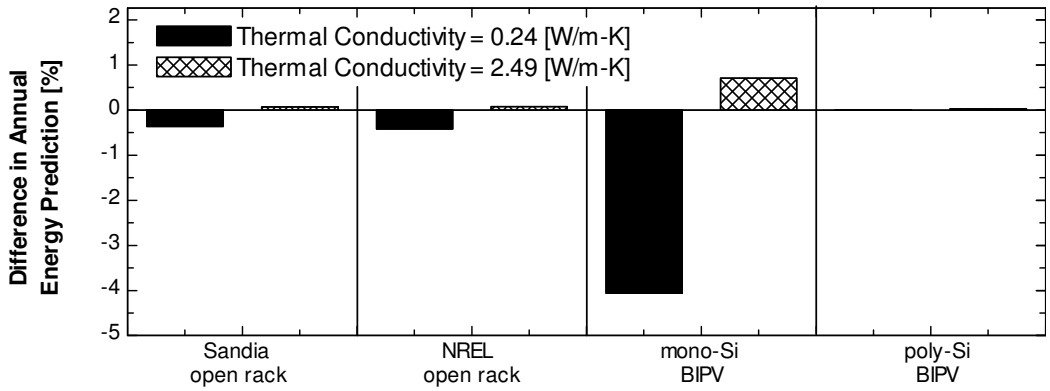

Figure 4.7: Sensitivity study on thermal conductivity

Spatially Uniform Module Temperature: The previous study of cover thermal conductivities suggests that cover thickness is only important in absorbed radiation calculations and not as a thermal resistance between the cell temperature and environmental conditions. Additionally, Chapter 3 discussed the inaccuracies of the backside thermal resistance. Previous sensitivity studies also found low model sensitivity to the backside thermal resistance. For these reasons, a simulation was completed assuming uniform module temperature rather than a temperature gradient between the cell and each end. The BIPV modules were assumed to be backside insulated.

The results of simulating each module assuming a uniform module temperature are shown in Figure 4.8 and suggest that the assumption of uniform module temperature causes less than 1% difference in annual energy production for each module studied. Since backside resistance values are difficult to calculate, this difference caused by assuming a uniform temperature can most likely be tolerated. Another more accurate solution may be to add some temperature difference, ΔT, to the calculated uniform temperature. This temperature difference could then be modified based on mounting and incident radiation, similar to the equation proposed by King et al. (2004).

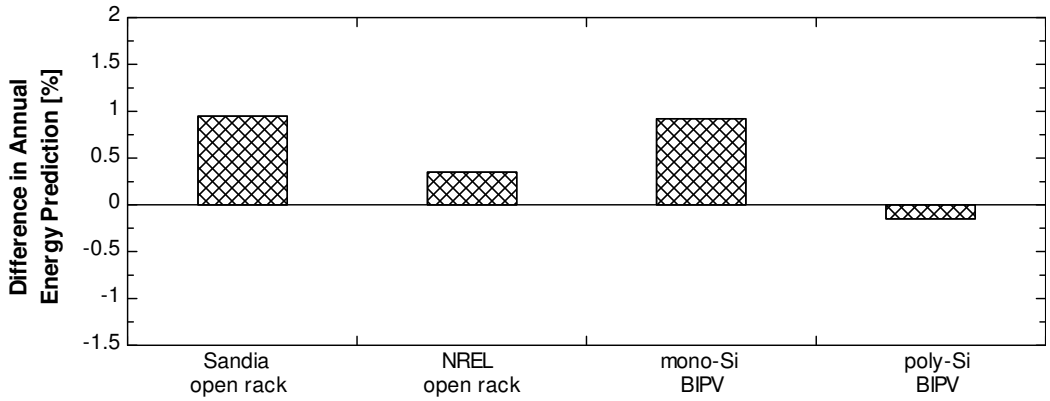

Figure 4.8: Sensitivity study on uniform module temperature.

Cover (Long-Wave) Emissivity: Similar to thermal conductivity, assuming the cover material is known, the emissivity can be found through either the cover's manufacturer's data, if known, or in material property reference books. The published emissivity of photovoltaic glass is typically 0.84 (PPG Industries, Inc., 2008). Bejan and Kraus (2003) provide a range of glass emissivities from 0.88 to 0.95. Since these values are greater than the published emissivity, a value of 1 is used as a worst case for the sensitivity study. Since the emissivity of the ETFE cover has been approximated as 1, the value of a typical glass cover (0.84) is applied for the sensitivity study.

The results of simulating each module with an incorrect emissivity are shown in Figure 4.9 and suggest that the effect of an inaccurate value of emissivity results in an error of less that 2% of the annual energy productions. The error, however, is much more significant for BIPV mounted modules (mono-Si and poly-Si) than for open rack modules. Following studies in this section will also display the trend of changes in inputs affecting heat transfer rates between the module and environment having a greater effect on BIPV simulation results. The cause of this disparity between mountings was described in Section 3.4.3.

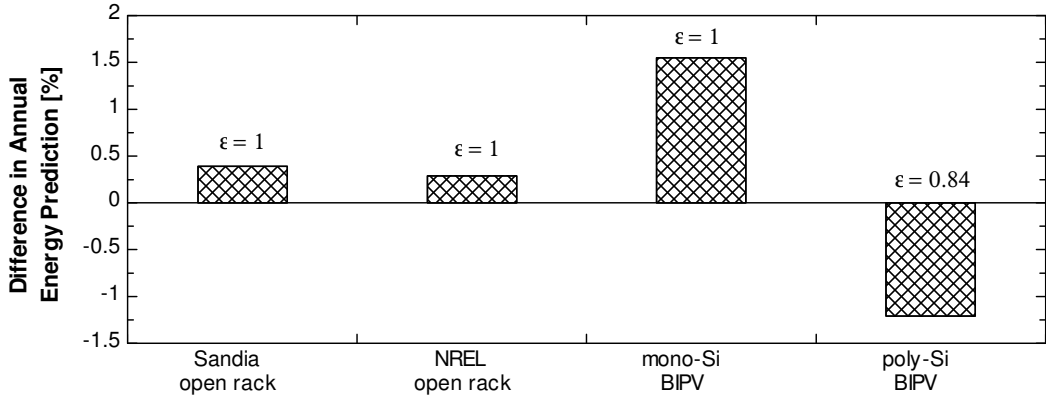

Figure 4.9: Sensitivity study on cover emissivity.

4.7.2 Dimensioning

Characteristic Length: This value is used in the Reynolds number equations, which is then used in heat transfer correlations. A representative characteristic length has been calculated by Equation (2.10) as the product of 4 times the area divided by the perimeter was found in previous reports to be accurate. While this observation is directly applicable for single module arrays, arrays consisting of multiple modules separated by some distance, however, complicate the definition of length (L) and width (W). This complication arises from the distance between the modules. Considering an infinitesimally small distance, the modules basically form one larger module. Considering a much larger distance, each module can be treated as thermally independent. Unfortunately, the cut-off distance between thermally treating the array as one large module or multiple separate modules is ambiguous.

The NREL modules (like all previously studied modules) were assumed thermally independent (Equation (2.10)) due to the gap between the modules in the array. A sensitivity study is completed to evaluate the steady state energy balance model assuming multiple modules in an array were thermally dependent and therefore treated as one larger module. The characteristic length in this case is calculated using Equation (4.10). Results of a simulation completed applying this new characteristic length show a -1.60% difference in annual energy prediction error for the NREL system. The sign of this error makes sense, as temperature will increase with larger characteristic lengths, causing a decrease in predicted energy output. The mono-Si and poly-Si systems consist of a single module, and the modules in the Sandia system are spaced by approximately one meter. Therefore these systems should not be characterized as a larger array.

$$L_{char,array} = \frac{4 \bullet L_{panel} \bullet \#_{panels\ in\ length\ direction} \bullet W_{panel} \bullet \#_{panels\ in\ width\ direction}}{Perimeter_{array}} \tag{4.10}$$

4.7.3 Backside Properties

Module Backside Emissivity: A value of 0.7 is currently applied in the model. Module backsheets are sometimes laminated. For example, NIST reports a mylar-tedlar backsheet. Tedlar (DuPont™, 2009) reports a solar reflectance of 69%. Reflectance of long-wave radiation is not reported. Assuming that long-wave radiation is reflected similarly, the emissivity of a backsheet could be as low as 0.3. Therefore the lower end of the range of emissivities studied is 0.3 while the upper end is set to the physical limit of 1. Results (Figure 4.10) of simulations show that this range of emissivities only causes a ±0.3% change in annual energy prediction error. Note that this input only applies to open rack modules.

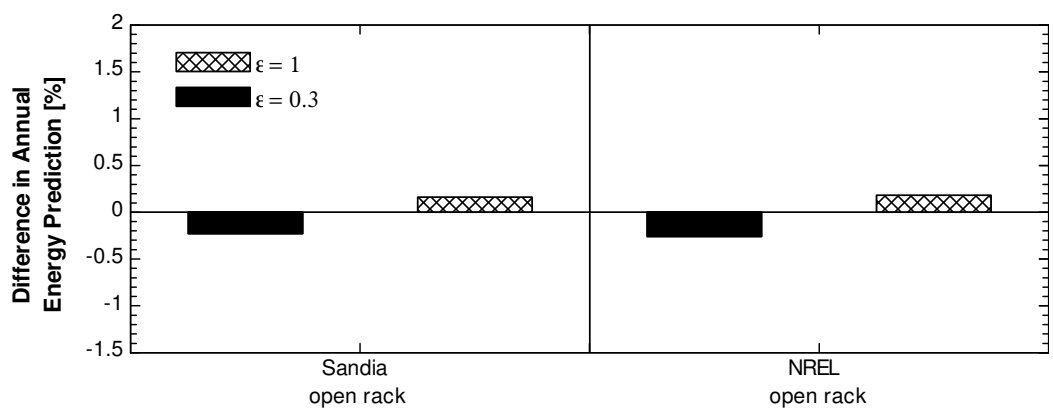

Figure 4.10: Sensitivity study on module backside emissivity.

4.7.4 Weather Inputs

Wind Speed (Possible Geographical Uncertainty): Previous validation efforts for the BIPV systems showed that the wind speed at the building wall was difficult to predict from wind speed measurements taken at the roof of the building. It follows that the wind

speed provided in TMY files may not be correct for each simulation location it is applied to. A sensitivity study is completed to determine the effects of incorrectly estimating wind speed. The results, found in Figure 4.11, show that incorrectly predicting the wind speed can have a large effect on results. This effect is not unexpected as forced convection is an important contributor of heat rejection. The results also show that the same change to wind speeds for the BIPV modules has a larger effect. This observation is explained in Section 3.4.3.

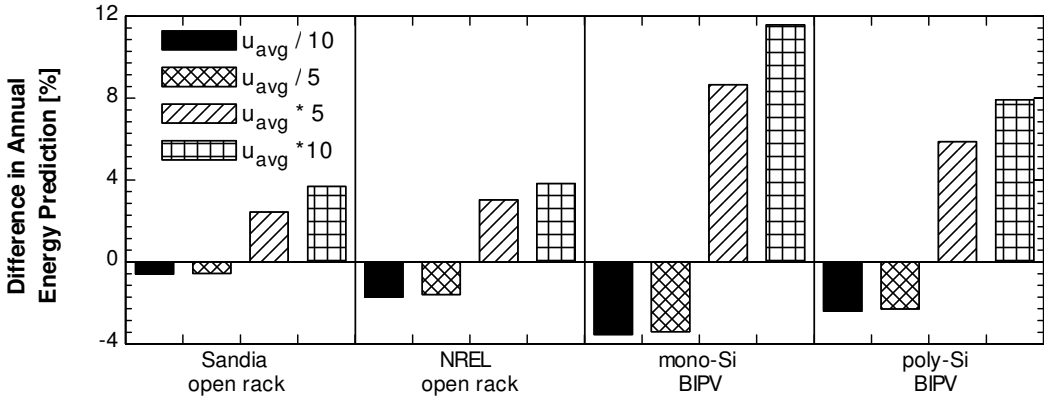

Figure 4.11: Sensitivity study on wind speed.

Ground Temperature: The ground temperature is required for the model because the module will radiate to the ground. Previous simulations assumed a ground temperature equal to the ambient temperature. This formula is simple and has the potential to be developed into more complex, and possibly more accurate predictor of ground temperature. A sensitivity study is completed to determine the impact of an assumed constant error in the ground temperature input. A range of ±10°C is studied, and the results are shown in Figure 4.12. The results show that for the applied range of values, the impact on the BIPV model is around 1% and more significant than the impact on the open rack model. A study of ground temperature models may lead to improvement or

less uncertainty in this model. It is important to note that the impact of uncertainty in ground temperature would decrease for BIPV modules mounted at tilt angles closer to horizontal (due to decreased view factors between the module and ground).

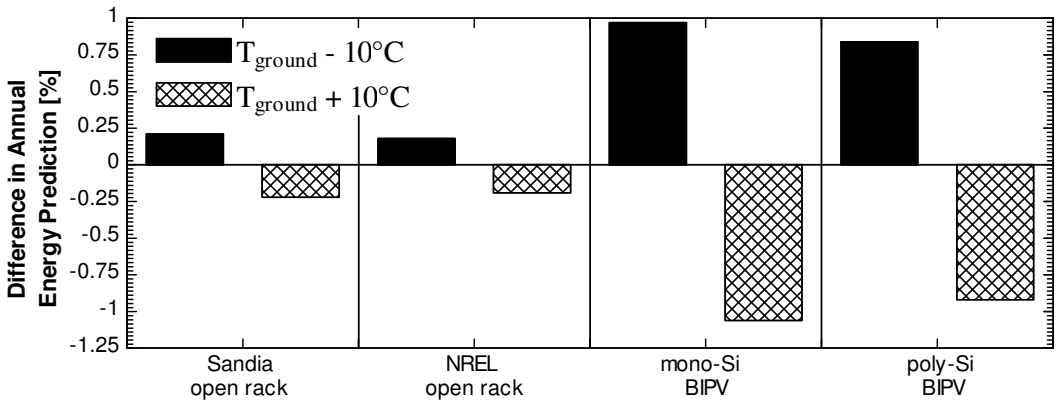

Figure 4.12: Sensitivity study on ground temperature.

<u>Sky Temperature:</u> A sky temperature is required for the model because the module cover also radiates to the sky. Current simulations apply either Equation (3.2) or Equation (3.3) to predict the sky temperature for the open rack and BIPV modules, respectively. A sensitivity study is completed to determine the impact of an assumed constant error in the sky temperature input. A range of ±5°C is studied. The results in Figure 7 show that for the applied range of values, the impact on the models for all of the modules is less than ±0.5%. This impact would increase, however, for backside insulated modules mounted at tilt angles closer to horizontal (due to increased view factors between the module and sky).

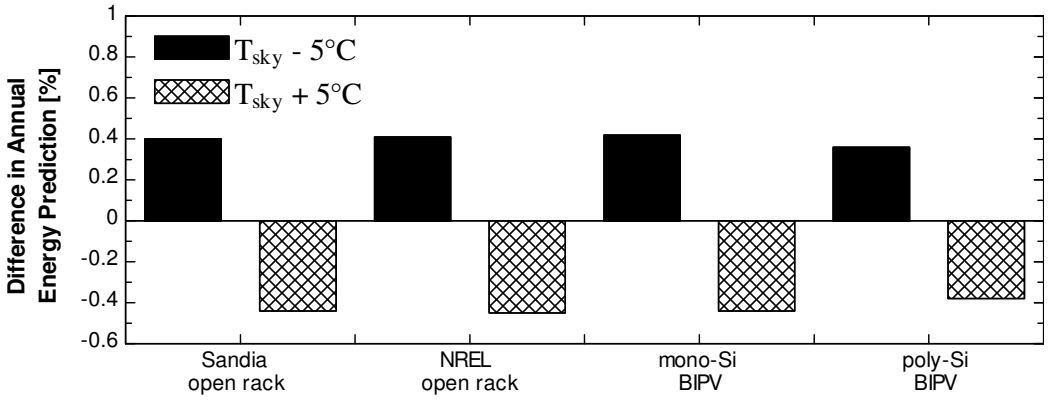

Figure 4.13: Sensitivity study on sky temperature.

Atmospheric Pressure: This has been held constant at 1 atmosphere. Atmospheric pressure varies with altitude, however, which may affect heat transfer rates for the Sandia and NREL modules. Therefore a simulation is completed with an atmospheric pressure of 0.8 atmospheres for these two modules. Results of this simulation show a difference of -0.62%. This effect is due to a decrease in the density of air at lower pressures, which causes a decrease in the Reynolds, Prandtl, and Grashof numbers. These decreases result in smaller forced and free heat transfer coefficients. Although depending on required level of uncertainty atmospheric pressure may be not critical, it is easy to adjust for based on altitude; therefore, altitude will be an input to future models.

4.7.5 Module Mounting and Surroundings

View Factors: View factor calculations are detailed in Section 3.1.3. In all practical cases, the assumption in this section that the ground is an infinite horizontal plane with respect to the module will be somewhat incorrect since the ground extending in front of the module can feature different terrains and constructions. Therefore it is possible that the true view factors between the module and the sky and ground, respectively, may be different than the value calculated. For this sensitivity study, the view factor between the

module and the ground is increased by 0.1 and 0.2 to simulate potential obstacles near the module that may increase the view factor from the module to the ground temperature. Results of this study are shown in Figure 4.14 and show that the range of view factors studied only causes a maximum difference of -0.6%. It is also important to note that, similar to some previous results, the difference for the BIPV modules is significantly larger than for the open rack modules.

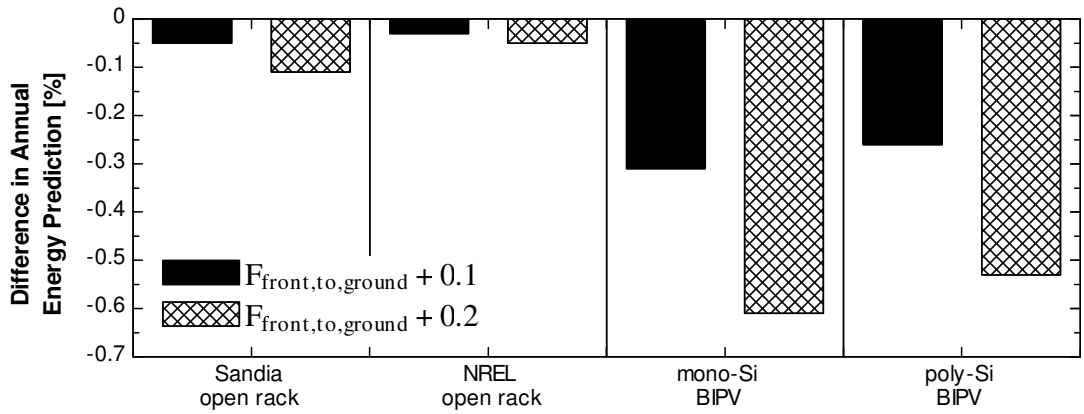

Figure 4.14: Sensitivity study on view factors

4.7.6 Modifications to Steady State Energy Balance Model Based on Sensitivity Study

The findings of the sensitivity study suggest that a steady state energy balance developed up to this point can be simplified to assume the entire module is at a uniform, time-dependent temperature. This simplification is important because it negates the need to predict thermal resistances.

The findings also suggest the use of a location specific atmospheric pressure. Fortunately this value is available in TMY datasets.

Simulations results updated to reflect the findings of the sensitivity study are shown in Figure 4.15.

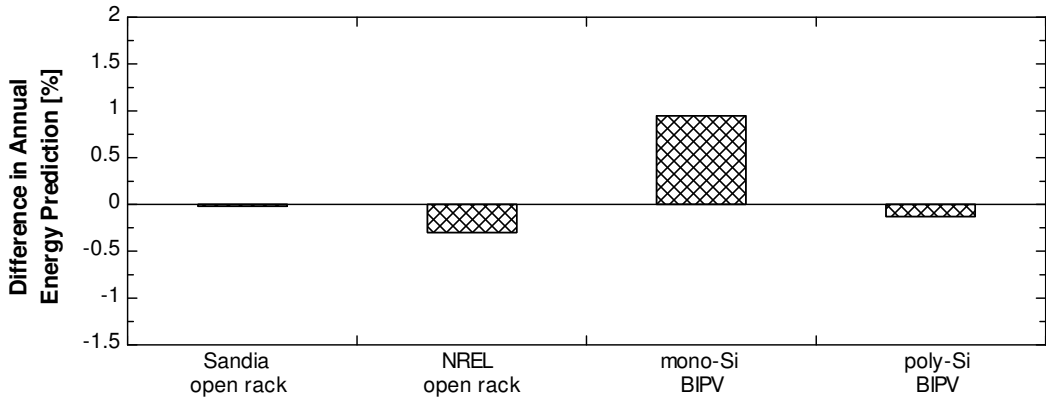

Figure 4.15: Sensitivity study accounting for lumped steady state energy balance model and location specific atmospheric pressure.

4.8 The Effect of Adjusting Wind Speed with Respect to Difference between Measurement and Module Heights

The sensitivity study in Section 4.7.4 showed that wind speed is an important input to the steady state energy balance model. The previous sections detailed the adjustment of wind speed with respect to the difference between measurement and module heights. The correct magnitude of this adjustment is unclear, so it is interesting to simulate the models again without adjusting the wind speed input. Figure 4.16 shows results of simulations that do not adjust wind speed for height. Note that the modified (uniform temperature, location specific pressure) steady state energy balance detailed in the previous section was applied. Therefore the results for the steady state energy balance and Duffie and Beckman models change for the Sandia module and the Skoplaki and King models change for the NREL module. The results show that using the measured wind speed (either at the module or at the free stream height) tends to improve the results of all of the cell temperature models except the Duffie and Beckman model. The actual difference

between the wind speed measured at the module and the free stream is unknown for each module, so the correct adjustment can not be specified. This analysis does provide insight into the slight differences between the results of the cell temperature models for rack mounted modules.

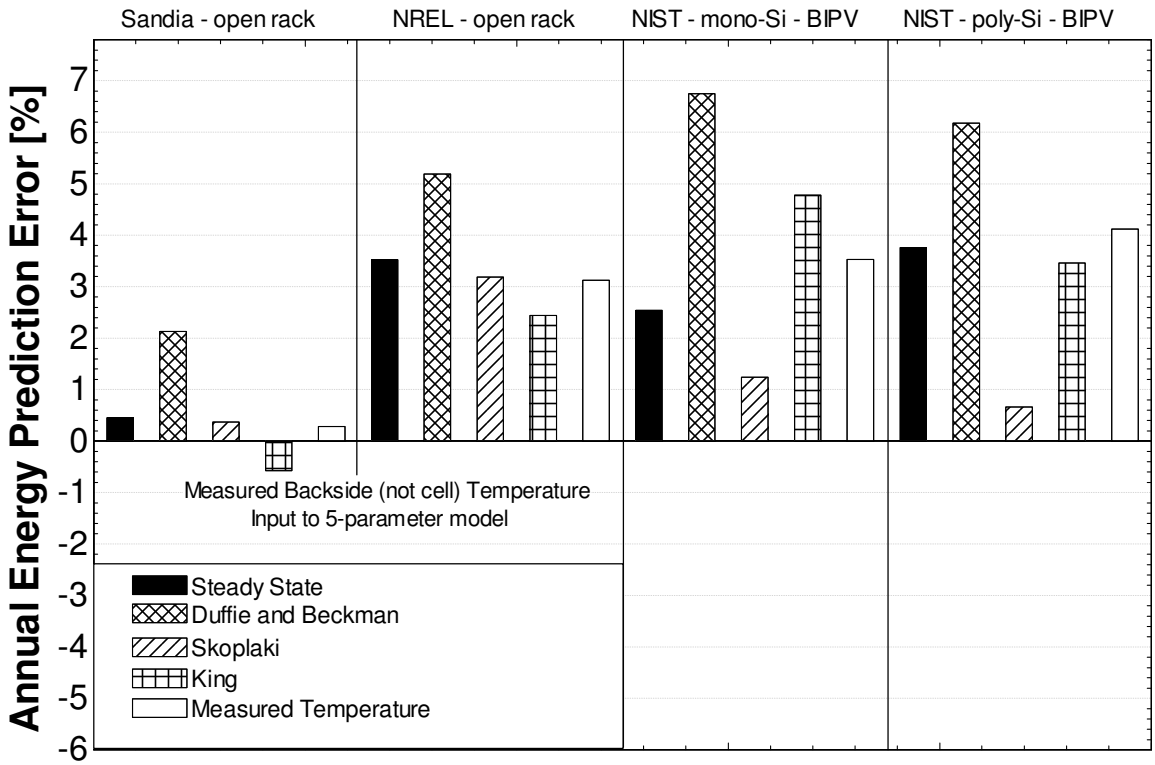

Figure 4.16: Annual energy prediction error for the modified steady state energy balance. Wind speed is not adjusted for measurement height.

4.9 Effect of Inaccurate NOCT Measurements on the Duffie and Beckman Cell Temperature Model

Results in Section 4.6 noted the variability between different cell temperature models for the BIPV modules, which can also be observed in Figure 4.16. It is possible that this variability is due to the suggestion in Chapter 3 that the NOCT was more difficult to measure under BIPV mounting conditions. Table 4.3 shows the NOCTs corresponding to the Skoplaki, Duffie and Beckman, and steady state energy balance cell temperature

models, respectively, for each module. Recall that a NOCT value is inherent in the Skoplaki model and adjustable by the mounting coefficient, the reported NOCT is an input to the Duffie and Beckman model, and the NOCT model (similar to steady state energy balance) can be used to predict a NOCT value (note that a uniform temperature NOCT model must be used for the Sandia and NREL modules as the materials are not known). Table 4.3 shows that there is less variability between these NOCT values for rack mounted modules than there is for the BIPV modules. This observed variability of NOCT values for BIPV conditions supports the previous hypothesis that the NOCT values are more difficult to measure under BIPV conditions.

Table 4.3: Comparison of NOCT values used by the Skoplaki, Duffie and Beckman, and steady state energy balance temperature models.

	Open Rack - Sandia	Open Rack - NREL	BIPV (mono-Si)	BIPV (poly-Si)
Assumed NOCT (Skoplaki) [C]	47	47	85	85
Reported NOCT (Duffie and Beckman) [C]	46	44	67	62
Predicted NOCT (NOCT Model) [C][1]	50	50	77	70
Standard Deviation [C]	**2.1**	**2.9**	**9.0**	**11.4**

[1] Uniform module temperature is applied for the Sandia and NREL modules

With this information on NOCT values, it is worthwhile to revisit the difference between the energy prediction results from the cell temperature model and results applying measured temperature. For the open rack modules, characterized by low variability between NOCT inputs, all results are within 2.5% of results found by applying the measured temperature and also within 2.5% of the results from the other cell temperature models. These results suggest that a relatively simple cell temperature model (Skoplaki or Duffie and Beckman) will typically be accurate within this range. For the BIPV modules, which are characterized by high variability between NOCT inputs, results from the cell temperature model begin to differ from the results found by applying the

measured temperature and the results from the other cell temperature models. Additionally, the difference between the NOCT applied by the model and the predicted NOCT in Table 4.3 identifies the sign of the difference between the results from the Skoplaki and Duffie and Beckman cell temperature models and the results found by applying the measured temperature. For example, the Skoplaki model assumed a BIPV NOCT of 85°C, which is the highest NOCT listed in the table. The results found by applying the Skoplaki model under-predicted performance relative to the results found by applying measured temperature, suggesting the Skoplaki model was over-predicting temperature. Comparatively, the Duffie and Beckman model assumed the lowest BIPV and over-predicts performance, suggesting it under-predicts temperature.

Given this finding, it is interesting to revisit the performance of the Duffie and Beckman cell temperature model when a more accurate NOCT is applied. Figure 4.17 shows the results of the Duffie and Beckman cell temperature model applying the NOCT predicted by the NOCT model. When the predicted NOCT is applied to the Duffie and Beckman model, the results found by applying that model are improved in the BIPV case, and the accuracy is similar to the original results in the open rack case. It should be noted that this approach assumes that the predicted NOCT is more accurate than the measured and assumed NOCT values, at least for BIPV modules. This finding suggests that with proper NOCT inputs, simple cell temperature models may be accurate for some BIPV installations.

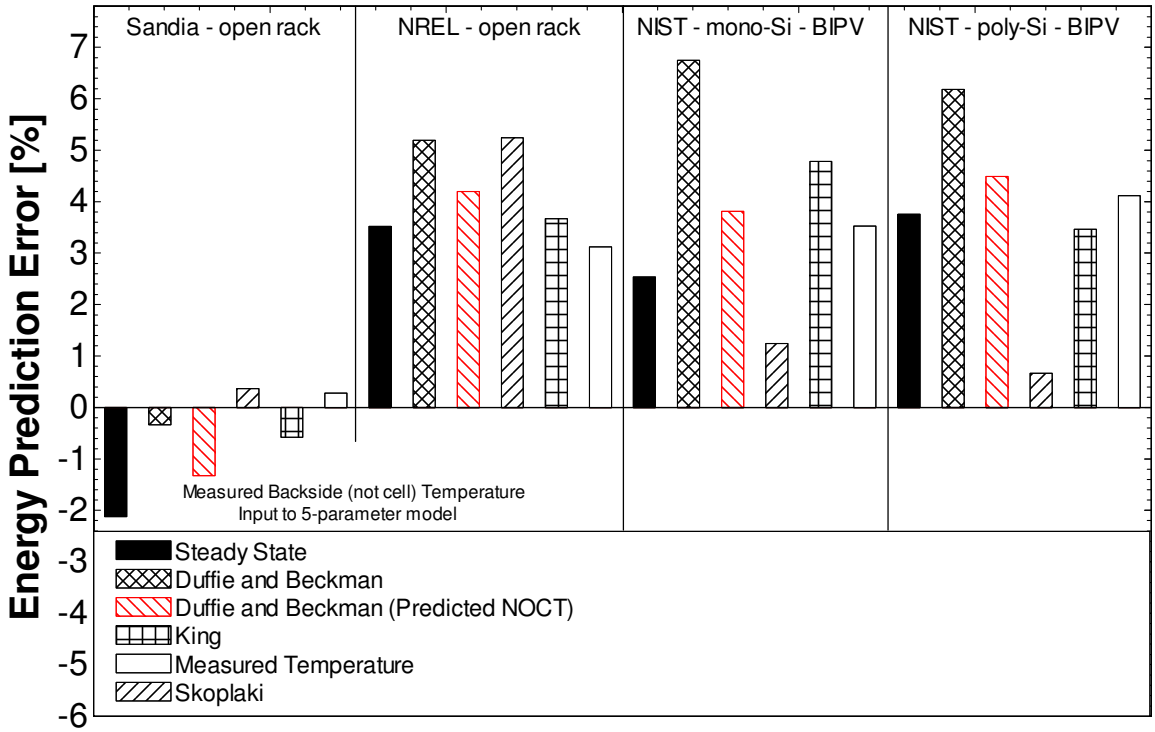

Figure 4.17: Annual energy prediction error for the modified steady state energy balance. The Duffie and Beckman model applies NOCTs (Table 4.3) predicted by the NOCT model in Chapter 3.

4.10 Summary

This chapter developed the steady state energy balance model for rack mounted modules. Three additional cell temperature models commonly cited in literature were also introduced. Then two rack mounted modules and datasets were described. A filtering procedure to provide consistency between datasets was introduced. Annual simulation results applying hourly data were presented for each combination of modules and cell temperature models and showed that all of the cell temperature models were within 7% of the measured annual energy. All cell temperature models were within 3.5% when compared to the results of the five parameter model applying measured temperature. Greater variability between cell temperature models was observed for the BIPV modules. This variability in results was attributed to variability in the NOCT inputs of different cell

temperature models. A sensitivity study was completed that suggested the steady state energy balance model can assume uniform module temperature and location specific atmospheric pressure without a significant loss of accuracy.

The sensitivity study also found that using array rather than module dimensions to calculate characteristic length used in heat transfer correlations has a significant effect. Finally, the study found that not adjusting wind speed for measurement height for the rack mounted modules improved all cell temperature models except the Duffie and Beckman model. Both of these findings will require additional research to be fully resolved.

At this point, the steady state energy balance model has been developed and validated for BIPV and rack mounted modules. Additionally, the results of the steady state energy balance have been at least as accurate as the other cell temperature models studied. The steady state energy balance model potentially adds value to the existing library of cell temperature models because it is highly adaptable to various mounting specifications, does not require the reported NOCT, and only requires data found on the manufacturers datasheet. The next chapter will focus on developing the steady state energy balance model for various building and rooftop mounting configurations.

5. Development of Model for Roof and Wall Mounted Modules

The previous chapter adapted the steady state energy balance model to rack mounted modules and showed annual simulation results for two rack mounted and two BIPV modules applying the developed steady state energy balance and three other cell temperature models. The results showed that the steady state energy balance model is overall as least as accurate as the other models evaluated for the rack mounted modules and more accurate than the Duffie and Beckman and Skoplaki models for BIPV modules studied. Therefore, since the steady state energy balance model is developed from accepted heat transfer correlations rather than empirical formulates, it can be adapted to various mounting configurations that are not as easily accounted for with the other models. The hope is that this model will help a user specify the most efficient mounting configuration.

PV modules are often mounted on the roofs of residences and commercial buildings. Many studies have been completed in the past decade that have focused on specific aspects of modeling roof and wall mounted modules (for example: Mittelman et. al., 2009, Gan, 2009, and Brinkworth et. al., 2000). None of the studies currently examined, however, are completely adaptable to a variety of mounting and weather conditions. An attempt is made here to develop a first approximation of an adaptable model by applying limiting assumptions to inherently complex calculations. Future research will be needed to determine the accuracy and robustness of this model as validation data are lacking.

Roof mounted modules can be generally grouped into four different mounting configurations: (1) integrated (2) flush, (3) gap, and (4) rack. Models characterizing each

of these mounting configurations are further described below. For each configuration, except the integrated mounting configuration, the roof temperature is required. Accurately determining the roof temperature is nontrivial, as many factors contribute to the roof temperature (e.g., thermal resistance and capacity of roof, interaction with outdoor environment, and interaction with attic). Therefore, due to lack of experimental data, simplifying assumptions must be made in order to estimate a roof temperature. The models discussed below assume that the roof is well insulated and independent of the attic temperature. In general this assumption calculates a higher roof temperature that allows less heat transfer from the backside of the module. Therefore this assumption is conservative in terms of calculated PV performance. The temperature of the roof under this assumption is calculated by an energy balance. In order to simplify the model, it is assumed that the roof underneath the module does not interact with the "uncovered" area of the roof. Then the inputs to this energy balance are dependent on the conditions experienced by the portion of the roof underneath the module.

A few other simplifying assumptions are required:

- The edges of the modules are assumed adiabatic.
- The module remains parallel to the slope of the roof for all mounting configurations except the open rack mounting.

The temperature calculations for the PV module for each mounting configuration are presented in the following sections.

5.1 Integrated Mounting Configuration

An integrated mounting configuration refers to modules that are integrated into the structure such that the backside of the module is directly in contact with the attic environment. Figure 5.1 shows an example of this configuration. Assuming the attic temperature is known, the steady state energy balance model can be applied to these mountings. The backside heat transfer is described by the tilted plate free convection heat transfer correlation applied in the rack mounted model and radiative heat transfer.

Figure 5.1: Example of an integrated mounting configuration (Philadelphia Solar, 2009).

5.2 Flush Mounting Configuration

A flush mounting configuration refers to modules with backsides directly in contact with the roof. The backside of a module for this mounting, by definition, will not experience free convection heat transfer with the ambient air. Residential modules such as PV shingles and tiles are examples of this configuration (Figure 5.2). The steady state energy balance model applied to the NIST modules can be applied to a flush mounted module with an assumption that the backside of the module is adiabatic.

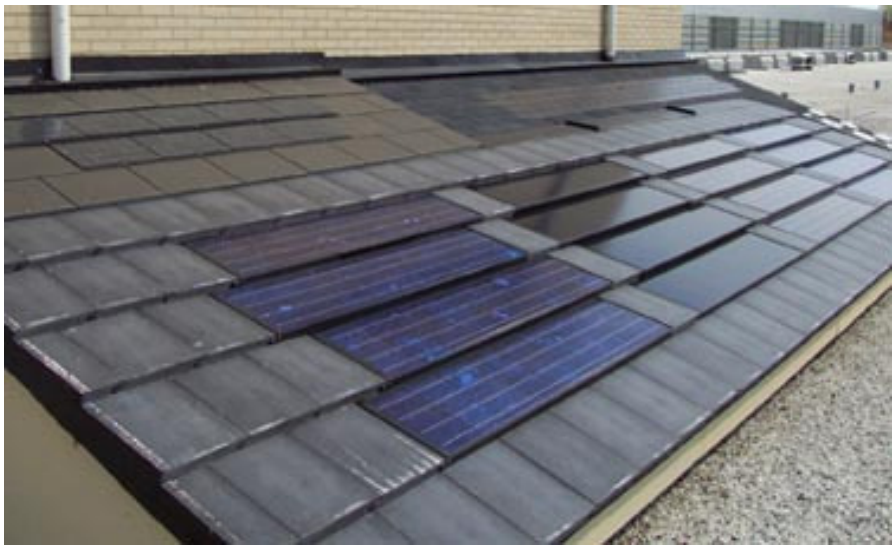

Figure 5.2: Example of flush mountings configurations (NIST, 2006).

5.3 Gap Mounting Configuration

A gap mounting configuration refers to modules that are separated from the roof by a gap or channel. At some point in the channel, thermal boundary layers on both sides of the channel intersect. After this intersection, the temperature of the air flowing through the gap becomes greater than the ambient temperature, thereby decreasing the heat transfer from the backside of the module. If the ratio of gap width (distance between module and roof) to module height (distance between gutter end and ridge end of module) is less than one (this ratio (*R*) is defined by Equation (5.1)), channel flow is assumed to be significant and the module is considered gap mounted. Once the module is mounted at a distance such that the thermal boundary from the module and the thermal boundary from the roof do not intersect (where *R* is greater than one), the module is treated as if it were simply an open rack module mounted on the roof.

$$\mathrm{R} = \frac{\text{gap width}}{\text{module height}} \tag{5.1}$$

The heat transfer from the backside of the module for the gap mounting may be affected by both convection (free and forced) and radiation. In addition to the roof temperature assumption, the mounting structures supporting the module create additional modeling difficulties by impeding free or forced convection, depending on the structure. This analysis will consider three different types of mounting structures:

5.3.1 Mounting Structures Are Parallel to the Ridge of the Roof

Figure 5.3 shows an example of this orientation. These structures will impede free convection and forced convection from perpendicular winds while accommodating forced convection from parallel (with respect to the mounting structure) winds. In this case, free convection will be neglected, leaving only forced convection and radiative heat transfer. The wind speed through the structure is estimated by projecting the wind speed to the line parallel to the mounting structure. For example, if the angle between the wind direction and the ridge of the roof is γ and the measured wind speed is u_{meas}, then the wind speed through the channel is calculated by Equation.(5.2). The Nusselt number for turbulent forced convection in the channel (uniform temperature) is calculated by Equation (5.3) (Nellis and Klein, 2009). The friction factor in this equation can be solved with Equation (5.4), where e represents the roughness of the channel and D_h represents the hydraulic diameter and is solved by Equation (5.5). The roughness is estimated as 5 mm.

$$u_{channel} = u_{meas}\text{abs}\left(\cos\left(\lambda\right)\right) \tag{5.2}$$

$$\overline{Nu} = \frac{\frac{f_{fd}}{8}\left(\mathrm{Re}-1000\right)\mathrm{Pr}}{1+12.7\left(\mathrm{Pr}^{\frac{2}{3}}-1\right)\sqrt{\frac{f_{fd}}{8}}}\left(1+\left(\frac{L}{D_h}\right)^{-0.7}\right) \tag{5.3}$$

$$f_{fd} = \left\{-2.0\log_{10}\left[\frac{2e}{7.54D_h}-\frac{5.02}{\mathrm{Re}}\log_{10}\left(\frac{2e}{7.54D_h}+\frac{13}{\mathrm{Re}}\right)\right]\right\}^{-2} \tag{5.4}$$

$$D_h = \frac{4Area}{Perimeter} \tag{5.5}$$

Figure 5.3: Example of mounting structure oriented parallel to ridge of roof (South Ayrshire Council, 2010).

5.3.2 Mounting Structures Are Perpendicular to the Ridge of the Roof

Figure 5.4 shows an example of this orientation. Such structures will accommodate free convection and also forced convection from parallel winds while impeding forced convection from perpendicular winds. The wind speed through the channel is calculated by Equation (5.2) where γ is now the angle between the wind direction and a line perpendicular to the ridge of the roof.

The free convection heat transfer for a vertical channel is predicted by the Equation (5.6) (Nellis and Klein, 2009), where the Rayleigh number is calculated by Equation (5.7),

$$\overline{Nu} = \frac{Ra}{24}\frac{S}{L}\left[1-\exp\left(\frac{-35}{Ra}\frac{L}{S}\right)\right]^{0.75} \tag{5.6}$$

$$Ra = \frac{gS^3\beta\left(T_s - T_{amb}\right)}{\upsilon\alpha} \tag{5.7}$$

where S is the width of the channel, and L is the length of the channel (in the direction of free convection). These equations are developed for a situation where both sides of the channel are at the same temperature (T_s). To adapt to the situation where each side is at a different, above ambient, temperature, the temperature input to the Rayleigh number is calculated by Equation (5.8).

$$T_s = \frac{T_1 + T_2}{2} \tag{5.8}$$

Finally, to adjust this correlation for a channel inclined θ degrees from horizontal, the technique used in Nellis and Klein (2009) to calculate the heat transfer of an inclined plate is replicated. Therefore, the gravity vector is adjusted by Equation (5.9).

$$g = 9.81\,\mathrm{MAX}\left[0.1, \sin\left(\theta\right)\right] \tag{5.9}$$

The forced convection is calculated in the same technique presented in for the mounting structures parallel to the ridge. Free and forced convection coefficients will then be combined by the correlation used in previous models, shown in Equation (5.10).

$$\overline{h}_{total} = \sqrt[3]{\left(\overline{h}_{forced}{}^{3} + \overline{h}_{free}{}^{3}\right)} \tag{5.10}$$

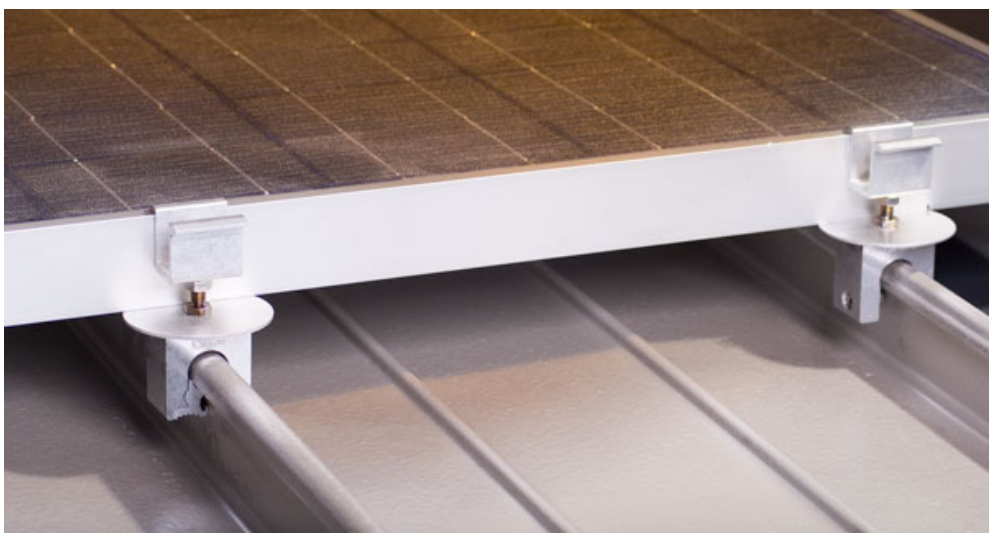

Figure 5.4: Example of mounting structure oriented perpendicular to ridge of roof (Green-Trust.Org, 2007).

5.3.3 Mounting Structures Do Not Significantly Impede the Flow of Air in Either Direction

In this case, all wind directions are assumed to create flow underneath the module; therefore, the measured wind speed is directly applied to forced convection correlations. Figure 5.5 shows an example of this orientation. The channel flow correlations for both free and forced convection will be calculated and combined in the same method as previous sections. The characteristic length for forced convection, however, will be calculated by Equation (5.11).

$$L_{char} = \frac{4Area}{Perimeter} \tag{5.11}$$

Figure 5.5: Example of mounting structure that does not significantly impede the flow of air in either direction (Comfort Zone Mechanical Air, Inc., 2010).

5.4 Rack Mounting Configuration

A rack mounting configuration is supported by structures similar to those supporting open rack modules mounted on the ground. Figure 5.6 shows an example of this configuration. In this case, the distance between the module and the roof is adequate such that the flow of air behind the module is not significantly altered by the channel formed between the module and the roof, and the open rack model can be applied. The roof temperature is assumed to be equal to the ambient temperature for this configuration.

Figure 5.6: An example of a rack mounting configuration (U.S. Environmental Protection Agency, 2010).

5.5 Application to Building Mounted Modules

All of models presented, with the exception of the model for the rack mounting configuration, also apply to modules mounted on the sides of buildings. In this case, the options of wall temperature assumptions are the same as the options of roof temperature assumptions presented earlier. In fact, the integrated mounting configuration has been validated for BIPV modules at NIST (Chapter 2).

6. FORTRAN Implementation

This project is in support of SAM and the steady state energy balance model developed in the previous chapters is planned to be integrated into the photovoltaic simulation tool in SAM. The current cell temperature model available in SAM is adapted from the 5-parameter model presented in Duffie and Beckman (2006) and detailed in Chapter 4. This model is not adaptable to the various mounting configurations discussed throughout this study. In order create an adaptable model, several parameters, inputs, and assumptions must be added to the FORTRAN code that currently implements the five parameter performance model in SAM (based on TRNSYS Type 194). These additions are discussed in the following subsections. The entire FORTRAN code, along with descriptions of parameters, inputs, and outputs is included in Appendix H.

6.1 New Parameters: Pre-Defined Options

6.1.1 Mounting Location

This parameter will include three options: ground, roof, or wall. This selection will determine whether the code uses ground, roof, or wall temperature as the surroundings temperature for radiative heat transfer from the backside of the module.

6.1.2 Mounting Configuration

This parameter defines the mounting configuration of the module, as discussed in Chapter 5. This selection will determine the appropriate set of heat transfer equations to solve to find the cell temperature. It is proposed that if “ground” is selected as the mounting location, open rack will be the default mounting.

6.1.3 Mounting Structure Orientation

This parameter defines the mounting structure orientation, as discussed in Section 5.3. This selection will determine the appropriate heat transfer correlations to solve for the convective heat transfer on the backside of a gap mounting configuration. This selection is irrelevant for other mounting configurations.

6.1.4 Heat Transfer Dimensions

Section 4.7.2 showed that choosing array rather than module dimensions can have an impact on the results of a simulation. For this reason, there is an option to simulate the array with either module or array dimensions. It is highly recommended, however, that roof and building mounted modules apply array dimensions when the modules are mounted closely to one another. This is especially true for gap mounting configurations where the channel flow between the backside and the roof or wall will be less affected by slight gaps between modules.

6.2 New Parameters: User-Defined Values

6.2.1 Module Dimensions

6.2.1.1 Length

This parameter is the dimension of the edge that is at the inclination angle of the module, because it is used as an input to free convection correlations.

6.2.1.2 Width

This parameter is the remaining dimension that defines the cover area of the module.

6.2.2 Gap Mounting Dimensions

6.2.2.1 Gap Spacing

This parameter defines the distance between the module and the roof for gap mounting configurations. Note that this selection is irrelevant for other mounting configurations.

6.2.3 Cover Properties

6.2.3.1 Cover Emissivity

The parameter defines the emissivity of the cover. The default value is set to 0.84 (the emissivity of glass).

6.3 Redundant Parameter

6.3.1 Area

The proposed model requires both the length and width of the module. Therefore, the area of the module becomes redundant and can be defined inside of the code.

6.4 New Input

6.4.1 Wind Direction

The gap integrated mounting model is dependent on wind direction, as detailed in Section 5.3. This selection can be set to a constant or left at the default value for other mounting configurations.

As results from simulating the NIST BIPV modules in Section 3.2 showed, building effects can cause significant differences between wind speed measured on the roof and wind speed measured at the module. The final manipulation of wind speed measurements for the NIST dataset required site-specific information such as wind speed measurement height, module height, and nearby buildings. Additionally, multiple

correlations were evaluated before the wind speed was accurately adjusted. For these reasons it is recommended that the user make changes to the measured wind speed based on site-specific experience and research.

6.4.2 Attic Temperature

This temperature is required for integrated mounting configuration modules on the roof. This selection can be set to the ambient temperature or left at the default value for other mounting configurations and locations.

6.4.3 Indoor Temperature

This temperature is required for integrated mounting configuration modules on building walls. This selection can be set to the ambient temperature or left at the default value for other mounting configurations and locations.

6.5 Pre-Set Assumptions that Users Could Potentially Define

6.5.1 Sky Temperature

The sky temperature has been predicted using the Berdahl and Martin (1984) correlation (Section 3.1.1). It is possible, however, that the model user may have measurements of the surroundings temperature. In this case, an input is included for the measured values which defaults to the Berdahl and Martin correlation if it is not used. Alternatively, TRNSYS Type 69 could be used to import the sky temperature.

6.5.2 Ground Temperature

The ground temperature has been previously assumed to be equal to the ambient temperature. It was also suggested that more accurate correlations could be determined. Therefore, the model user may have measurements or a different ground temperature model that could supply temperature to code. As with the sky temperature, an input can be provided that defaults to the current ground temperature model if it is not used.

7. Conclusions and Recommendations

7.1 Conclusions

An energy balance model to predict the cell temperature of mono-Si and poly-Si photovoltaic modules was developed and validated using field measurements. The energy balance model considers convection and radiative exchange with the ambient environment as well as conduction through the cover, cell, and the backsheet substrate. The convection heat loss is predicted using established free and forced convection heat transfer correlations and the radiative heat transfer calculations are based on first-principles rather than empirical relations. Both a transient model that accounts for the thermal capacitance and temperature of each material in the cell and a steady energy balance model that creates a thermal resistance network between the cell and ends of the module were developed.

The datasets used for model validation included mono-Si and poly-Si technologies in a building-integrated photovoltaic (BIPV) implementation at the NIST headquarters facilities in Gaithersburg, MD; mono-Si technology in a rack-mounted configuration at the Sandia National Labs in Albuquerque, NM; and a heterojunction with intrinsic thin layer (HIT) technology in a rack-mounted configuration at NREL in Golden, CO. Datasets at each location were available for a minimum of a one year period. Each data set was independently screened for quality control purposes.

Simulation results for both the mono-Si and poly-Si modules showed that the steady state model applying hourly data produced similar long term energy prediction results as the transient model applying five minute data. The RMSE errors were predictably greater for

the steady state model than for the transient model, as the steady state model tends to over predict during the morning and under predict in the afternoon because the model does not account for the thermal capacitance of a BIPV module. This result is likely to be true for any BIPV module experiencing “symmetric” weather, and caution should be taken when applying this assumption to a module experiencing asymmetric mounting. This result also indicates that modelers attempting to more accurately predict the performance at each time step (diagnostic models, for example) likely need to have data available in short time steps to account for transient effects such as intermediate cloud cover and varying wind speeds. Time constants of BIPV modules were calculated to be between 5 and 15 minutes, so the shorter time steps should be at least in this range. These transient simulations also require the thermal capacity and conductivity of the materials composing the modules, although these values are typically not available.

Annual system performance validation for the two open rack modules (mono-Si and HIT) and two BIPV (mono-Si and poly-Si) modules showed that the five parameter model applying the nodal, steady state energy balance model calculates annual results within 2.5% of results found with the five parameter model applying measured temperatures and within 4% of measured results. Additionally, assumptions of a spatially uniform module temperature and location specific atmospheric pressure can be applied to the model with less than 1% effect on results. The accuracy of this model lends confidence that the steady state energy balance model can be accurately adapted to various mountings by applying accepted heat transfer. This is an important benefit of the developed model, as other models evaluated are not easily adaptable. Models for roof and wall mounted modules are proposed in this research but not currently validated.

The results of the nodal, steady state energy balance model compare well with the results of three other previously-published cell temperature models (Duffie and Beckman (2006), Skopaki (2008), and King (2004)) evaluated for the open rack modules. The Duffie and Beckman and Skoplaki models were found to be less accurate than the steady-state model developed in this study for the BIPV modules. The relative inaccuracy of these models is a result of not adequately accounting for the effects of higher module operating temperatures due to the BIPV mounting. The Duffie and Beckman model uses the reported NOCT to account for various mounting configurations. The procedure to measure NOCT, however, was shown to be inaccurate under some testing conditions. The Duffie and Beckman model produces more accurate results when a NOCT predicted with the steady state energy balance model is applied.

NOCTs calculated with the steady state energy balance model for the mono-Si and poly-Si modules evaluated in this research do not agree with the NOCTs measured by NIST. The correction factor chart provided in the procedure to measure NOCT likely assumes laminar flow while the experimental results have suggested that wind induced forced convection is turbulent. Additionally, the published correction factor chart (IEC, 2005 and ASTM, 2008) does not account for various model mounting configurations that affect the difference between the cell and ambient temperatures at various testing conditions. Recommendations for improving the accuracy of NOCT measurements are included in Section 3.4.5.

7.2 Recommendations for Future Work

A large source of uncertainty in photovoltaic modeling is applying the correct wind speed and this is a problem for both simulations using TMY datasets and during the course of validations that rely on near-site measured wind speeds. For the simulations applying TMY datasets, there is potential for a large difference in wind speeds between the measurements at the TMY site compared with the PV installation location. This difference appears especially likely when considering both BIPV modules and urban settings. For validation efforts, the height of the wind speed measurement, relative to the module, becomes important. For example, a sensitivity study showed around a 2% difference between adjusting wind speeds between the module height and free stream and applying the measured wind speed. While an adjustment is likely required, the magnitude of the adjustment is currently not known. Additionally, it is likely this adjustment is dependent on the testing location.

A sensitivity study showed that a more accurate value of ground temperature may help remove uncertainty from results. It is likely that the current assumption that the ground temperature is equal to the ambient temperature can be improved.

The choice of using either array dimensions or individual module dimensions is also important when modeling a multiple-module array. For example, a sensitivity study showed that modeling with array rather than module dimensions resulted in a -1.6% decrease in predicted energy output. This complication arises from the distance between the modules in an array. Considering the limits of such a mounting, at a small distance the modules basically form one larger module, while at a much larger distance each

module can be treated as thermally independent. Research into the modeling of large arrays would help to provide clarity in this area.

The size of a module may affect heat transfer correlations. The model developed for this research assumes that the heat transfer coefficient is the same on both sides of a module for any wind direction. As a module becomes larger, winds from a direction perpendicular to the plane of the module will likely not transfer as much energy from the leeward side of the module because the turbulent wake flow near the edges due to the pressure drop will be far removed from the center of the module. Defining the correct characteristic length also becomes more difficult for rectangular modules and arrays with one dimension significantly larger than the other. In this case, the heat transfer induced by wind speeds in the direction of the longer dimension will be less than the heat transfer induced by wind speeds in the shorter direction. Research into these areas will increase understanding of the effect of module size and wind direction on the heat transfer coefficient.

Validation efforts are required to determine the accuracy and robustness of the models proposed for roof and building mounted modules. Further validation efforts will also provide a larger sample size of results to help to determine the average and standard deviations of the accuracy of cell temperature models over a range of locations and mounting configurations, as this information is currently not available in literature. Additionally, extensive residual analyzes may help determine conditions where models perform poorly.

Finally, manufacturers able to provide additional information without compromising their intellectual property would help facilitate modeling efforts. Helpful information would include: cover material, cover thickness, cover emissivity, backsheet emissivity, and backsheet thermal resistance.

References

ASTM, 2008. Standard Test Methods for Electrical Performance of Nonconcentrator Terrestrial Photovoltaic Modules and Arrays Using Reference Cells. *Annual Book of ASTM Standards*, E 1036 – 8.

Bansal, N.P., Doremus, R.H., 1986. *Handbook of Glass Properties*, Elsevier. Online version: http://knovel.com/web/portal/browse/display?_EXT_KNOVEL_DISPLAY_bookid=2266&VerticalID=0

Beckman, W.A., 2009. Personal Communication.

Bejan, A., Kraus, A.D., 2003. *Heat Transfer Handbook*. John Wiley & Sons. Online version: http://knovel.com/web/portal/browse/display?_EXT_KNOVEL_DISPLAY_bookid=725&VerticalID=0

Berdahl, P., Martin, M., 1984. Emissivity of Clear Skies. *Solar Energy*, Vol 32, Page 5663.

Boyd, M. T., 2010. Evaluation and Validation of Equivalent Circuit Photovoltaic Solar Cell Performance Models. M.S. Thesis, Mechanical Engineering, University of Wisconsin-Madison.

Brandrup, J., Immergut, E.H., Grulke, E.A., Abe, A., Bloch, D.R., 2005. *Polymer Handbook (4th Edition)*, John Wiley & Sons. Section B.

Brinkworth, B.J., Marshall, R. H., Ibarahim, Z., 2000. A Validated Model of Naturally Ventilated PV Cladding. *Solar Energy*, Volume 69, Issue 1, Pages 67-81.

Comfort Zone Mechanical Air, Inc., 2010. http://www.comfortzone-air.com/_Media/100_0186.jpg. Accessed 2010, 11/19.

Davis, M.W., Fanney, A.H., Dougherty, B.P., 2001. Prediction of Building Integrated Photovoltaic Cell Temperatures. *ASME Journal of Solar Energy Engineering*, Volume 123, Issue 3, Pages 200-210.

De Soto, W., Klein S.A., Beckman W.A., 2006. Improvement and validation of a model for photovoltaic array performance. *Solar Energy*, Volume 80, Issue 1, Pages 78-88.

Del Cueto, J.A., 2000. Model For The Thermal Characteristics Of Flat-Plate Photovoltaic Modules Deployed At Fixed Tilt. *28th IEEE Photovoltaic Specialists Conference*, Pages 1441-1445.

Dougherty, B.P., 2010. Personal Communication.

Dougherty, B.P., Fanney, A.H., Davis, M.W., 2004. Measured Performance of Building Integrated Photovoltaic Panels: Round 2. *ASME International Solar Energy Conference*, Pages 421-430.

Duffie, J.A., Beckman, W.A., 2006. *Solar Engineering of Thermal Processes*, third ed. John Wiley & Sons Inc., New York.

DuPont™ 2009. Dupont™ Tedlar® PVF Films. Data Sheet. http://www2.dupont.com/Photovoltaics/en_US/assets/downloads/pdf/Tedlar_for_PV.pdf

Eicker, U., 2003. *Solar Technologies for Buildings*, John Wiley & Sons., New York. Pages 88-90.

Emmel M, G., Abadie M, O., & Mendes N., 2007. New external convective heat transfer coefficient correlations for isolated low-rise buildings. *Energy and Buildings*, 39, 335.

Fanney, A.H., Dougherty, B.P., 2001. Building Integrated Photovoltaic Test Facility. *Journal of Solar Energy Engineering*, Volume 123, Issue 3, Pages 194-199.

Fuentes M.K., 1987. A Simplified Thermal Model for Flat-Plate Photovoltaic Arrays. Sandia National Laboratories Report: SAND85-0330.

Gan, G., 2009. Numerical determination of adequate air gaps for building-integrated photovoltaics. *Solar Energy*, Volume 83, Issue 1, Pages 1253-1273.

Green-Trust.Org, 2007. http://www.green-trust.org/wordpress/2010/08/25/standing-seam-metal-roof-with-solar-panels/. Accessed 2010, 11/19

IEC 61215, 2005: Crystalline silicon terrestrial photovoltaic (PV) modules – Design qualification and type approval.

Incropera, F.P., Dewitt, D.P., Bergman, T.L., Lavine, A.S., 2006. *Fundamentals of Heat and Mass Transfer*, sixth edition, John Wiley & Sons Inc., New York.

Ito, N., Kimura, K., Oka, J., 1972. A field experiment study on the convective heat transfer coefficient on exterior surface of a building. *ASHRAE Transactions 78*, Pages 184 – 191.

Jones, A.D., Underwood, C.P., 2001. A Thermal Model For Photovoltaic Systems. *Solar Energy*, Volume 70, No. 4, Pages 349-359.

King, D.L., Boyson, W.E., Kratochvil, J.A., 2004. Photovoltaic Array Performance Model. Sandia National Laboratories. Report: SAND2004-3535.

Klein, S.A. (2010). EES – Engineering Equation Solver, F-Chart Software. http://www.fchart.com.

Krauter, S., Preiss, A., Ferretti, N., Grunow, P., 2008. PV Yield Prediction for Thin Film Technologies and the Effect of Input Parameters Inaccuracies. *23rd European Photovoltaic Solar Energy Conference*.

Loveday, D.L., and Taki, A.H., 1996. Convective heat transfer coefficients at a plane surface on a full-scale building façade. *International Journal of Heat and Mass Transfer*, Vol 39, Issue 8, Pages 1729-1742.

Manwell J, F., McGowan J, G., & Rogers A, L., 2002. *Wind energy explained theory, design and application*, first ed. John Wiley & Sons Ltd.

Marion, B., 2009. Personal Communication.

Mittelman, G., Alshare, A., Davidson, J.H., 2009. A model and heat transfer correlation for rooftop integrated photovoltaics with a passive air cooling channel. *Solar Energy*, Volume 83, Issue 1, Pages 1150-1160.

Muller, M., 2010. Measuring and Modeling Nominal Operating Cell Temperature (NOCT). Presented at the PV Performance Modeling Workshop, 22-23 September 2010, Albuquerque, New Mexico. http://www.nrel.gov/docs/fy10osti/49505.pdf

Myers, D.R., Stoffel, T.L., Reda, I., Wilcox, S.M., Adreas, A.M., 2002. Recent Progress in Reducing the Uncertainty in and Improving Pyranometer Calibrations. *ASME Journal of Solar Energy Engineering*, Volume 124, Pages 44-50.

Nellis, G., and Klein, S.A., 2009. *Heat Transfer*, Cambridge University Press.

NIST, 2006. http://www.nist.gov/public_affairs/techbeat/tb2006_0622.htm. Accessed 2010, 11/23.

NREL, 2010. Solar Advisor Model. https://www.nrel.gov/analysis/sam/. Accessed 2010, 12/11.

Philadelphia Solar, 2009. http://www.philadelphia-solar.eu/philadelphia_solar_roof_integration.html. Accessed 2010, 11/23.

PPG Industries, Inc., 2008. Solarphire PV High-Transmissive Glass. Data Sheet. http://www.ppg.com/en/solutionbyindustry/energy/solar/Documents/FinalSolarphirePVproductdatasheet.pdf. Accessed 2010 4/19.

PV Resources, 2010. Large-scale photovoltaic power plants ranking 1 – 50. http://www.pvresources.com/en/top50pv.php. Accessed 2010, 12/10.

Sharples, S., 1984. Full-scale measurements of convective energy losses from exterior building surfaces. *Building and Environment*, Vol 19, Pages 31-39.

Sharples, S., Charlesworth, P.S., 1997. Full-scale measurements of wind-induced convective heat transfer from a roof-mounted flat plate solar collector. *Solar Energy*, Vol 62, Issue 2, Pages 69-77.

Shrestha, B.L., Palomino, E.G., TamixhMani, G., 2009. Temperature of rooftop photovoltaic modules: Air gap effects. *Proceedings of SPIE*, Volume 7412.

Skoplaki, E., Boudouvis, A.G., Palyvos, J.A., 2008. A simple correlation for the operating temperature of photovoltaic modules of arbitrary mounting. *Solar Energy Materials & Solar Cells*, Volume 92, Pages 1393-1402.

Skoplaki. E., Palyvos. J.A., 2009. On the temperature dependence of photovoltaic module electrical performance: A review of efficiency/power correlations. *Solar Energy*, Vol 83, Pages 614-624.

South Ayrshire Council, 2010. http://www.south-ayrshire.gov.uk/sustainable-development/energy/renewables.aspx Accessed 2010, 11/19.

Sparrow, E.M., Ramsey, J.W., Mass, E.A., 1979. Effect of Finite Width on Heat Transfer and Fluid Flow about an Inclined Rectangular Plate. *Journal of Heat Transfer*, Vol 101, Pages 199-204.

Swinbank, W.C., Roy, Q.J., 1963. Long-Wave Radiation from Clear Skies. *J. Roy. Meteorol. Soc*, Vol 89, Page 339.

Test, F.L., Lessmann, R.C., Johary, A., 1981. Heat Transfer During Wind Flow over Rectangular Bodies in the Natural Environment. *Journal of Heat Transfer*, Vol 103, Pages 262-267.

U.S. Environmental Protection Agency, 2010. http://www.epa.gov/oaintrnt/facilities/corvallis_solar.htm. Accessed 2010, 11/23.

Weather Underground, 2010. History for Washington, DC. http://www.wunderground.com/history/airport/KDCA/2002/1/22/DailyHistory.html?req_city=Washington&req_state=DC&req_statename=District+of+Columbia. Accessed 2010 1/18.

Wegley, H.L., Ramsdell, J. V., Orgill, M. M., and Drake, R.L., 1980. A Sitting Handbook for Small Wind Energy Conversion Systems, Battelle Pacific Northwest Lab., PNL-2521, Rev. 1, NTIS.

Appendix A: Module Properties

Table A.1: Measured mono-Si performance and physical data (Boyd, 2010)

Relevant Performance Data (mono-Si module at NIST)	Values Measured by NIST
I_{sc} [A]	4.37
V_{oc} [V]	42.93
I_{mp} [A]	3.96
V_{mp} [V]	33.68
P_{mp} [W]	133.4
α_{Isc} [A/°C]	0.00175
β_{Voc} [V/°C]	-0.152
NOCT [°C]	43.7
Length [m]	1
Width [m]	1.2

Table A.2: Material properties of the components of the mono-Si module (Davis et al. 2001)

Property	Cover	PV Cell	Backsheet	Insulation
Thickness (th) [m]	0.006	0.0003	0.00017	0.1016
Density (ρ) [kg/m^3]	2500	1650	1475	55
Capacitance (c) [J/kg-K]	835	700	1130	1210
Conductivity (k) [W/m-K]	1.04	150	0.14	0.0294
Emissivity (ε) [-]	0.84	-	0.893	0.9

Table A.3: Measured poly-Si performance and physical data (Boyd, 2010)

Relevant Performance Data (poly-Si module at NIST)	Values Measured by NIST
I_{sc} [A]	5.05
V_{oc} [V]	42.77
I_{mp} [A]	4.61
V_{mp} [V]	33.45
P_{mp} [W]	154.2
α_{Isc} [A/°C]	0.0036
β_{Voc} [V/°C]	-0.131
NOCT [°C]	39.5
Length [m]	1
Width [m]	1.2

Table A.4: Properties of ETFE cover of poly-Si module (Brandup et al., 2005)

Property	ETFE
Thickness (th) [mm]	0.05
Density (ρ) [kg/m^3]	1600
Capacitance (c) [J/kg-K]	1950
Conductivity (k) [W/m-K]	0.238
Emissivity[1] (ε) [-]	0.84

[1] Initial Estimate

Table A.5: Mono-Si (Sandia) performance and physical data

Relevant Performance Data (mono-Si module at Sandia)	Values Found in Manufacturer's Datasheet
I_{sc} [A]	5.75
V_{oc} [V]	47.7
I_{mp} [A]	5.25
V_{mp} [V]	40
P_{mp} [W]	210
α_{Isc} [A/°C]	0.0035
β_{Voc} [V/°C]	-0.1368
NOCT [°C]	45±2
Length [m]	1.6
Width [m]	0.8
Cover Material	Glass
Cover Thickness [mm]	3.2
Cover Emissivity [-]	0.84

Table A.6: HIT (NREL) performance and physical data

Relevant Performance Data (mono-Si module at NREL)	Values Found in Manufacturer's Datasheet
I_{sc} [A]	3.83
V_{oc} [V]	68.7
I_{mp} [A]	3.59
V_{mp} [V]	55.8
P_{mp} [W]	200
α_{Isc} [A/°C]	0.00088
β_{Voc} [V/°C]	-0.172
NOCT [°C]	44.2
Length [m]	1.319
Width [m]	0.984
Cover Material	Glass
Cover Thickness[1] [mm]	3.2
Cover Emissivity [-]	0.84

[1] Estimate

Appendix B: Monthly Simulation Results (Sections 2.8 and 2.9)

B.1: Mono-Si

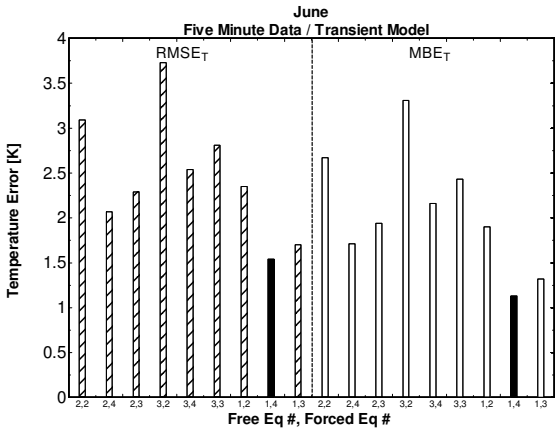

Figure B.1 - 1

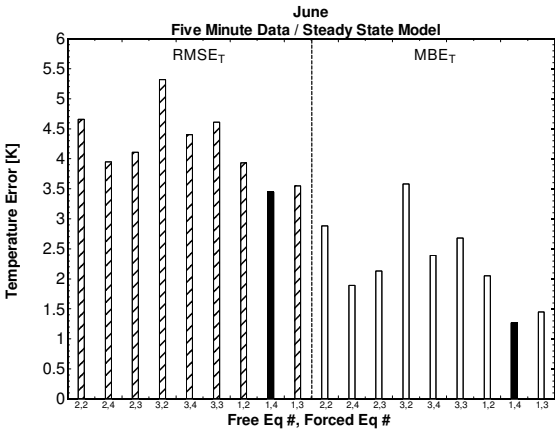

Figure B.1 - 3

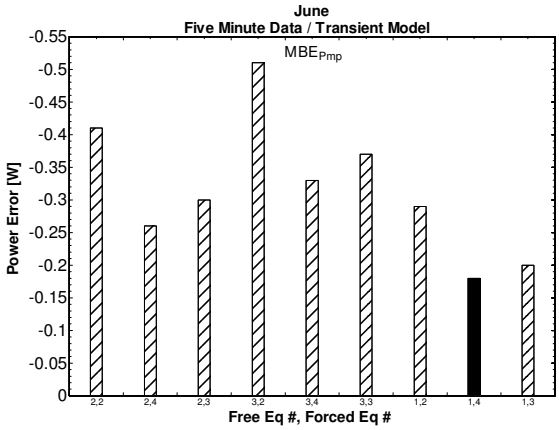

Figure B.1 - 2

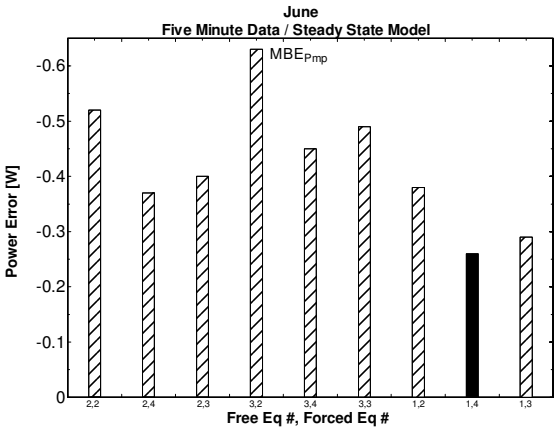

Figure B.1 - 4

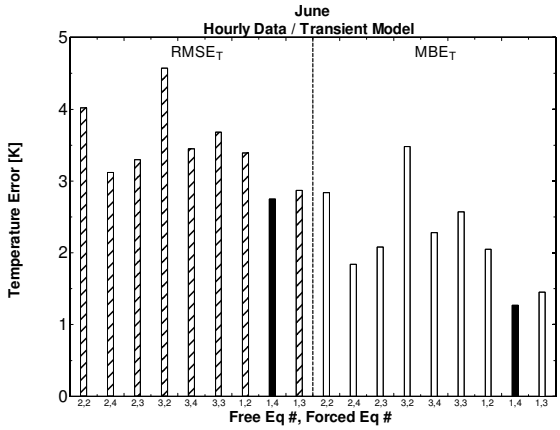

Figure B.1 - 5

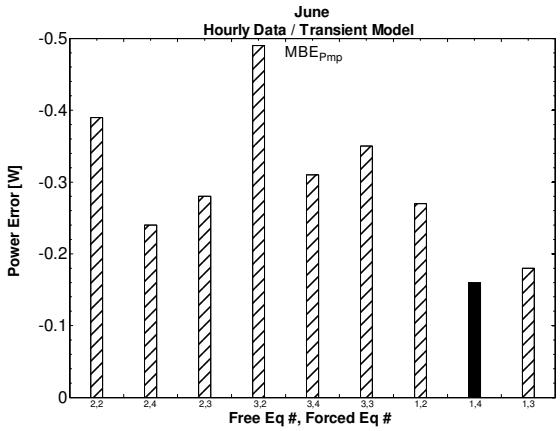

Figure B.1 - 6

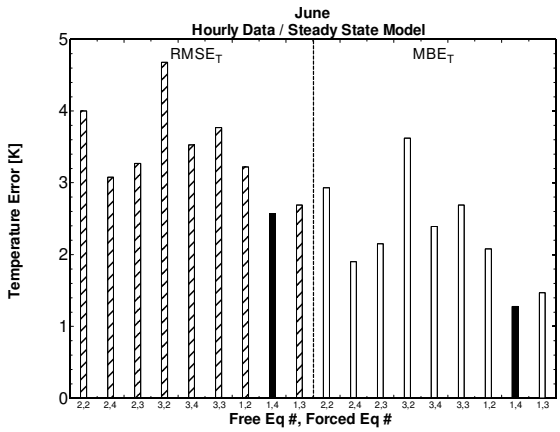

Figure B.1 - 7

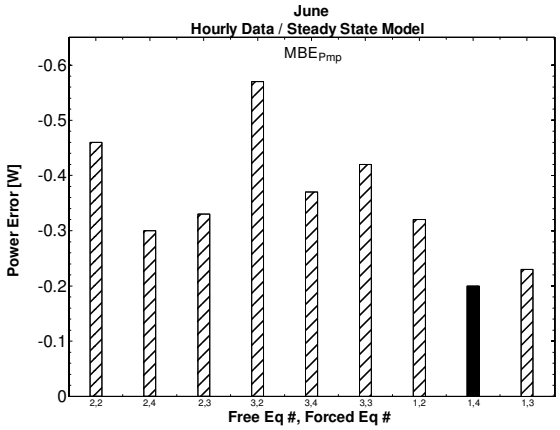

Figure B.1 - 8

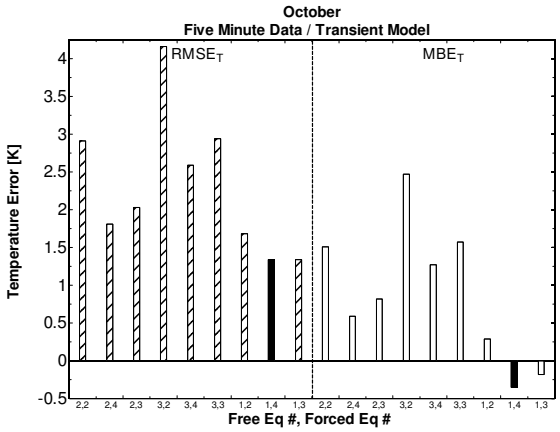

Figure B.1 - 9

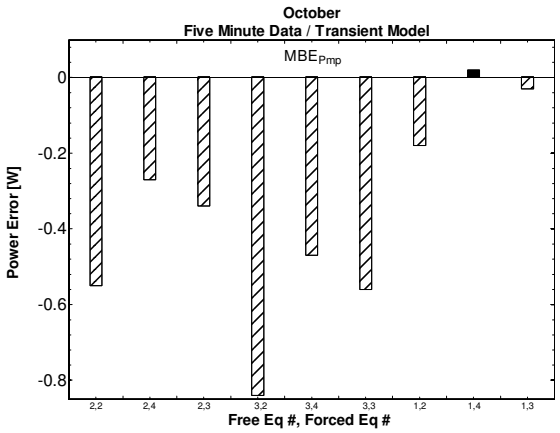

Figure B.1 - 10

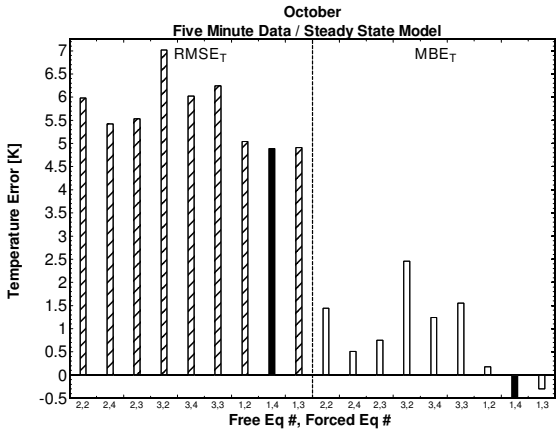

Figure B.1 - 11

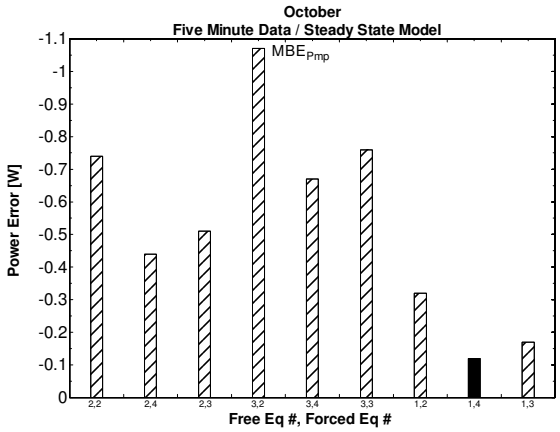

Figure B.1 - 12

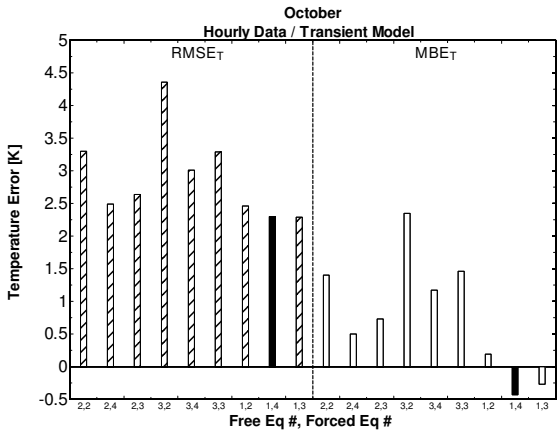

Figure B.1 - 13

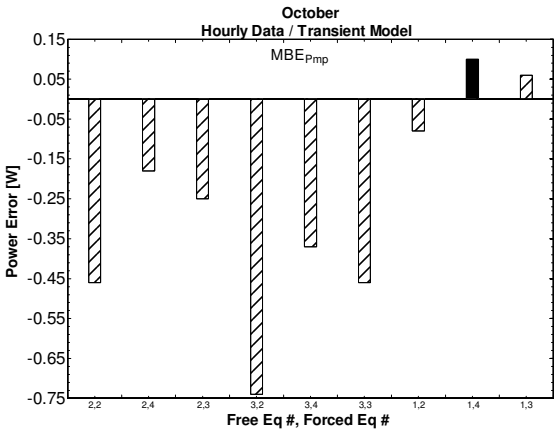

Figure B.1 - 14

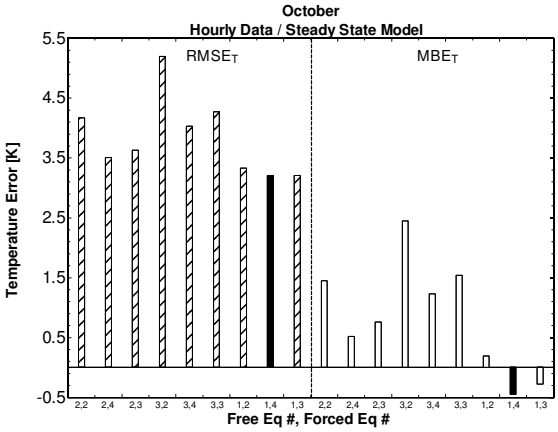

Figure B.1 - 15

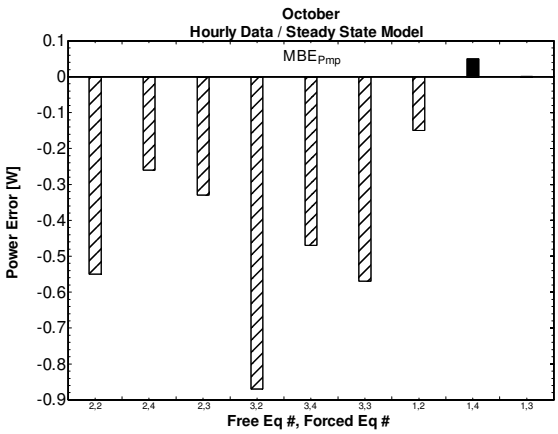

Figure B.1 - 16

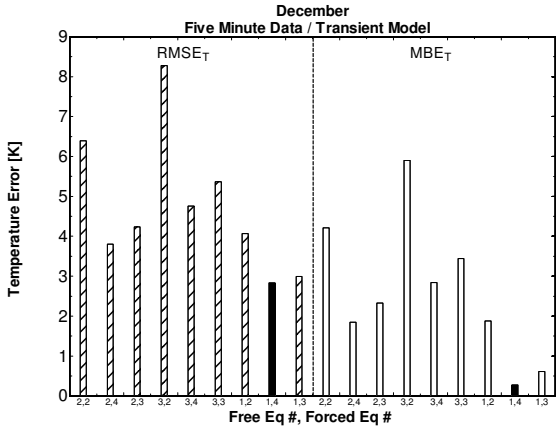

Figure B.1 - 17

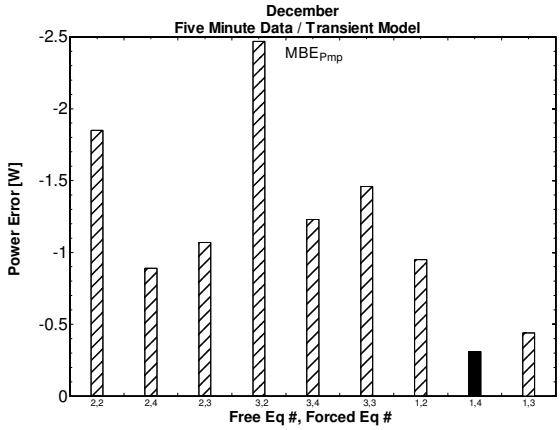

Figure B.1 - 18

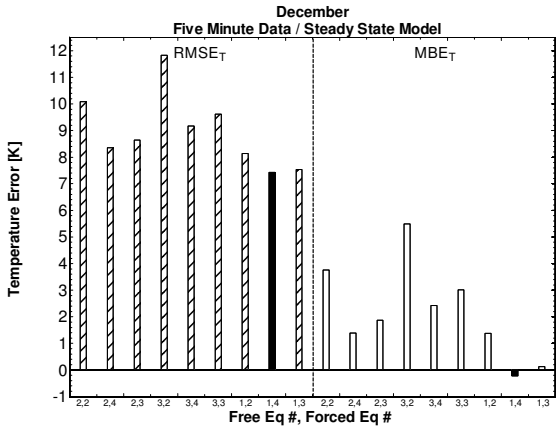

Figure B.1 - 19

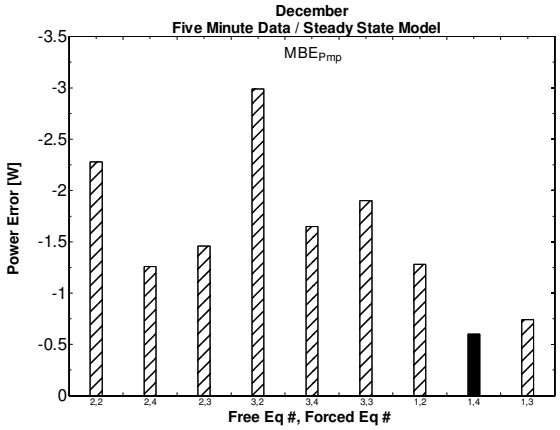

Figure B.1 - 20

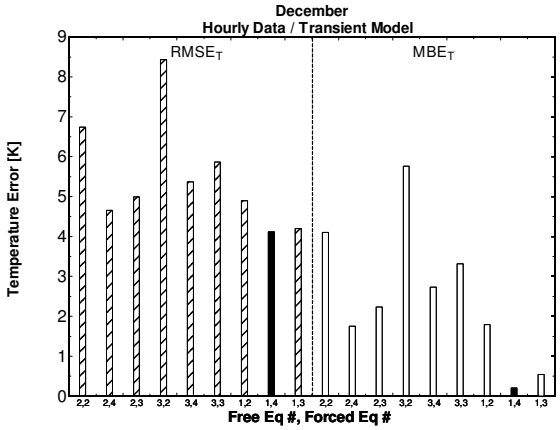

Figure B.1 - 21

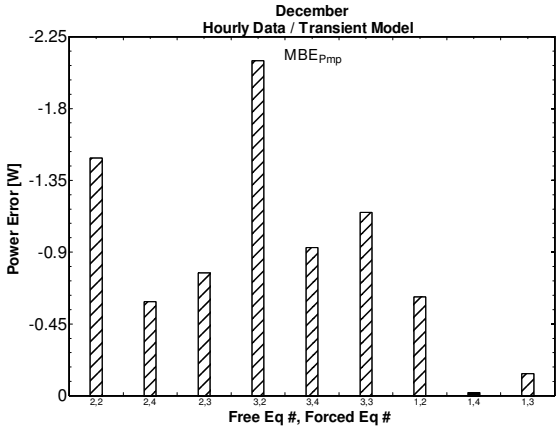

Figure B.1 - 22

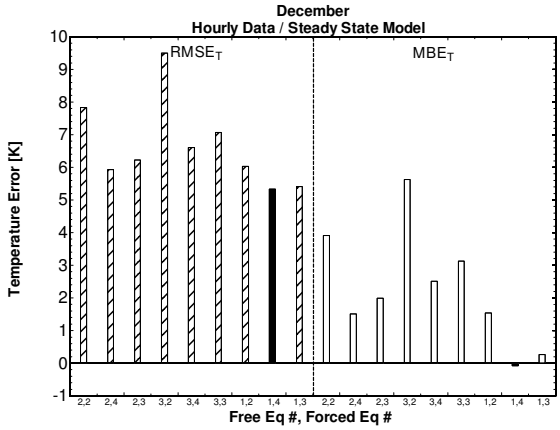

Figure B.1 - 23

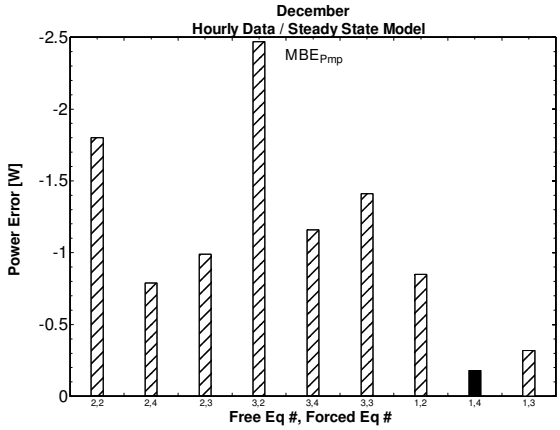

Figure B.1 - 24

B.2: Poly-Si

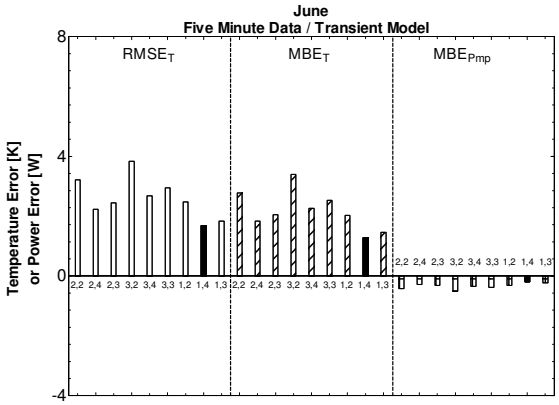

Figure B.2 - 1

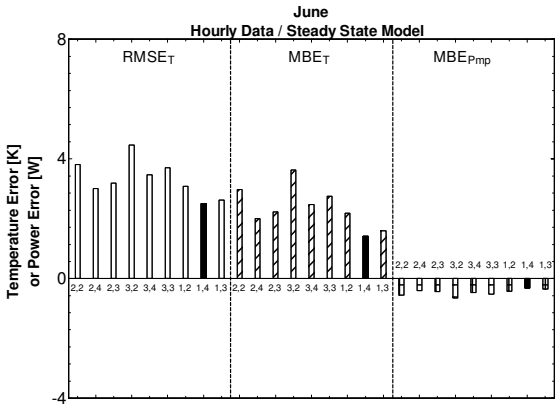

Figure B.2 - 2

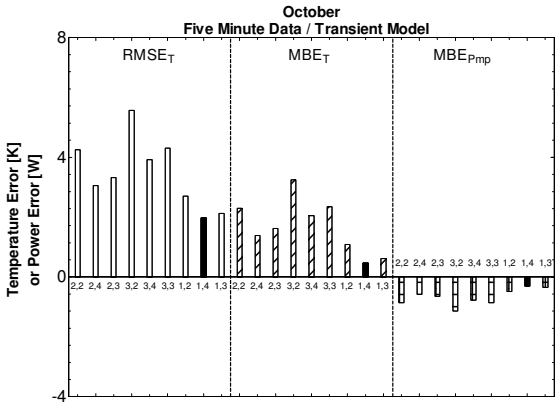

Figure B.2 - 3

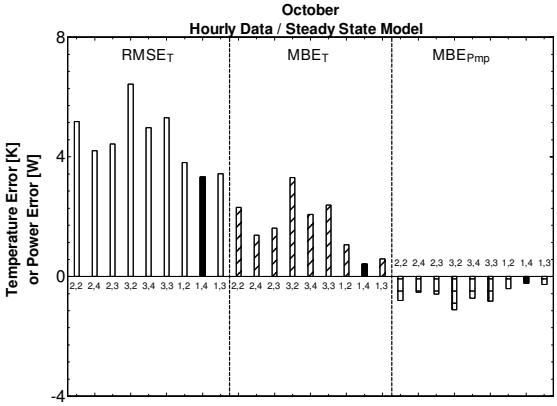

Figure B.2 - 4

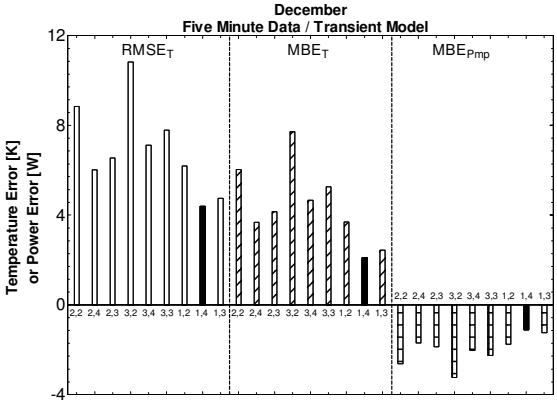

Figure B.2 - 5

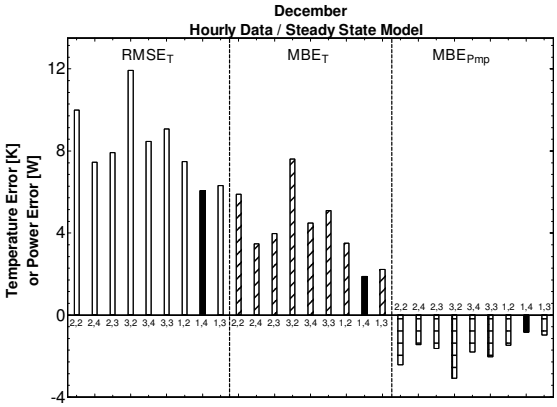

Figure B.2 - 6

Appendix C: Adjusting Rooftop Wind Speed Measurements

Table C.1: Values of surface roughness length for various types of terrain (Manwell et al., 2002).

Terrain Description	z0
Very smooth, ice or mud	0.01
Calm open sea	0.20
Blown sea	0.50
Snow surface	3.00
Lawn grass	8.00
Rough pasture	10.00
Fallow field	30.00
Crops	50.00
Few Trees	100.00
Many trees, hedges, few buildings	250.00
Forest and woodlands	500.00
Suburbs	1500.00
Centers of cities with tall buildings	3000.00

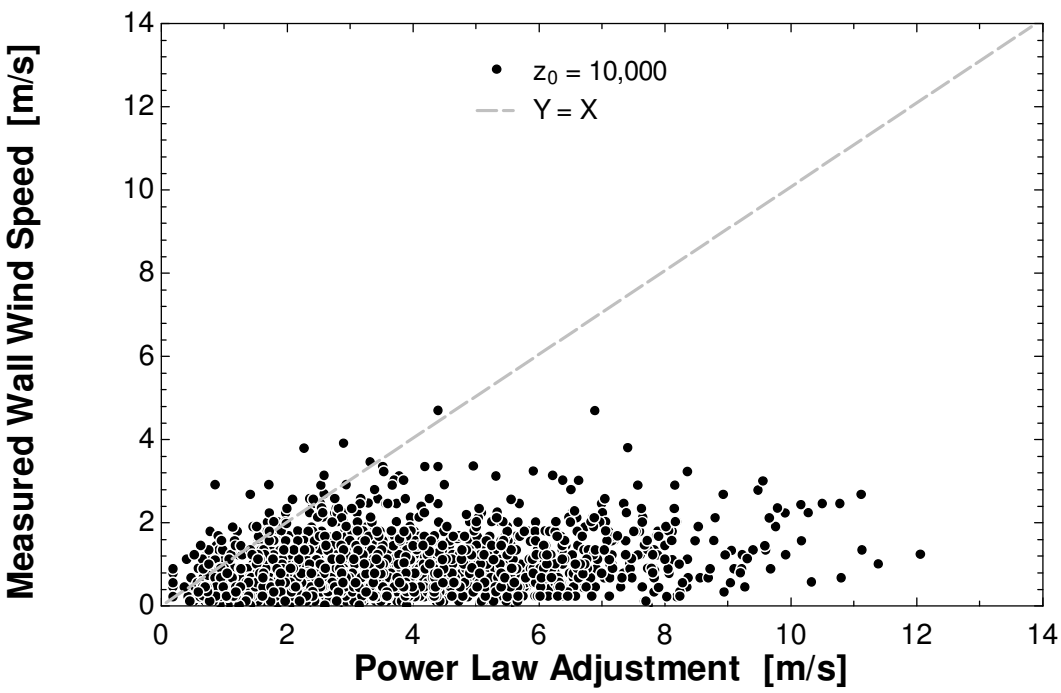

Figure C.1: Measured wind speed at the module versus rooftop wind speed adjusted to the height of the module using the power law for the month of December. A maximum surface roughness length of 10000 was used.

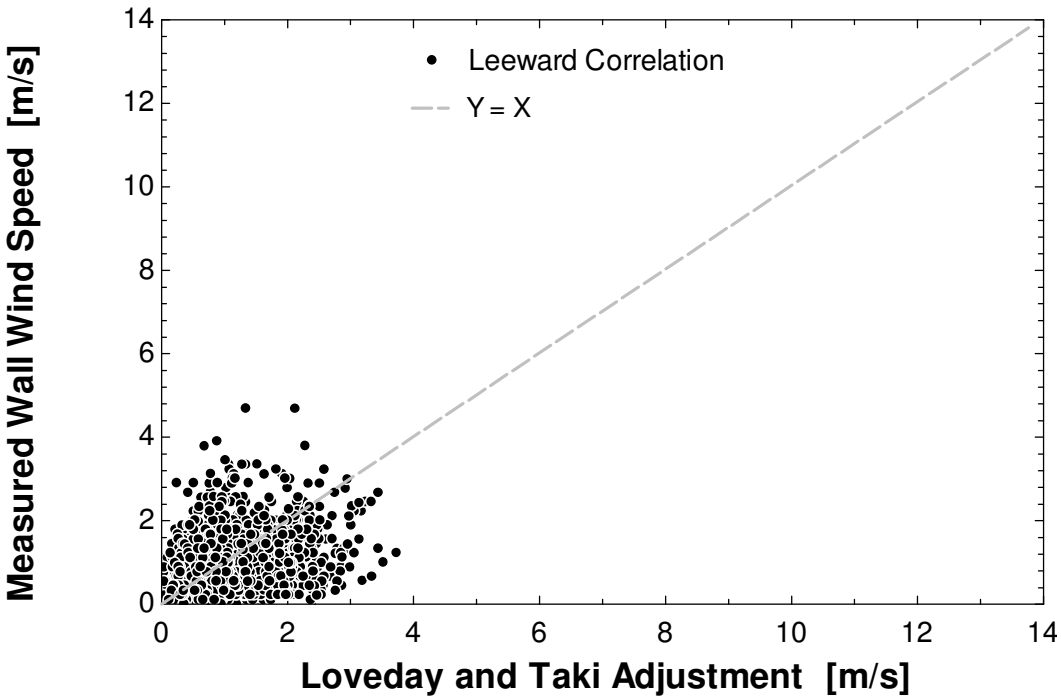

Figure C.2: Measured wind speed at the module versus rooftop wind speed adjusted to the height of the module using the procedure detailed in Section 3.2.2. The leeward correlation was used for all wind directions.

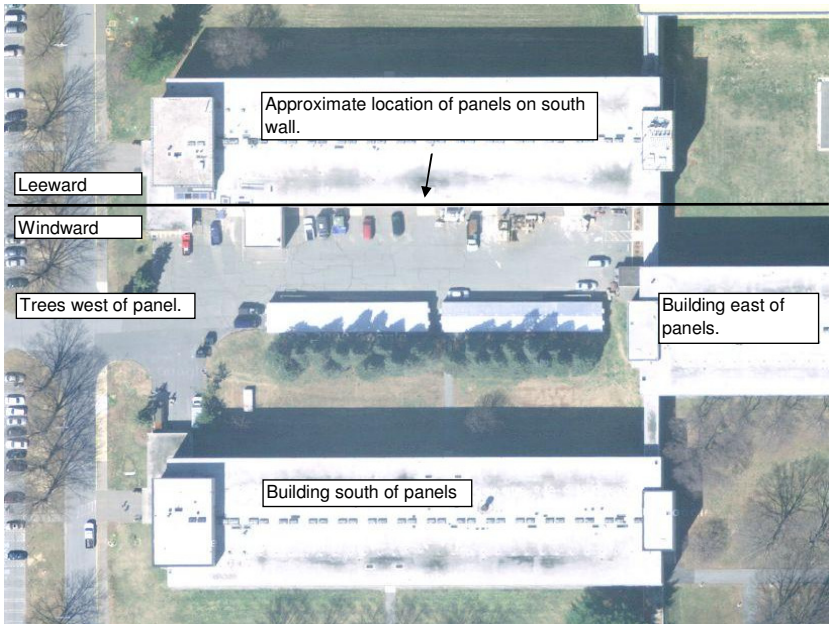

Figure C.3: Aerial photograph of NIST campus near photovoltaic modules. Leeward and windward directions are shown, along with obstructions in the windward direction.

Figure C.4: View of modules on south wall of NIST and building to the east of the modules.

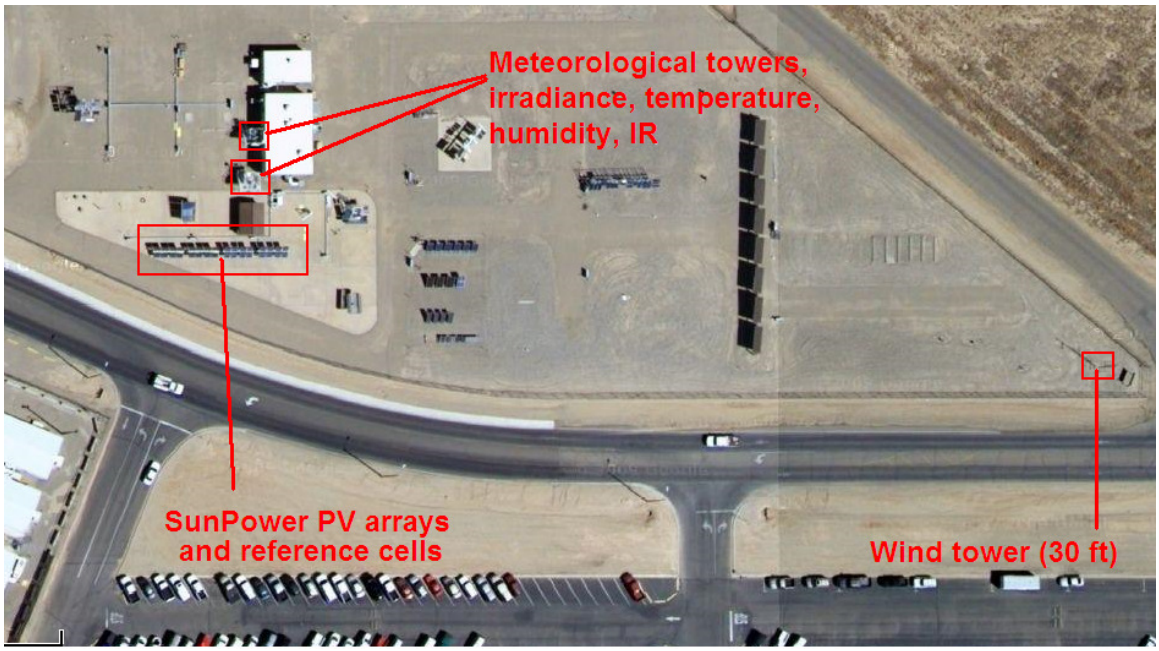

Figure C.5: Aerial view of Sandia site

Figure C.6: The five modules on the top of the structure are the HIT array at NREL (Marion, 2009).

Appendix D: Free Convection Calculations (Nellis and Klein, 2009)

Horizontal Heated Upward Facing

The Rayleigh number and the average Nusselt are based on the characteristic length scale of plate, Equation D.1.

$$L_{char} = \frac{Surface\ Area}{Perimeter} \tag{D.1}$$

The average Nusselt number is the weighted average of the laminar and turbulent Nusselt numbers:

$$\overline{Nu}_{L_{char}} = \left(\overline{Nu}^{10}_{L_{char},lam} + \overline{Nu}^{10}_{L_{char},turb}\right)^{\frac{1}{10}} \tag{5.12}$$

The laminar Nusselt number is:

$$\overline{Nu}_{L_{char},lam} = \frac{1.4}{\ln\left(1 + \frac{1.4}{0.835 C_{lam} Ra^{0.25}_{L_{char}}}\right)} \tag{5.13}$$

where C_{lam} is:

$$C_{lam} = \frac{0.671}{\left[1 + \left(\frac{0.492}{\Pr}\right)^{\frac{9}{16}}\right]^{\frac{4}{9}}} \tag{5.14}$$

The turbulent Nusselt number is:

$$\overline{Nu}_{L_{char},turb} = C_{turb,U} Ra^{\frac{1}{3}}_{L_{char}} \tag{5.15}$$

where $C_{turb,U}$ is:

$$C_{turb,U} = 0.14\left(\frac{1 + 0.0107\Pr}{1 + 0.01\Pr}\right) \tag{5.16}$$

Horizontal Heated Downward Facing

The average Nusselt number is taken to be the laminar Nusselt number:

$$\overline{Nu}_{L_{char}} = \frac{2.5}{\ln\left\{1+\frac{2.5}{0.527 Ra_{L_{char}}^{0.20}}\left[1+\left(\frac{1.9}{\Pr}\right)^{0.9}\right]^{\frac{2}{9}}\right\}} \tag{5.17}$$

Appendix E: Filtering Datasets

Table E.1: Monthly energy prediction errors for NIST mono-Si BIPV with different filtering criteria applied to input data (Section 4.5.2). One filter rejects time periods with large zenith angles while the other filter does not.

	Monthly Energy Prediction Errors	
	No zenith angle filter	Zenith angle filter
Jan	2.39%	1.70%
Feb	4.00%	3.47%
Mar	4.39%	4.06%
Apr	0.00%	0.00%
May	0.74%	0.74%
Jun	-0.62%	-0.62%
Jul	6.28%	6.27%
Aug	0.94%	0.94%
Sep	2.26%	2.17%
Oct	5.01%	4.81%
Nov	4.44%	3.71%
Dec	4.16%	3.10%
Total	3.25%	2.86%

Table E.2: HIT data rejected by I-V curve filter.

Month	Day	Times														
1	2	11.75	12.00													
1	5	11.00	11.25	11.50	11.75	12.00	12.25									
1	6	10.50														
1	10	10.00	12.50													
1	12	11.25	11.50	11.75	12.00	12.25	12.50	12.75	13.00	13.25	13.50	13.75	14.00			
1	13	11.25	11.50	11.75	12.00	12.25	12.50	12.75	13.00	13.25	13.50					
1	14	10.50	10.75													
1	18	11.25	12.25	12.50	12.75											
1	19	12.00	12.25	12.50	12.75	13.00	13.25	13.50	13.75							
1	20	11.75	12.00	13.25												
1	22	11.75	12.00	12.25	12.50	12.75										
1	24	12.00	12.25	12.75												
1	26	10.75	11.00	11.25	11.75	12.00	12.25	12.50	12.75	13.00	13.25	13.50	13.75	14.00	14.25	14.50
1	27	11.00	11.25	11.50	11.75	12.00	12.25									
1	30	12.50	12.75	13.00	13.50											
1	31	11.50	11.75	12.00	12.25	12.50	12.75	13.00								
2	2	10.75	11.00	11.25	11.50	11.75	12.00									
2	3	11.50														
2	6	11.25														
2	7	12.25	12.50	12.75	13.00	13.75	14.00	14.25								
2	8	11.50	11.75	12.00	14.00	14.25	14.50	14.75								
2	9	11.50	11.75	12.00	12.25	12.50	12.75	13.00	13.25	13.50	13.75	14.00	14.25			
2	10	11.75	12.00	12.25	12.75	13.00	13.25	13.50								
2	11	13.00	13.25	13.75												
2	12	13.25	13.50	13.75												
2	13	12.25														
2	15	12.00														
2	16	11.75	12.00													
2	18	10.50	10.75	11.00	11.25	11.50	11.75	12.00	12.25	12.50						
2	20	13.25														
2	21	11.75	12.00	12.25	12.50											
2	22	12.50														
2	23	11.75	12.00	12.25	13.25	13.75	14.00	14.25	14.50							
2	24	11.00	11.75	13.00	13.25											
2	25	13.25														
2	27	12.00														
2	28	14.50														
3	1	11.25	11.50	11.75	12.00	12.25	12.50	12.75	13.00	13.25	13.75	14.50				
3	3	13.50														
3	4	12.00	12.50	12.75	13.00	13.25										
3	6	12.25	12.50	12.75	13.00	13.25	13.50	13.75	14.00	14.75	15.25					
3	7	11.00	11.75	13.00												
3	8	10.50	10.75	11.00	11.25	11.50	11.75	12.00	12.25	12.50	12.75	13.00	13.25	13.50	13.75	
3	9	11.00	11.25	11.50	11.75	12.00	12.25	12.50	12.75	13.00	13.25					
3	13	11.50	12.50													
3	14	11.00	11.25	11.50	11.75	12.25										
3	15	9.75	10.00	10.25	10.50	10.75	11.00	11.25	11.50	12.25	12.50	12.75	13.00	13.25	13.50	13.75
3	16	10.50	10.75	11.00	11.25	11.50	11.75	12.00								
3	18	12.00														
3	20	12.50	12.75													
3	21	10.75	11.00	11.25	11.50	11.75	12.00	12.25	12.50	12.75	13.00	13.25				
3	22	10.00	10.25	10.50	10.75	11.00	11.25	12.00	12.25	12.50	12.75	13.25				
3	23	10.00	10.25	10.50	10.75	11.00	11.25	11.50	11.75	12.00	12.25	12.50	12.75	13.00	13.25	13.50
3	25	11.50														
3	28	12.75	13.25	13.75												
3	29	11.00	11.25	11.50	11.75	12.00	12.25	12.50	12.75	13.00	13.25	13.50	13.75	14.00		
4	1	10.75	11.00	11.25	11.50	11.75	12.00	12.25	12.50	12.75	13.00	13.25	13.50			
4	3	10.75														
4	4	11.25														
5	9	10.25														
5	17	14.25														
5	25	13.50														
6	10	10.75														

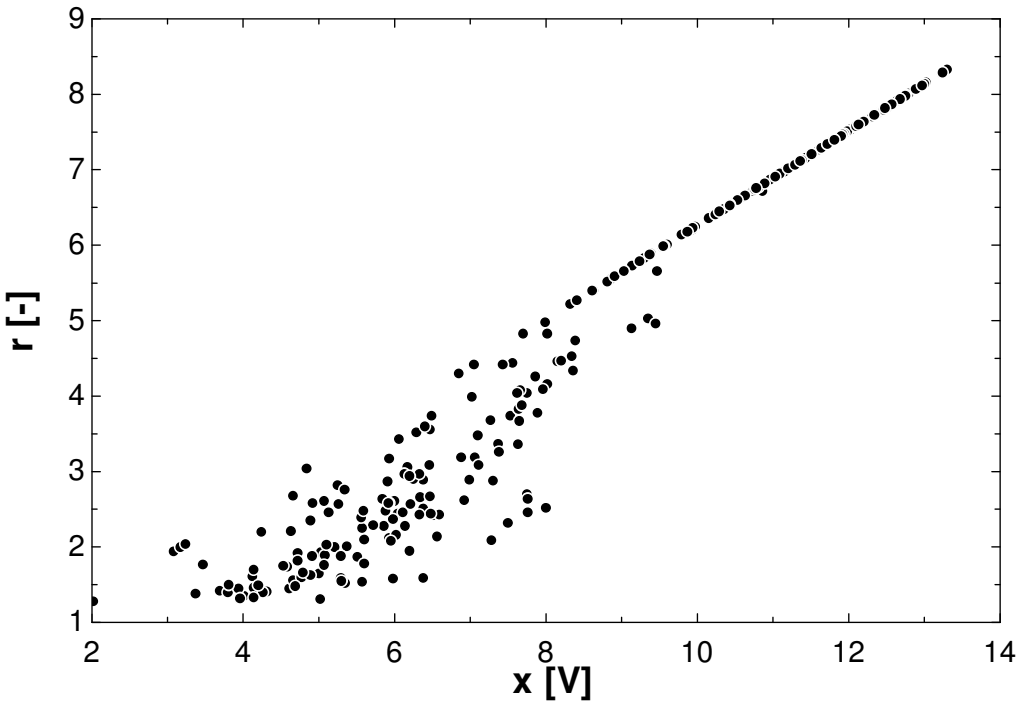

Figure E.1: Plot of r vs. x (Figure 4.3) for points rejected by maximum power point tracking filter.

Appendix F: Module Temperature and Performance Code (EES)

```
$UnitSystem SI  MASS  DEG  PA  K  J
$TABSTOPS   0.25  0.60  0.75  1  2.5 in
$Complex Off

"Procedure to calculate free convection on tilted plate"
PROCEDURE FC_plate_tilted_turb(Fluid$, T_s, T_infinity, P, L, W, angle : h, Nusselt, Ra)
{Inputs:
Fluid$ - string name of a fluid in EES database
T_s - surface temperature of heated/cooled side of plate [C],  [K]
T_infinity - bulk temperature of fluid  [C],  [K]
P - ambient pressure [bar], [Pa], [kPa] or [MPa]
L - length of plate [m]
W - width of plate [m]
angle - tilt of the plate from horizontal

Outputs:
h - average heat transfer coefficient [W/m^2-K]
Nusselt - average Nusselt number [-]
Ra - Raleigh number [-]}
                    g = g#
                    T_avg=(T_s+T_infinity)/2
                    rho=density(Fluid$,T=T_avg,P=P)
                    k=conductivity(Fluid$,T=T_avg)
                    beta=VolExpCoef(Fluid$,T=T_avg)
                    mu=viscosity(Fluid$,T=T_avg)
                    Pr=Prandtl(Fluid$, T=T_avg)
                    nu=mu/rho

{vertical relation adjusted for angle}
"This portion of the code differs from model in EES:
uses Churchill and Chu correlation (Incropera et al., 2006)"
                    Gr=g*sin(angle)*BETA*abs(T_s-T_infinity)*L^3/nu^2
                    Ra=Gr*Pr
                    {call FC_plate_vertical_ND(Ra,Pr:Nusselt)}
                    Nusselt = (0.825 + (0.387*Ra^(1/6))/(1+(0.492/Pr)^(9/16))^(8/27))^2
                    h_vertical=Nusselt*k/L
                    Nusselt_vertical=Nusselt
                    Ra_vertical=Ra

{horizontal up relation}
                    L=L*W/(2*(L+W))
                    Gr=max(1e-6,cos(angle))*g*BETA*abs(T_s-T_infinity)*L^3/nu^2
                    Ra=Gr*Pr
                    if (Ra>1000) then
                              call FC_plate_horizontal1_ND(Ra,Pr:Nusselt)
                              h_horiz1=Nusselt*k/L
                    else
                              h_horiz1=0.1
                    endif
                    Ra_horiz1=Ra
                    Nusselt_horiz1=h_horiz1*L/k

{horizontal down relation}
```

```
                Gr=max(1e-6,-cos(angle))*g*BETA*abs(T_s-T_infinity)*L^3/nu^2
                Ra=Gr*Pr
                if (Ra>1000) then
                        call FC_plate_horizontal2_ND(Ra,Pr:Nusselt)
                        h_horiz2=Nusselt*k/L
                else
                        h_horiz2=0.1
                endif
                Ra_horiz2=Ra
                Nusselt_horiz2=h_horiz2*L/k

                if (h_horiz1>h_horiz2) then
        h=h_horiz1
        Nusselt=Nusselt_horiz1
        Ra=Ra_horiz1
                else
        h=h_horiz2
        Nusselt=Nusselt_horiz2
        Ra=Ra_horiz2
                endif
                if (h_vertical>h) then
        h=h_vertical
        Nusselt=Nusselt_vertical
        Ra=Ra_vertical
                endif
                h2=max(h_vertical,h_horiz1,h_horiz2)
end

"******************* SUBPROGRAM TO CALCULATE POWER
                ***********************************"
Subprogram Power( S_HDKR1, T_cell1_K, E_g_ref, C, refTable$, RowModule:P_mp_mod1)
"This subprogam calculates power using the 5-parameter model most
recently detailed by Boyd, 2010."
"!Avoid using Common$ command to import variables to subprogram!"

numSeries       = Lookup(refTable$, RowModule, 'numSeries') "number of modules in parallel"
I_L_ref         = Lookup( refTable$, RowModule, 'I_L_ref' )       "light current at SRC"
I_o_ref         = Lookup( refTable$, RowModule, 'I_o_ref' )"reverse-saturation current at SRC"
a_ref           = Lookup( refTable$, RowModule, 'a_ref' )         "ideality factor at SRC"
R_sh_ref        = Lookup( refTable$, RowModule, 'R_sh_ref' )    "shunt resistance at SRC"
R_s_ref         = Lookup( refTable$, RowModule, 'R_s_ref' )      "series resistance at SRC"
T_c_ref         = Lookup( refTable$, RowModule, 'T_c_ref' )    "cell temperature at SRC"
T_K_ref         = ConvertTemp( C, K, T_c_ref )    "reference temperature"
alpha_I_sc= Lookup( refTable$, RowModule, 'alpha_I_sc' ) "short circuit temp coef"
S_ref           = Lookup( refTable$, RowModule, 'S_ref' )     "A CONSTANT VALUE"
S\S_ref         = S / S_ref "ratio of absorbed at simulation conditions to SRC conditions"
T_K             = T_cell1_K
S               = S_HDKR1

"SOLVING FOR FIVE OPERATING PARAMETERS"
 "temperature and radiation dependence of light current"
I_L             = S\S_ref * ( I_L_ref  +  alpha_I_sc * ( T_K  -  T_K_ref ) )
"temp. dep. of rev. sat. current"
I_o             = I_o_ref * ( T_K / T_K_ref )^3 * exp( E_g_ref / (k#*T_K_ref)  -  E_g / (k#*T_K) )
 "temperature dependence of material bandgap energy"
```

```
E_g             = E_g_ref * ( 1  -  C * ( T_K  -  T_K_ref ) )
a               = a_ref * T_K/T_K_ref     "temperature dependence of a"
R_sh            = R_sh_ref / S\S_ref     "radiation dependence for R_sh"
R_s             = R_s_ref      "no temperature dependence assumed for R_s"

"SOLVING FOR MAX POWER"
"Characteristic equation for current evaluated for max power"
I_mp_mod1       = ( I_L  -  I_o * ( exp( (V_mp_mod+I_mp_mod1*R_s)/a ) - 1 )  -  ( V_mp_mod + &
                                        I_mp_mod1 * R_s ) / R_sh )
"Derivative of characteristic equation for power (I*V) set to 0 and evaluated for max power"
0               = I_mp_mod1  +  V_mp_mod * dI\dV_mp_mod
P_3             = exp( (V_mp_mod  +  I_mp_mod1 * R_s) / a )
dI\dV_mp_mod    = ( -I_o / a * P_3  -  1 / R_sh ) / ( 1  +  (I_o * R_s) / a * P_3  +  R_s / R_sh )
I_mp_mod        = I_mp_mod1
P_mp_mod1       = I_mp_mod * V_mp_mod    "max power"

"SOLVING FOR SHORT CIRCUIT"
I_sc_mod1       = ( I_L  -  I_o * ( exp( I_sc_mod1*R_s/a ) - 1 )  -  I_sc_mod1 * R_s / R_sh )
I_sc_mod        = I_sc_mod1

"SOLVING FOR OPEN CIRCUIT"
I_L             = I_o * ( exp( V_oc_mod / a ) - 1 )  +  V_oc_mod / R_sh

end
"************************ END POWER SUBPROGRAM *******************"
"!********************** SUBPROGRAM FINDTEMPSS ********************!"
SubProgram FindTempSS (  S_HDKR, Length_defined, u_measured, epsilon_2, Q_abs, &
R_1, Area, T_amb, T_indoor, epsilon_1, F1, T_sky, F2, R_2, E_g_ref,C,refTable$,RowModule,&
T_prop, P_atm, Length, Width, Beta, numSeries, numParallel, T_1, T_2, T_3, Pmp_pred_total, &
u_infinity  )

"Steady state energy balance temperature model"
T_ground        = T_amb   "Ground temperature = ambient temperature"
u_infinity      = u_measured
fluid$          = 'air'
k_out           = CONDUCTIVITY(fluid$, T=T_prop)    "Thermal Conductivity of Air"
rho_out         = Density(fluid$, P=P_atm, T=T_prop)  "Density of Air"
mu_out          = Viscosity(fluid$, T=T_prop)          "Viscosity of Air"
Pr_out          = Prandtl(fluid$, T=T_prop)            "Prandtl Number of Air"
Re_air_s        = max(0.01 [m/s], rho_out*u_infinity*Length_defined/mu_out) "Reynolds Number"
cp_out          = cp(fluid$, T=T_prop)        "Specific Heat of Air"
"Nusselt Number: Incropera et al., 2006.  Eq 7.38, A = 0"
Nusselt_bar_forced_s   = 0.037 * Re_air_s^(4/5) * Pr_out^(1/3)
h_bar_forced_s   = Nusselt_bar_forced_s * k_out / Length_defined "Heat transfer coef."

"Solve for free convection heat transfer coefficient - COVER"
Call FC_plate_tilted_turb(Fluid$, T_1, T_amb, P_atm, Length, Width, beta: &
                                    h_bar_free_up, Nusselt_free_up, Ra_free_up)
"Combine Free and Forced Convection - COVER"
h_bar_top       = (h_bar_forced_s^(3) + h_bar_free_up^(3))^(1/3)

"Solve for free convection heat transfer coefficient - BACKSIDE"
Call FC_plate_tilted_turb(Fluid$, T_3, T_amb, P_atm, Length, Width, &
                    180 [deg] - beta: h_bar_free_down, Nusselt_free_down, Ra_free_down)
 "Combine Free and Forced Convection - BACKSIDE"
```

```
h_bar_bottom      = (h_bar_forced_s^(3) + h_bar_free_down^(3))^(1/3)

"Absorbed Radiation Minus Power Flux"
q_flux_solar      = max(0.01 [W/m^2], S_HDKR) - (Pmp_pred/Area)

"Define backside temps based on Mounting"
T_back            = T_amb
T_back_sky        = T_sky
T_back_gr         = T_ground

"Energy Balance on Node 1"
Q_abs + (T_2 - T_1)/R_1 - (h_bar_top*Area*(T_1 - T_amb) + epsilon_1*F1*&
sigma#*Area*(T_1^4 - T_sky^4) + epsilon_1*F2*sigma#*Area*(T_1^4 - T_ground^4)) = 0

"Energy Balance on Node 2"
q_flux_solar*Area + (T_3 - T_2)/(R_2) - (T_2 - T_1)/(R_1) = 0

"Energy Balance on Node 3"
-(T_3 - T_2)/(R_2) - (h_bar_bottom*Area*(T_3 - T_back) + epsilon_2*F2*sigma#*&
Area*(T_3^4 - T_back_sky^4) + epsilon_2*F1*sigma#*Area*(T_3^4 - T_back_gr^4)) = 0

T_cell            = T_2
"Call subprogram to calculate power"
Call Power( S_HDKR, T_cell, E_g_ref, C, refTable$, RowModule : Pmp_pred )
Pmp_pred_total    = numSeries * Pmp_pred * numParallel "Calculate total power"

end
"!************* END SUBPROGRAM FINDTEMP ***********************************!"
"******** START SUBPROGRAM FINDTEMPDUFFIE ****************************"
Subprogram FindTempDuffie( T_NOCT_C, S_HDKR, u_measured, T_amb, E_g_ref,&
C,refTable$,RowModule,numSeries,numParallel,S_HDKR_NOCT,T_cell,Pmp_pred_total)

"Duffie and Beckman (2006) temperature model"
T_NOCT            = convertTemp( C, K, T_NOCT_C )
T_amb_NOCT_C              = 20 [C]
T_amb_NOCT        = convertTemp( C, K, T_amb_NOCT_C )
u_infinity        = u_measured

(T_module - T_amb) / (T_NOCT - T_amb_NOCT) = ( 9.5 / ( 5.7 + 3.8*u_infinity ))*&
((S_HDKR - Pmp_pred) / S_HDKR_NOCT)

T_cell            = T_module
Call Power( S_HDKR, T_cell, E_g_ref, C, refTable$, RowModule : Pmp_pred )
Pmp_pred_total    = numSeries * Pmp_pred * numParallel

end
"******* END PROGRAM FINDTEMPDUFFIE *************************************"
"!**START SUBPROGRAM FINDTEMPSKOPLAKI ******************************!"
Subprogram FindTempSkoplaki( S_HDKR, u_measured, T_amb, G_T, omega_m, &
E_g_ref, C, refTable$, RowModule, numSeries, numParallel, T_cell, Pmp_pred_total )

"Sloplaki et al. (2008) temperature model"
u_infinity        = u_measured
T_module          = T_amb + omega_m * ( 0.32 / ( 8.91 + 2 * u_infinity )) * G_T
T_cell            = T_module
```

```
Call Power( S_HDKR, T_cell, E_g_ref, C, refTable$, RowModule : Pmp_pred )
Pmp_pred_total   = numSeries * Pmp_pred * numParallel

end
"!*** END SUBPROGRAM FINDTEMPSKOPLAKI ******************************!"
"***** START SUBPROGRAM FINDTEMPKING *********************************"
Subprogram FindTempKing( S_HDKR, G_T, T_amb, u_measured, a_king, b_king,&
DELTA_T_King, G_T_ref_King, E_g_ref, C, refTable$, RowModule, numSeries, &
numParallel, T_cell, Pmp_pred_total )

 "King et al. (2006) temperature model"
u_infinity          = u_measured
T_m_King            = G_T * exp(a_King + b_King*u_infinity) + T_amb
T_module            = T_m_King + (G_T / G_T_ref_King) * DELTA_T_King
T_cell              = T_module
Call Power( S_HDKR, T_cell, E_g_ref, C, refTable$, RowModule : Pmp_pred )
Pmp_pred_total   = numSeries * Pmp_pred * numParallel

end
"******* END SUBPROGRAM FINDTEMPKING ***********************************"
"!**START PROCEDURE WIND ADJUSTMENT FINDTEMP ****************!"
procedure AdjustWind( Building_Code, u_avg, z_0_M, height_meas, height_panel: u_infinity )

"!POWER LAW ADJUSTMENT"
"Building Code = 0: Do not adjust for building proximity"
alpha_wind_0      = 0.096 * log10( z_0_M ) + 0.016 * ( log10(z_0_M) )^2 + 0.24
u_adjusted_0      = u_avg*(height_panel/height_meas)^(alpha_wind_0)

"! LOVEDAY & TAKI METHOD AS DETAILED IN DEC-JAN REPORT !"
"Building Code = 2: Assume leeward for all wind directions"
height_LD_roof  = 39 [m]
height_LD_wall  = 19.25 [m]
alpha_wind_0      = 0.096 * log10( z_0_M ) + 0.016 * ( log10(z_0_M) )^2 + 0.24
u_infinity_LD_roof          = u_avg*(height_LD_roof/height_meas)^(alpha_wind_0)
u_infinity_LD_wall          = 0.157*u_infinity_LD_roof - 0.027
u_adjusted_2                = u_infinity_LD_wall*(height_panel/height_LD_wall)^(alpha_wind_0)

if( Building_Code = 0 ) then u_infinity := u_adjusted_0
if( Building_Code = 2 ) then u_infinity := u_adjusted_2

end
"* PROCEDURE TO CALCULATE COVER PROPERTIES
DEPENDENT ON INCIDENCE ANGLES*******"
procedure Transmission( n_air, n_glaz, K, L, theta`: tau·alpha, alpha)

"transmittance-absorptance product & absorptance (with reflectance = 0)"
theta               = MAX(1e-9 [deg], theta` )
theta_r             = arcSin( n_air / n_glaz * sin( theta ))    "Snell's Law"
tau·alpha           = exp(( -K * L) / cos( theta_r )) * ( 1 - 1/2 * (( sin( theta_r - theta))^2&
                          / ( sin( theta_r + theta))^2 + ( tan ( theta_r - theta))^2 &
                          / ( tan ( theta_r + theta))^2 ))   "Eq 5.12.4, Duffie & Beckman"
tau_a               = exp(( -K * L) / cos( theta_r ))    "Eq 5.2.2, Duffie & Beckman"
alpha               = 1 - tau_a     "Eq 5.3.5, Duffie & Beckman"

end
```

```
"*****************END PROCEDURE*************************************"
"!********************** I N P U T S ****************************************!"
directory$        = 'Directory_of_EES_file'
row               = 1
module$           =  'Name_of_Module'

"Lookup File Containing Weather and Performance Data"
lktPathIn$        = concat$(directory$,concat$(module$,'*NAME*.lkt'))
"Lookup File Containing Module Data and Information"
refTable$         = concat$(directory$,'*NAME*.lkt')
RowModule         = LOOKUP$ROW( refTable$, 'Module', module$)

"Inputs"
day               = Lookup( lktPathIn$, row, 'Day' )
month             = Lookup( lktPathIn$, row, 'Month' )
Time_STD          = Lookup( lktPathIn$, row, 'Time' )
T_amb_C           = Lookup( lktPathIn$, row, 'T_amb' )
T_indoor_C        = Lookup( lktPathIn$, row, 'T_indoor' )
G                 = Lookup( lktPathIn$, row, 'G' )
G_bn              = Lookup( lktPathIn$, row, 'G_bn' )
G_d               = Lookup( lktPathIn$, row, 'G_d' )
u_avg             = Lookup( lktPathIn$, row, 'u_avg' )
T_dew_F           = Lookup( lktPathIn$, row, 'T_dew' )
Pmp_meas          = Lookup( lktPathIn$, row, 'Pmp' )
T_meas_C          = Lookup( lktPathIn$, row, 'T_module' )

"CHOOSE METHOD TO CALCULATE WIND SPEED"
"! Does wind speed need to be adjusted for proximity to building? !"
Building_Code     = Lookup(refTable$, RowModule, 'Building Code')
"! Surface roughness (Manwell) for panel location !"
z_0_M             = Lookup(refTable$, RowModule, 'z_0_Manwell')
"! Measurement and panel heights !"
height_meas       = Lookup(refTable$, RowModule, 'height_meas_wind')
height_panel      = Lookup(refTable$, RowModule, 'height_panel')
"! Call procedure to calculate wind adjustment for site !"
Call AdjustWind( Building_Code, u_avg, z_0_M, height_meas, height_panel: u_infinity )

"****************CALCULATIONS*************************************"
"Convert Input Units"
T_amb             = convertTemp( C, K, T_amb_C  )
T_dew_C           = convertTemp( F, C, T_dew_F )
T_meas            = convertTemp( C, K, T_meas_C )
T_indoor          = convertTemp( C, K, T_indoor_C )

"PROVIDE FREE STREAM (10 m) WIND SPEED"
z_0               = 250 [-]
alpha_w           = 0.096 * log10( z_0 ) + 0.016 * ( log10(z_0) )^2 + 0.24
h_wm              = 2.3 [m]
h_10              = 10 [m]
u_infinity        = u_10 * ( h_wm / h_10 ) ^ (alpha_w)

"Calculate Temperature with Steady State Model"
Call FindTempSS ( S_HDKR, L_char, u_infinity, eps_back, Q_abs, R_1,&
Area, T_amb, T_indoor, epsilon_1, F1, T_sky, F2, R_2, E_g_ref, C, refTable$,&
RowModule, T_prop, P_atm, Length, Width, Beta, numSeries, numParallel,&
```

```
T_cover_pred, T_cell_pred, T_back_pred, Pmp_pred, u_avg_adj)

"Calculate Temperature with Duffie and Beckman Model"
{Call FindTempDuffie( NOCT, S_HDKR, u_infinity, T_amb, E_g_ref, C, &
refTable$, RowModule, numSeries, numParallel, S_HDKR_NOCT, T_cell_pred, Pmp_pred )}

"Calculate Temperature with Skoplaki Model"
"u_infinity for BIPV, u_10 for rack mounted"
{Call FindTempSkoplaki( S_HDKR, u_10, T_amb, G_T_HDKR, omega_m,&
E_g_ref, C, refTable$, RowModule, numSeries, numParallel, T_cell_pred, Pmp_pred )}

"Calculate Temperature with King Model"
"u_infinity for BIPV, u_10 for rack mounted"
{Call FindTempKing( S_HDKR, G_T_HDKR, T_amb, u_10, a_king, b_king,&
DELTA_T_King, G_T_ref_King, E_g_ref, C, refTable$, RowModule,&
numSeries, numParallel, T_cell_pred, Pmp_pred )}

"Location"
lat             = Lookup( refTable$, RowModule, 'Latitude' )
long            = Lookup( refTable$, RowModule, 'Longitude' )
L_st            = Lookup( refTable$, RowModule, 'Standard Meridian TZ' )
rho_g           = 0.1    "Ground reflectance"

"Geometry"
beta            = Lookup( refTable$, RowModule, 'Beta' )
gamma           = Lookup( refTable$, RowModule, 'Gamma' )

"Panel Dimensions"
Length          = Lookup( refTable$, RowModule, 'Panel_Length' ) "Length (or height) of module"
Width           = Lookup( refTable$, RowModule, 'Panel_Width' )   "Width of module"
Area            = Length * Width"Area of module"
numSeries       = Lookup( refTable$, RowModule, 'numSeries' )    "Number of modules in parallel"
numParallel     = Lookup( refTable$, RowModule, 'numParallel' )  "Number of modules in series"

"Thermal Model Inputs"
                "King Model"
a_king          = Lookup( refTable$, RowModule, 'a_king' )
b_king          = Lookup( refTable$, RowModule, 'b_king' )
DELTA_T_King = Lookup( refTable$, RowModule, 'DELTA_T_King' )
G_T_ref_King    = 1000 [W/m^2]
                "Skoplaki Model"
omega_m         = Lookup( refTable$, RowModule, 'omega_m' )

"Panel Cover Properties"
n_glaz = Lookup(refTable$,RowModule,'Refrac Index (n_glaz)')"Refractive index of glass cover"
K               = Lookup( refTable$, RowModule, 'Glaz Ext. Coeff. (K)' )
L_1             = Lookup( refTable$, RowModule, 'Glaz Thick (L)' )   "Thickness of cover"
k_1             = Lookup( refTable$, RowModule, 'k_cover' )
S_ref           = Lookup( refTable$, RowModule, 'S_ref' )
S_HDKR_NOCT             = Lookup( refTable$, RowModule, 'S_ref_NOCT' )
epsilon_1       = Lookup( refTable$, RowModule, 'epsilon' )

"Internal Thermal Resistances"
R_1             = (L_1)/(k_1*Area)
R_2             = Lookup( refTable$, RowModule, 'R2' )
```

```
NOCT            = Lookup( refTable$, RowModule, 'NOCT' )

"Backside Emissivity"
eps_back        = 0.7

"Electrical Properties"
I_mp_ref        = Lookup( refTable$, RowModule, 'I_mpo' )
V_mp_ref        = Lookup( refTable$, RowModule, 'V_mpo' )
P_mp_ref        = I_mp_ref * V_mp_ref * numSeries

"Constants for Performance Model"
n_air           = 1 [-]    "Refractive index of air"

"matl. bandgap energy for Si at ref. - okay for all techs: Boyd 2010
** Must use value that 5 - parameters are calculated with if this is changed **!!"
E_g_ref         = 1.121 [eV] * Convert( eV, J )
"**Must use value that 5-parameters are calculated with if this is changed**!!"
C               = 0.0002677 [1/K]    "matl. bandgap % temp. depen. for Si"

"Environmental Conditions for Constant Fluid Properties"
"Either lookup or specify atmospheric pressure"
{P_atm          = Lookup(refTable$, RowModule, 'P_atm_site') * convert(atm, Pa)}
P_atm           = 1 [atm] * convert(atm, Pa)
"Temperature used to calculate fluid (air) properties"
T_prop          = 315 [K]

"Solar Angle and Time Equations"
n               = nDay_( month, day)
E               = EqnTime_( n )     "equation of time - minute correction"
time_sol        = Time_STD  +  ( 4 [min/°] * ( L_st  -  long )  +  E ) / 60 [min/hr]        "solar time"
omega           = 15 [ °/hr] * ( time_sol - 12.00 [hr] )    "Hour angle"
arctheta        = CosIncAng_( lat, n, omega, beta, gamma)
theta_b         = arcCos ( CosIncAng_( lat, n, omega, beta, gamma))   "Incidence Angle on Panel"

"Geometry Inputs For Radiation Models"
R_b = R_Beam_(lat,n,omega,beta,gamma)"ratio of beam radiation on tilted to horizontal surface"
theta_z   = arcCos( CosZenAng_( lat, n, omega ) ) "zenith angle"
theta_d  = 59.7 [ °]  -  0.1388 * beta  +  0.001497 [1/ °] * beta^2 "eff. diffuse inc. angle, eqn. 5.4.2"
theta_g  = 90[°] - 0.5788*beta+0.002693[1/ °]*beta^2 "eff. ground reflect. inc. angle, eqn. 5.4.1"

"Transmittance-absorptance products and incidence angle modifiers"
"transmittance-absorptance product at NORMAL incidence angle."
Call Transmission( n_air, n_glaz, K, L_1, 0 [ °] :   tau·alpha_n, alpha_n  )
"transmittance-absorptance product at BEAM incidence angle."
Call Transmission  (   n_air, n_glaz, K, L_1, theta_b :   tau·alpha_b, alpha_b  )
"transmittance-absorptance product at DIFFUSE incidence angle."
Call Transmission  (   n_air, n_glaz, K, L_1, theta_d :   tau·alpha_d, alpha_d  )
"transmittance-absorptance product at GROUND reflected incidence angle."
Call Transmission  (   n_air, n_glaz, K, L_1, theta_g :   tau·alpha_g, alpha_g)
K_tau·alpha_b  = tau·alpha_b / tau·alpha_n   "inc. angle modifier for BEAM component"
K_tau·alpha_d  = tau·alpha_d / tau·alpha_n   "inc. angle modifier for DIFFUSE component"
K_tau·alpha_g  = tau·alpha_g / tau·alpha_n   "inc. angle modifier for GROUND ref. component"

"RADIATION EQUATIONS"
G_b             = max( 0, G_bn * cos( theta_z ) )     "beam radiation on horizontal"
```

```
G_bd            = max(0.1 [W/m^2], G_b + G_d )     "total radiation on a horizontal surface"
G_ref           = 1000 [W/m^2]      "reference radiation for SRC"
"extraterrestrial radiation on a normal surf."
G_on            = 1367 [W/m^2] * ( 1 + 0.033 * cos( 360 [ °] * n / 365 ))
G_o             = G_on * cos( theta_z )     "extraterrestrial radiation on a horiz. surf."
S_ref1          = G_ref * tau·alpha_n     "absorbed radiation on a normal surf at SRC"

"Calculate Incident Radiation - HDKR Model"
"!Horizontal Surface!"
A_i             = G_bn / G_on    "Anisotropy index "
beta_h          = 0 [deg]      "Slope of horizontal plane"
f_HDKR          = sqrt( G_b / MAX(1e-9,G_bd) )   "Modulating factor"
"Incident radiation on a tilted surface"
G_HDKR    = ( G_b + G_d * A_i )  +  G_d * ( 1 - A_i ) * ( (1+cos(beta_h)) / 2 ) *&
                                (1+f_HDKR*(sin(beta_h/2))^3)+G_bd*rho_g*((1-cos(beta_h)) / 2 )
"!Panel Surface!"
"Incident radiation on a tilted surface"
G_T_HDKR    = ( G_b + G_d * A_i ) * R_b  +  G_d * ( 1 - A_i ) * ( (1+cos(beta)) / 2 )&
                    * ( 1 + f_HDKR * ( sin( beta/2 ) )^3 )+G_bd * rho_g * ( (1-cos(beta)) / 2 )

"Calculate Cell Absorbed Solar Radiation"
                "Component incident at BEAM incidence angle"
S_b_HDKR        = tau·alpha_n * ( G_b + G_d * A_i ) * R_b * K_tau·alpha_b
                "Component incident at DIFFUSE incidence angle"
S_d_HDKR        = tau·alpha_n * G_d * ( 1 - A_i ) * ( (1+cos(beta)) / 2 ) *&
                  ( 1 + f_HDKR * ( sin( beta/2 ) )^3 ) * K_tau·alpha_d
                "Ground reflected"
S_gr_HDKR       = tau·alpha_n * G_bd * rho_g * ( (1-cos(beta)) / 2 ) * K_tau·alpha_g
S_HDKR          =  S_b_HDKR  +  S_d_HDKR  +  S_gr_HDKR    "Total"

"Calculate Cover Absorbed Radiation"
Q_abs_b_HDKR = ( G_b + G_d * A_i ) * R_b * alpha_b
Q_abs_d_HDKR = G_d * ( 1 - A_i ) * ( (1+cos(beta)) / 2 ) *&
                   ( 1 + f_HDKR * ( sin( beta/2 ) )^3 ) * alpha_d
Q_abs_g_HDKR = G_bd * rho_g * ( (1-cos(beta)) / 2 ) * alpha_g
Q_abs_HDKR      = Q_abs_b_HDKR + Q_abs_d_HDKR + Q_abs_g_HDKR
Q_abs           = max(0.01 [W], Q_abs_HDKR * Area)

"View Factors"
F_ground        = F3D_27(Beta)
F_sky           = 1 - F_ground
F1              = F_sky
F2              = F_ground

"Sky Temperature: Choose Correlation"
T_sky           = T_amb * (0.711 + 0.0056 * T_dew_C + 0.000073 &
                * T_dew_C^2 + 0.013 * cos(time_sol))^(0.25)  "Berdahl and Martin"
{T_sky          = 0.0552 * T_amb^(1.5)    "Swinbank and Roy"}

"Important Panel Dimensions"
Perimeter       = 2*Width + 2*Length     "Perimeter of Panel"
L_char          = 4*Area / Perimeter
```

Appendix G: NOCT Prediction Code (EES)

```
$UnitSystem SI  MASS  DEG  PA  K  J

$TABSTOPS   0.25  0.60  0.75  1  2.5 in

"Procedure to calculate free convection on tilted plate"
PROCEDURE FC_plate_tilted_turb(Fluid$, T_s, T_infinity, P, L, W, angle : h, Nusselt, Ra)
{Inputs:
Fluid$ - string name of a fluid in EES database
T_s - surface temperature of heated/cooled side of plate [C],  [K]
T_infinity - bulk temperature of fluid  [C],  [K]
P - ambient pressure [bar], [Pa], [kPa] or [MPa]
L - length of plate [m]
W - width of plate [m]
angle - tilt of the plate from horizontal

Outputs
h - average heat transfer coefficient [W/m^2-K]
Nusselt - average Nusselt number [-]
Ra - Raleigh number [-]}

                g = g#
                T_avg=(T_s+T_infinity)/2

                rho=density(Fluid$,T=T_avg,P=P)
                k=conductivity(Fluid$,T=T_avg)
                beta=VolExpCoef(Fluid$,T=T_avg)
                mu=viscosity(Fluid$,T=T_avg)
                Pr=Prandtl(Fluid$, T=T_avg)
                nu=mu/rho

{vertical relation adjusted for angle}
"This portion of the code differs from model in EES:
uses Churchill and Chu correlation (Incropera et al., 2006)"
                Gr=g*sin(angle)*BETA*abs(T_s-T_infinity)*L^3/nu^2
                Ra=Gr*Pr
                {call FC_plate_vertical_ND(Ra,Pr:Nusselt)}
                Nusselt = (0.825 + (0.387*Ra^(1/6))/(1+(0.492/Pr)^(9/16))^(8/27))^2
                h_vertical=Nusselt*k/L
                Nusselt_vertical=Nusselt
                Ra_vertical=Ra

{horizontal up relation}
                L=L*W/(2*(L+W))
                Gr=max(1e-6,cos(angle))*g*BETA*abs(T_s-T_infinity)*L^3/nu^2
                Ra=Gr*Pr
                if (Ra>1000) then
                        call FC_plate_horizontal1_ND(Ra,Pr:Nusselt)
                        h_horiz1=Nusselt*k/L
                else
                        h_horiz1=0.1
                endif
                Ra_horiz1=Ra
                Nusselt_horiz1=h_horiz1*L/k
```

```
{horizontal down relation}
                    Gr=max(1e-6,-cos(angle))*g*BETA*abs(T_s-T_infinity)*L^3/nu^2
                    Ra=Gr*Pr
                    if (Ra>1000) then
                              call FC_plate_horizontal2_ND(Ra,Pr:Nusselt)
                              h_horiz2=Nusselt*k/L
                    else
                              h_horiz2=0.1
                    endif
                    Ra_horiz2=Ra
                    Nusselt_horiz2=h_horiz2*L/k

                    if (h_horiz1>h_horiz2) then
        h=h_horiz1
        Nusselt=Nusselt_horiz1
        Ra=Ra_horiz1
                    else
        h=h_horiz2
        Nusselt=Nusselt_horiz2
        Ra=Ra_horiz2
                    endif
                    if (h_vertical>h) then
        h=h_vertical
        Nusselt=Nusselt_vertical
        Ra=Ra_vertical
                    endif
                    h2=max(h_vertical,h_horiz1,h_horiz2)
end

"* PROCEDURE TO CALCULATE COVER PROPERTIES
DEPENDENT ON INCIDENCE ANGLES*******"
procedure Transmission( n_air, n_glaz, K, L, theta`: tau·alpha, alpha)

"transmittance-absorptance product & absorptance (with reflectance = 0)"
theta               = MAX(1e-9 [deg], theta` )
theta_r             = arcSin( n_air / n_glaz * sin( theta ))    "Snell's Law"
tau·alpha           = exp(( -K * L) / cos( theta_r )) * ( 1 - 1/2 * (( sin( theta_r - theta))^2&
                              / ( sin( theta_r + theta))^2 + ( tan ( theta_r - theta))^2 &
                              / ( tan ( theta_r + theta))^2 ))   "Eq 5.12.4, Duffie & Beckman"
tau_a               = exp(( -K * L) / cos( theta_r ))    "Eq 5.2.2, Duffie & Beckman"
alpha               = 1 - tau_a     "Eq 5.3.5, Duffie & Beckman"

end

"! ************************ I N P U T S ************************************************!"
"Verify Module-Dependent Parameters Contained in Lookup Table"
directory$          = 'Directory_of_EES_file'
refTable$           = concat$(directory$,'*NAME*.lkt')
RowModule           = LOOKUP$ROW( refTable$, 'Module', module$)
module$             =  'Name_of_Module'

"ESTIMATED BACKSIDE EMISSIVITY"
eps_backside        = 0.7
"PANEL SLOPE AT NTE CONDITIONS"
```

```
"IEC Standards"
beta                = 45 [deg]  "IEC Value"
"ASTM Standard"
"Panel should be normal to the sun at noon"

"SOLVING FOR R2 WITH KNOWN NOCT, OR NOCT WITH KNOWN R2"
"Known NOCT, solve for R2"
{T_cell_C                   = NOCT_provided}

                    " OR "
"Known R2, solve for NOCT"
R2                  = Lookup( refTable$, RowModule, 'R2' )

"ENVIRONMENTAL CONDITIONS DURING TESTING"
T_amb_C             = 20 [C]    "5[C] < T_amb_C < 35[C]"
u_wind              = 1 [m/s]   "0.25 [m/s] < u_wind < 1.75 [m/s]"

"INPUTS FOR HDKR RADIATION MODEL"
"Ground reflectivity"
rho_g               = 0.1       "Reflectance of Surroundings"
"Radiation Values"
G_T                 = 800 [W/m^2]  "NOCT specified"
G_T_HDKR            = G_T
G_d / G_bd          = 0.15

"Geometry and Time"
theta               = 0 [deg] "Assume beam radiation is normal to panel"
theta_z             = Beta    "Which makes zenith angle equal to slope of panel"
n                   = 220     "Use Eq. 1.6.1a and try to find average declination as calculated in report for
                    average slope at NOCT"

"! ************************ E N D     O F     I N P U T S
                    ************************************************************************
                    ***** !"

"Panel Dimensions - Needed for heat transfer coefficients"
Length              = Lookup( refTable$, RowModule, 'Panel_Length' )
W                   = Lookup( refTable$, RowModule, 'Panel_Width' )
Area                = Length * W
Perimeter           = 2*Length + 2*W
L_char              = 4*Area / Perimeter

"Define Backside Resistance - OR - comment out and solve"
"View Factors Dependent on Slope"
F1                  = F3D_27(180[deg] - Beta)  "Panel to sky (front)"
F2                  = 1 - F1       "Panel to ground (front)"
F_ground            = F3D_27( Beta )
F_sky               = 1 - F_ground

"Environmental Conditions During Testing"
T_amb               = convertTemp(C,K, T_amb_C)
NOCT_provided       = Lookup( refTable$, rowModule, 'NOCT Uninsulated' )

"Environmental Conditions at NTE "
T_amb_C_NTE         = 20 [C]
```

```
u_wind_NTE      = 1 [m/s]
T_amb_NTE       = convertTemp(C,K, T_amb_C_NTE)

"Results of Steady State Energy Balances Below"
"Cell Temperature at Environmental Conditions During Testing"
T_cell          = convertTemp(C, K, T_cell_C)

"Cell Temperature at NTE"
T_cell_NTE_C    = convertTemp(K,C,T_cell_NTE)

"Calculated Correction Factor "
cf              = (T_cell_NTE_C - 20 [C]) - (T_cell_C - T_amb_C)
DELTA_T         = T_cell_C - T_amb_C  "May be of interest"

"Panel Properties"
eps_cover       = Lookup( refTable$, rowModule, 'epsilon')
L_A             = Lookup(refTable$, rowModule, 'Glaz Thick (L)')  "Cover Thickness"
k_A             = Lookup(refTable$, rowModule, 'k_cover')  "Cover Conductivity"
R_A             = (L_A/(k_A * Area))
R1              = R_A   "Easier to Relate to similar variables"
L\k1            = R1*Area

"Fluid Properties"
P_atm           = 101000 [Pa]  "Atmospheric Pressure"
Fluid$          = 'Air'

"Cover and Air Properties"
n_air           = 1[-]    "air refraction index"
n_glaz          = Lookup( refTable$, rowModule, 'Refrac Index (n_glaz)' )  "glazing refractive index"
K               = Lookup( refTable$, rowModule, 'Glaz Ext. Coeff. (K)' )   "glazing extinction
                coefficient"
L               = L_A    "glazing thickness"

"GEOMETRY AND TIME"
R_b  = cos(theta)/cos(theta_z)    "ratio of radiation on tilted to horizontal surface"
theta_d  = 59.7 [°]  -  0.1388 * beta  +  0.001497 [1/°] * beta^2   "eff. diffuse inc. angle, eqn. 5.4.2"
theta_g  = 90[°] - 0.5788*beta+0.002693 [1/°] * beta^2   "eff. ground reflect. inc. angle, eqn. 5.4.1"

"Transmittance-absorptance products and incident angle modifiers"
"transmittance-absorptance product at NORMAL incidence angle."
Call Transmission( n_air, n_glaz, K, L_1, 0 [ °] :   tau·alpha_n, alpha_n  )
"transmittance-absorptance product at BEAM incidence angle."
Call Transmission  (   n_air, n_glaz, K, L_1, theta_b :   tau·alpha_b, alpha_b  )
"transmittance-absorptance product at DIFFUSE incidence angle."
Call Transmission  (   n_air, n_glaz, K, L_1, theta_d :   tau·alpha_d, alpha_d  )
"transmittance-absorptance product at GROUND reflected incidence angle."
Call Transmission  (   n_air, n_glaz, K, L_1, theta_g :   tau·alpha_g, alpha_g)
K_tau·alpha_b  = tau·alpha_b / tau·alpha_n   "inc. angle modifier for BEAM component"
K_tau·alpha_d  = tau·alpha_d / tau·alpha_n   "inc. angle modifier for DIFFUSE component"
K_tau·alpha_g  = tau·alpha_g / tau·alpha_n   "inc. angle modifier for GROUND ref. component"

"RADIATION EQUATIONS"
G_b             = max( 0, G_bn * cos( theta_z ) )     "beam radiation on horizontal"
G_bd            = max(0.1 [W/m^2], G_b + G_d )     "total radiation on a horizontal surface"
G_ref           = 1000 [W/m^2]      "reference radiation for SRC"
```

```
"extraterrestrial radiation on a normal surf."
G_on            = 1367 [W/m^2] * ( 1 + 0.033 * cos( 360 [ °] * n / 365 ))
G_o             = G_on * cos( theta_z )     "extraterrestrial radiation on a horiz. surf."
S_ref1          = G_ref * tau·alpha_n     "absorbed radiation on a normal surf at SRC"

"Calculate Incident Radiation - HDKR Model"
"!Horizontal Surface!"
A_i             = G_bn / G_on    "Anisotropy index "
beta_h          = 0 [deg]      "Slope of horizontal plane"
f_HDKR          = sqrt( G_b / MAX(1e-9,G_bd) )   "Modulating factor"
"Incident radiation on a tilted surface"
G_HDKR    = ( G_b + G_d * A_i )  +  G_d * ( 1 - A_i ) * ( (1+cos(beta_h)) / 2 ) *&
                              (1+f_HDKR*(sin(beta_h/2))^3)+G_bd*rho_g*((1-cos(beta_h)) / 2 )
"!Panel Surface!"
"Incident radiation on a tilted surface"
G_T_HDKR    = ( G_b + G_d * A_i ) * R_b  +  G_d * ( 1 - A_i ) * ( (1+cos(beta)) / 2 )&
                 * ( 1 + f_HDKR * ( sin( beta/2 ) )^3 )+G_bd * rho_g * ( (1-cos(beta)) / 2 )

"Calculate Cell Absorbed Solar Radiation"
                "Component incident at BEAM incidence angle"
S_b_HDKR        = tau·alpha_n * ( G_b + G_d * A_i ) * R_b * K_tau·alpha_b
                "Component incident at DIFFUSE incidence angle"
S_d_HDKR        = tau·alpha_n * G_d * ( 1 - A_i ) * ( (1+cos(beta)) / 2 ) *&
                  ( 1 + f_HDKR * ( sin( beta/2 ) )^3 ) * K_tau·alpha_d
                "Ground reflected"
S_gr_HDKR    = tau·alpha_n * G_bd * rho_g * ( (1-cos(beta)) / 2 ) * K_tau·alpha_g
S_HDKR          =  S_b_HDKR  +  S_d_HDKR  +  S_gr_HDKR    "Total"

"Calculate Cover Absorbed Radiation"
Q_abs_b_HDKR  = ( G_b + G_d * A_i ) * R_b * alpha_b
Q_abs_d_HDKR   = G_d * ( 1 - A_i ) * ( (1+cos(beta)) / 2 ) *&
                         ( 1 + f_HDKR * ( sin( beta/2 ) )^3 ) * alpha_d
Q_abs_g_HDKR   = G_bd * rho_g * ( (1-cos(beta)) / 2 ) * alpha_g
Q_abs_HDKR     = Q_abs_b_HDKR + Q_abs_d_HDKR + Q_abs_g_HDKR
Q_abs                                  = max(0.01 [W], Q_abs_HDKR * Area)

"Radiation heat transfer from Cover to Surroundings"
sigma           = sigma#
T_sky           = (0.0552*T_amb^1.5)  "Swinbank and Roy Correlation"
T_ground        = T_amb
T_sky_NTE       = (0.0552*T_amb_NTE^1.5)
T_ground_NTE    = T_amb_NTE
Q_rcs           = F1*eps_cover*sigma*Area*(T_1^4 - T_sky^4) + &
                  F2*eps_cover*sigma*Area*(T_1^4 - T_ground^4)
Q_rcs_NTE       = F1*eps_cover*sigma*Area*(T_1_NTE^4 - T_sky_NTE^4)&
                  + F2*eps_cover*sigma*Area*(T_1_NTE^4 - T_ground_NTE^4)

"Convective Heat Transfer from Cover to Ambient Air"
Call FC_plate_tilted_turb(Fluid$, T_1, T_amb, P_atm, Length, W, beta: &
                                h_free_up, Nusselt_free_up, Ra_free_up)
Call FC_plate_tilted_turb(Fluid$, T_1_NTE, T_amb_NTE, P_atm, Length,&
        W, beta: h_free_up_NTE, Nusselt_free_up_NTE, Ra_free_up_NTE)

T_film_up_NTE  = (T_amb_NTE + T_1_NTE)/2 "Film Temperature"
k_up_NTE        = CONDUCTIVITY(fluid$, T=T_film_up_NTE) "Thermal Conductivity of Air"
```

```
rho_up_NTE      = Density(fluid$, P=P_atm, T=T_film_up_NTE) "Density of Air"
mu_up_NTE       = Viscosity(fluid$, T=T_film_up_NTE) "Viscosity of Air"
Pr_up_NTE       = Prandtl(fluid$, T=T_film_up_NTE) "Prandtl Number of Air"
Re_air_W_up_NTE = max(0.01, rho_up_NTE * u_wind_NTE * L_char / mu_up_NTE)

T_film_up       = (T_amb + T_1)/2    "Film Temperature"
k_up            = CONDUCTIVITY(fluid$, T=T_film_up)    "Thermal Conductivity of Air"
rho_up          = Density(fluid$, P=P_atm, T=T_film_up)   "Density of Air"
mu_up           = Viscosity(fluid$, T=T_film_up)  "Viscosity of Air"
Pr_up           = Prandtl(fluid$, T=T_film_up)  "Prandtl Number of Air"
Re_air_W_up     = max(0.01, rho_up * u_wind * L_char / mu_up)

"Laminar Correlation - Davis et al., 2001"
{Nusselt_forced_up  = 0.86*Re_air_W_up^(1/2)*Pr_up^(1/3)}
{Nusselt_forced_up_NTE = 0.86*Re_air_W_up^(1/2)*Pr_up^(1/3)}
"Laminar Correlation - Davis et al., 2001"
{Nusselt_forced_up = 0.664*Re_air_W_up^(1/2)*Pr_up^(1/3)
Nusselt_forced_up_NTE = 0.664*Re_air_W_up_NTE^(1/2)*Pr_up_NTE^(1/3)}

"Turbulent Correlation - Incropera et al., 2006.  Eq 7.38, A = 0"
Nusselt_forced_up = 0.037*Re_air_W_up^(4/5)*Pr_up^(1/3)
Nusselt_forced_up_NTE = 0.037*Re_air_W_up_NTE^(4/5)*Pr_up_NTE^(1/3)

h_forced_up     = (Nusselt_forced_up * k_up / L_char)
h_forced_up_NTE         = (Nusselt_forced_up_NTE * k_up_NTE / L_char)
"Combining free and forced convection"
h_up            = ((h_forced_up^(3) + (h_free_up)^(3))^(1/3))
h_up_NTE        = ((h_forced_up_NTE^(3) + (h_free_up_NTE)^(3))^(1/3))
"Convective Heat Transfer from Cover to Ambient Air"
Q_cca           = h_up*Area*(T_1 - T_amb)
Q_cca_NTE       = h_up_NTE*Area*(T_1_NTE - T_amb_NTE)

"Radiation heat transfer from Backside to Surroundings"
Q_rbs           = F1*eps_backside*sigma*Area*(T_2^4 - T_ground^4)+&
                  F2*eps_backside*sigma*Area*(T_2^4 - T_sky^4)
Q_rbs_NTE       = F1*eps_backside*sigma*Area*(T_2_NTE^4 - T_ground_NTE^4)+&
                  F2*eps_backside*sigma*Area*(T_2_NTE^4 - T_sky_NTE^4)

"Convective Heat Transfer from Backside to Ambient Air"
beta_back       = 180 [deg] - Beta
Call FC_plate_tilted_turb(Fluid$, T_2, T_amb, P_atm, Length, W, beta_back:&
                              h_free_down, Nusselt_free_down, Ra_free_down)
Call FC_plate_tilted_turb(Fluid$, T_2_NTE, T_amb_NTE, P_atm, Length, W, beta_back:&
                            h_free_down_NTE, Nusselt_free_down_NTE, Ra_free_down_NTE)

T_film_down     = (T_amb + T_2)/2 "Film Temperature"
k_down          = CONDUCTIVITY(fluid$, T=T_film_down) "Thermal Conductivity of Air"
rho_down        = Density(fluid$, P=P_atm, T=T_film_down) "Density of Air"
mu_down         = Viscosity(fluid$, T=T_film_down) "Viscosity of Air"
Pr_down         = Prandtl(fluid$, T=T_film_down) "Prandtl Number of Air"
Re_air_W_down = max(0.01 [m/s], rho_down * u_wind * L_char / mu_down)

T_film_down_NTE = (T_amb_NTE + T_2_NTE)/2 "Film Temperature"
k_down_NTE      = CONDUCTIVITY(fluid$, T=T_film_down_NTE) "Thermal Conductivity of Air"
rho_down_NTE    = Density(fluid$, P=P_atm, T=T_film_down_NTE) "Density of Air"
```

```
mu_down_NTE   = Viscosity(fluid$, T=T_film_down_NTE) "Viscosity of Air"
Pr_down_NTE    = Prandtl(fluid$, T=T_film_down_NTE) "Prandtl Number of Air"
Re_air_W_down_NTE = max(0.01[m/s],rho_down_NTE*u_wind_NTE*L_char/mu_down_NTE)

"Laminar Correlation - Davis et al., 2001"
{Nusselt_forced_down = 0.664*Re_air_W_down^(1/2)*Pr_down^(1/3)
Nusselt_forced_down_NTE = 0.664*Re_air_W_down_NTE^(1/2)*Pr_down_NTE^(1/3)}

"Turbulent Correlation - Incropera et al., 2006.  Eq 7.38, A = 0"
Nusselt_forced_down = 0.037*Re_air_W_down^(4/5)*Pr_down^(1/3)
Nusselt_forced_down_NTE = 0.037*Re_air_W_down_NTE^(4/5)*Pr_down_NTE^(1/3)

h_forced_down = Nusselt_forced_down * k_down / L_char
h_forced_down_NTE = Nusselt_forced_down_NTE * k_down_NTE / L_char

"Combining free and forced convection"
h_down = ((h_forced_down^(3) + h_free_down^(3))^(1/3))
h_down_NTE  = ((h_forced_down_NTE ^(3) + h_free_down_NTE ^(3))^(1/3))

Q_cba              = h_down*Area*(T_2 - T_amb)
Q_cba_NTE       = h_down_NTE*Area*(T_2_NTE - T_amb_NTE)

"Steady State Energy Balance Equations"
(T_cell - T_1)/R_A + Q_abs*Area = Q_rcs + Q_cca          "Energy Balance at T1"
S_HDKR*Area = (T_cell - T_1)/R_A + (T_cell - T_2)/R2   "Energy Balance at T_cell"
(T_cell - T_2)/R2 = Q_rbs + Q_cba                "Energy Balance at T2"

"Steady State Energy Balance Equations"
"Energy Balance at T1"
(T_cell_NTE - T_1_NTE)/R_A + Q_abs*Area = Q_rcs_NTE + Q_cca_NTE
"Energy Balance at T_cell"
S_HDKR*Area = (T_cell_NTE - T_1_NTE)/R_A + (T_cell_NTE - T_2_NTE)/R2
"Energy Balance at T2"
(T_cell_NTE - T_2_NTE)/R2 = Q_rbs_NTE + Q_cba_NTE
```

Appendix H: Adaptable Model for TRNSYS (FORTRAN)

Parameters

	Name	Dimension	Unit	Type	Range	Default
1	Mode	dimensionless	-	integer	[1;1]	1
2	Module short-circuit current at reference conditions	Electric current	amperes	real	[0;+Inf]	0
3	Module open-circuit voltage at reference conditions	Voltage	V	real	[0;+Inf]	0
4	Reference temperature	Temperature	K	real	[0;+Inf]	0
5	Reference Insolation	Flux	W/m^2	real	[0;+Inf]	0
6	Module voltage at max power point and reference conditions	Voltage	V	real	[0;+Inf]	0
7	Module current at max power point and reference conditions	Electric current	amperes	real	[0;+Inf]	0
8	Temperature coefficient of Isc at (ref. cond)	any	any	real	[-Inf;+Inf]	0
9	Temperature coefficient of Voc at (ref. cond)	any	any	real	[-Inf;+Inf]	0
10	Number of cells wired in series	dimensionless	-	integer	[1;+Inf]	0
11	Number of modules in series	dimensionless	-	integer	[1;+Inf]	0
12	Number of modules in parallel	dimensionless	-	integer	[1;+Inf]	0
13	Module temperature at NOCT	Temperature	K	real	[0;+Inf]	0
14	Ambient temperature at NOCT	Temperature	K	real	[0;+Inf]	0
15	Insolation at NOCT	Flux	W/m^2	real	[0;+Inf]	0
16	Module area	Area	m^2	real	[0;+Inf]	0
17	tau-alpha product for normal incidence	dimensionless	-	real	[0;1]	0
18	Semiconductor bandgap	any	any	real	[-Inf;+Inf]	0
19	Value of parameter **a** at reference conditions	dimensionless	any	real	[0;+Inf]	1.9
20	Value of parameter **I_L** at reference conditions	Electric current	amperes	real	[0;+Inf]	5.4
21	Value of parameter **I_O** at reference conditions	Electric current	amperes	real	[0;+Inf]	0
22	Module series resistance	dimensionless	-	real	[-Inf;+Inf]	0.5
23	Shunt resistance at reference conditions	dimensionless	-	real	[-Inf;+Inf]	16
24	Extinction coefficient-thickness product of cover	dimensionless	-	real	[0;+Inf]	0.008
25	Module Width	Length	m	real	[0.01;+Inf]	1
26	Module Length	Length	m	real	[0.01;+Inf]	1
27	Module Cover Emissivity	dimensionless	-	real	[0.01;1]	0.84
28	Module Backside Emissivity	dimensionless	-	real	[0.01;1]	0.7
29	Mounting Configuration 1: Rack Mounting Configuration 2: Flush Mounting Configuration 3: Integrated Mounting Configuration 4: Gap Mounting Configuration	dimensionless	-	integer	[1;4]	1
30	Mounting Structure Orientation 1: None 2: North - South Supporting Structures 3: East - West Supporting Structures	dimensionless	-	integer	[1;3]	1
31	Mounting Location 1: Ground 2: Roof 3: Wall	dimensionless	-	integer	[1;3]	1
32	Heat Transfer Dimensions 1: Module Dimensions 2: Array Dimensions	dimensionless	-	integer	[1;2]	1
33	Gap Spacing	Length	m	real	[1E-7;+Inf]	0.1
34	Number of rows of modules in array	Length	m	integer	[1;+Inf]	1
35	Number of columns of modules in array	Length	m	integer	[1;+Inf]	1

Inputs

	Name	Dimension	Unit	Type	Range	Default
1	Total incident radiation on tilted surface	Flux	kJ/hr.m^2	real	[-Inf;+Inf]	0
2	Ambient temperature	Temperature	C	real	[-Inf;+Inf]	0
3	Load voltage	Voltage	V	real	[-Inf;+Inf]	0
4	Array slope	Direction (Angle)	degrees	real	[-Inf;+Inf]	0
5	Beam radiation on tilted surface	Flux	kJ/hr.m^2	real	[-Inf;+Inf]	0
6	Sky diffuse radiation on tilted surface	Flux	kJ/hr.m^2	real	[-Inf;+Inf]	0
7	Ground diffuse radiation on tilted surface	Flux	kJ/hr.m^2	real	[-Inf;+Inf]	0
8	Incidence angle on tilted surface	Direction (Angle)	degrees	real	[-Inf;+Inf]	0
9	Solar zenith angle	Direction (Angle)	degrees	real	[-Inf;+Inf]	0
10	Wind speed	Velocity	m/s	real	[-Inf;+Inf]	0
11	Dew Point Temp	Temperature	C	real	[-Inf;+Inf]	0
12	Atmospheric Pressure	Pressure	atm	real	[0.01;+Inf]	1
13	DayHour	Time	hr	real	[-Inf;+Inf]	12
14	WindDirection	Direction (Angle)	degrees	real	[-Inf;+Inf]	0
15	Attic Temp	Temperature	C	real	[-Inf;+Inf]	20
16	Indoor Temp	Temperature	C	real	[-Inf;+Inf]	20

Outputs

	Name	Dimension	Unit	Type	Range	Default
1	Array voltage	Voltage	V	real	[-Inf;+Inf]	0
2	Array current	Electric current	amperes	real	[-Inf;+Inf]	0
3	Array power	Power	W	real	[-Inf;+Inf]	0
4	Power at maximum power point	Power	W	real	[-Inf;+Inf]	0
5	Fraction of maximum power used	dimensionless	-	real	[-Inf;+Inf]	0
6	Voltage at MPP	Voltage	V	real	[-Inf;+Inf]	0
7	Current at MPP	Electric current	amperes	real	[-Inf;+Inf]	0
8	Open circuit voltage	Voltage	V	real	[-Inf;+Inf]	0
9	Short circuit current	Electric current	amperes	real	[0;1]	0
10	Array fill factor	dimensionless	-	real	[0;+Inf]	0
11	Array temperature	Temperature	K	real	[0;+Inf]	0
12	Conversion efficiency	dimensionless	-	real	[0;1]	0
13	MP eff	dimensionless	-	real	[0;1]	0

```
SUBROUTINE TYPE299(TIME,XIN,OUT,T,DTDT,PAR,INFO,ICNTRL,*)

C*********************************************************************
*************************
C 5-PARAMETER PHOTOVOLTAIC MODULE
C  This component implements the 5-Parameter PV model as presented by
C  DeSoto, Klein, and Beckman, to appear in Solar Energy Journal, 2005
C
C  The parameters at the reference condition must be provided as
parameters.  An
C  EES distributable program is available for this purpose.
C  2005.11.00 - SAK - Written for TRNSYS 16.1
C  2005.12.01 - DAA - Added the electrical units for RCHECK
C  2005.12.15 - DAA - Corrected the calculation of EEFREF and IL, based
on module-values,
C                     as well as the calculation of the maximum power
for the array.
C  2005.12.16 - DAA/SAK Added outputs in order to be consistent with
Type94.
C                     Corrected calculation of maximum power.  Added
initialization of outputs.
C                     Changed input1, instead of Beam Normal, now it
uses beam on horizontal.
C  2006.01.15 - DAA - Added the first parameter, MODE, for future
upgrades
C  2006.02.23 - DAA - Created a second MODE that reads the parameters
from a text file
```

```
C  2006.09.22 - DAA - Modified inputs to use similar ones than those
used by Type94.  Deleted
C                      the option MODE=2, as this is not necessary: it
is handled by EES plugin.
C  2006.11.18 - DAA - Modified cell temperature equation, to take into
account wind speed
C  2006.12.20 - DAA - Added MODE = 2, which models a PV module coupled
with an inverter
C  2007.01.23 - DAA/WAB Fixed calculation of incidence angle modifiers
for diffuse and ground
C                     reflected radiation.
C
C*********************************************************************
*************************
! Copyright © 2006 Solar Energy Laboratory, University of Wisconsin-
Madison. All rights reserved.

!export this subroutine for its use in external DLLs.
!DEC$ATTRIBUTES DLLEXPORT :: TYPE299

C    USE STATEMENTS
      USE TrnsysConstants
      USE TrnsysFunctions

      IMPLICIT NONE !force explicit declaration of variables

C    TRNSYS DECLARATIONS
      DOUBLE PRECISION XIN,OUT,TIME,PAR,T,DTDT,STORED,TIME0,DELT
      INTEGER*4 INFO(15),NPMAX,NI,NO,ND,NSMAX,IUNIT,ITYPE,ICNTRL,NP
      CHARACTER*3 YCHECK,OCHECK1,OCHECK2

C    SET THE MAXIMUM NUMBER OF
PARAMETERS(NP),INPUTS(NI),OUTPUTS(NO),DERIVATIVES(ND), AND STORAGE
SPOTS(NSMAX)
C    THAT MAY BE SUPPLIED FOR THIS TYPE
      PARAMETER (NPMAX=40,NI=16,NO=14,ND=0)

C    REQUIRED TRNSYS DIMENSIONS
      DIMENSION XIN(NI),OUT(NO),PAR(NPMAX),YCHECK(NI),
     &      OCHECK1(13), OCHECK2(14)

C    COMMON BLOCK DEFININTIONS
      COMMON /ARRAY194/ A, IL, IO, RS, RSH
      COMMON /PARAM194/ SERCELL,TCR,IMR,VMR,ISCR,VOCR,MVOC,MISC,EG

C    LOCAL VARIABLE DECLARATIONS
      INTEGER NSER, NPRL
      DOUBLE PRECISION I,  !current [amps]
     & CURRENT5194, !function, determines current as function of
voltage for the 5 parameter model
     & V,        !load voltage [volts]
     & IO_REF,   !reverse saturation current at reference conditons [A]
     & IO,       !reverse saturation current, dependent on temperature
[A]
     & TA,       !ambient temperature [Kelvin (K), but input in °C]
     & A_REF,    !modified ideality factor at reference conditions
```

```
& A,         !modified ideality factor
& KB,        !Boltzmann constant [J/K]
& IL_REF,    !photocurrent at reference conditions [A]
& IL,        !photocurrent, dependent on insolation [A]
& ISC,       !short circuit current [A]
& TC,        !cell temperature [K]
& VOC,       !open circuit voltage [V]
& ISCR,      !short circuit current at reference [A]
& VOCR,      !open circuit voltage at reference [V]
& TCR,       !reference cell temperature [K]
& SUNR,      !reference irradiance [W/m^2]
& VMR,       !reference max. power point voltage [V]
& IMR,       !reference current at max. power [A]
& MISC,      !temperature coefficient: short circuit current [A/K]
& EG_REF,    !bandgap energy at reference conditions[eV]
& EG,        !bandgap energy at cell temperature[eV]
& SERCELL,   !Number of cells in series in module
& TCNOCT,    !cell temperature at NOCT [K]
& TANOCT,    !ambient temperature at NOCT [K]
& SUNNOCT,   !irradiance at NOCT [K]
& AREA,      !collector area [m^2]
& TAU_AL,    !transmittance-absorptance product
& EFFREF,    !reference max. power efficiency
& IMP,       !current at max. power [A]
& VMP,       !max. power point voltage [V]
& P,         !power [W]
& PMAX,      !maximum power point along IV curve [W]
& MVOC,      !temperature coefficient: open circuit voltage [V/K]
& THETAZ,
& RS,        !series resistance (constant)
& RSH_REF,   !shunt resistance at reference conditons
& RSH,       !shunt resistance
& SLOPE,     !slope of PV array [degrees]
& OPENVOLTN194,
& SUNDIR,
& SUNGND,
& SUNDIFF,
& THETA,
& TADIFF,
& TAGND,
& TADIR,
& TAMAX,
& SUNEFF,
& SUNBN,
& SUNTILT,
& RHO,
& AMASS,
& MAM,
& a0,    !coefficient for effect of air mass on incident radiation
& a1,
& a2,
& a3,
& a4,
& n2,
& KL,
& RefrAng1,
```

```
     & RefrAng2,
     & RefrAng3,
     & TransSurf1,
     & TransSurf2,
     & TransSurf3,
     & TransCoverABS1,
     & TransCoverABS2,
     & TransCoverABS3,
     & TransCoverDiff,
     & tau1,
     & tau2,
     & tau3,
     & THETA2,
     & THETA3,
     & THETA3X,
     & UTIL,            !COLLECTION EFFICIENCY
     & FF,                    !FILL FACTOR
     & V_max_inv,             !Inverter maximum voltage
     & V_min_inv,             !Inverter minimum voltage
     & P_max_inv,             !Inverter maximum power
     & eta_inverter,
     & P_mp_array,            !Array power at maximum power point
     & V_mp_array,            !Array voltage at maximum power point
     & I_mp_array,            !Array current at maximum power point
     & V_oc_array,            !Array open circuit voltage
     & I_vmin,
     & P_vmin,
     & I_vmax,
     & P_vmax,
     & V_max_prime,
     & X(2),
     & Y(1),
     & V_WIND,                !Wind speed
     & TARE,                        !Inverter tare
     & VMPLOW,                !Lower limit for maximum power point
     & VMPUP,                       !Upper limit for maximum power
point
     & VMPOLD, VMPNEW,  !Intermediate variables for maximum power point
calculation
     & G, Iplus,                    !Intermediate variable for maximum
power point calculation
     & IVSLOPE,
     & DPDV,                        !Slope of Power curve curve
     & MYCOEF1,
     & TDEW,                  !INPUT
     & P_atm,                 !INPUT
     & t_hr,                  !INPUT: time
     & WD,                    !INPUT: wind direction
     & T_attic,               !INPUT: Attic Temperature
     & T_in,                  !INPUT: Indoor Temperature
     & Width,                 !Parameter: Width of panel
     & Length,                !Parameter: Length (height) of panel
     & EmisC,                 !Parameter: Emissivity of Cover
     & EmisB,                 !Parameter: Emissivity of Panel Backside
(make this constant?)
     & W_gap,                 !Parameter: Space between gap and roof
```

```
     & Nrows,                 !Parameter: Number of rows of modules in
array
     & Ncols,                 !Parameter: Number of columns of modules
in array
     & T_prop,                !Constant: Temperature at which to
evaluate properties of air
     & k_air,                 !Constant: Thermal conductivity of air
     & mu_air,                !Constant: Dynamic viscosity of air
     & Pr_air,                !Constant: Prandtl Number of air
     & sigma,                 !Constant: Stefan-Boltzmann constant
     & cp_air,                !Constant: specific heat of air
     & FREECONVECTION194,     !Function: Calculate free convection
coefficient
     & CHANNELFLOW194,        !Function: Calculate forced convection
coefficient for gap mounted module
     & CHANNELFREE194,        !Function: Calculate free convection
coefficient for gap mounted module
     & L_char,                !Solve for: Characteristic Length of
panel
     & Fcs,                   !Solve for: view factor from cover to sky
     & Fcg,                   !Solve for: view factor from cover to
ground
     & Fbs,                   !Solve for: view factor from backside to
sky
     & Fbg,                   !Solve for: view factor from backside to
ground
     & rho_air,               !Solve for: density of air at film temp
     & Re_forced,             !Solve for: Reynolds Number of air
     & Nu_forced,             !Solve for: Nusselt number forced
convection
     & h_forced,              !Solve for: Heat transfer coefficient,
forced convection
     & h_free_c,              !Solve for: Heat transfer coefficient,
free convection, cover
     & h_free_b,              !Solve for: Heat transfer coefficient,
free convection, backside
     & h_conv_c,              !Solve for: Total convective heat
transfer coefficient of cover
     & h_conv_b,              !Solve for: Total convective heat
transfer coefficient of backside
     & h_sky,                 !Solve for: Heat transfer coefficient for
radiative heat transfer to sky
     & h_ground,              !Solve for: Heat transfer coefficient for
radiative heat transfer to ground
     & T_sky,                 !Solve for: Sky Temperature
     & T_ground,              !Solve for: Ground Temperature
     & P_guess,               !Solve for: Guess for Pmp, iterate as
necessary
     & TC1,                   !Solve for: New cell temperature
     & err_TC,                !Solve for: Change between n and n-1 cell
temperature predictions
     & err_P,                 !Solve for: Change between n and n-1
power predictions
     & QDIFF,                 !Solve for: Absorbed diffuse radiation:
cover
```

```
     & QGND,                   !Solve for: Absorbed ground radiation:
cover
     & QDIR,                   !Solve for: Absorbed direction radiation:
cover
     & QHDKR,                  !Solve for: Total absorbed radiation:
cover
     & SHDKR,                  !Solve for: HDKR absorbed cell radiation
for energy balance
     & T_back,                 !Solve for: Back temperature for
integrated mounting
     & h_radbk,                !Solve for: Heat transfer coefficient for
radiative heat transfer to specified backside temp
     & T_rw,                   !Solve for: Roof or wall temperature
     & A_c,                    !Solve for: Cross Sectional Area for gap-
mounted module
     & L_str,                  !Solve for: Distance between mounting
structures (creates channel)
     & per_c,                  !Solve for: Cross Sectional Perimeter
     & D_h,                    !Solve for: Hydraulic Diameter
     & per_cw,                 !Solve for: Cross Sectional Perimeter,
wetted
     & e_r,                    !Solve for: Surface Roughness of gap
     & Re_dh,                  !Solve for: Reynolds number for gap
mounted module
     & AR,                     !Solve for: Aspect Ratio of channel
     & h_fo,                   !Solve for: Forced convection, backside
gap mounted
     & h_fr,                   !Solve for: Free convection, backside gap
mounted
     & m_dot,                  !Solve for: Mass flow rate of air through
gap
     & T_cr,                   !Solve for: Average of cell and roof temp
     & T_m,                    !Solve for: Mean temperature of air
leaving gap
     & Q_fo,                   !Solve for: Forced convective heat
transfer to air in gap
     & Q_fr,                   !Solve for: Free convective heat transfer
to air in gap
     & Q_conv,                 !Solve for: Total convective heat
transfer from module backside, gap mounted
     & L_charB,                !Solve for: Characteristic length for
calculation of backside convection correlations, gap mounted
     & rho_bk                  !Solve for: density of air at backside
film temp for integrated mounting


      INTEGER  NS,          !the number of double precision storage
spots required for this instance of Type194
     & MODE,              !Component mode - for future upgrades
     & LU_INV,            !Logical unit number of the file that contains
the inverter parameters (for mode 2)
     & NX(2),
     & h_iter,                !Iteration number for radiative heat
transfer coefficients
     & p_iter,         !Iteration number for power prediction
     & MC,             !Mounting Configuration
```

```
     & MSO,            !Mounting Structure Orientation
     & ML,             !Mounting Location
     & HTD             !Heat Transfer Dimensions

C    DATA STATEMENTS
      DATA KB/8.618E-5/ !Boltzmann constant [eV/K]  note units
      DATA a0/0.918093/,a1/0.086257/,a2/-0.024459/,a3/0.002816/,
     &     a4/-0.000126/ !Air mass modifier coefficients as indicated
in DeSoto paper
      DATA T_prop/315./,k_air/0.02676/,mu_air/1.927E-5/,Pr_air/0.724/
!Viscosity in units of N-s/m^2
      DATA sigma/5.66961E-8/,cp_air/1005.5/
      DATA
YCHECK/'IR1','TE1','VO1','DG1','IR1','IR1','IR1','DG1','DG1',
     &      'VE1','TE1','PR4','TD1','DG1','TD1','TD1'/
      DATA OCHECK1/'VO1','CU1','PW2','PW2','DM1','VO1',
     &              'CU1','VO1','CU1','DM1','TE1','DM1','DM1'/
      DATA OCHECK2/'VO1','CU1','PW2','PW2','DM1','VO1',
     &              'CU1','VO1','CU1','DM1','TE1','DM1','DM1','DM1'/



C-----------------------------------------------------------------------
----------------------------
C    GET GLOBAL TRNSYS SIMULATION VARIABLES
      TIME0   = getSimulationStartTime()
      DELT    = getSimulationTimeStep()

C-----------------------------------------------------------------------
----------------------------
C    SET THE VERSION INFORMATION FOR TRNSYS
      IF(INFO(7).EQ.-2) THEN
        INFO(12)=16
        RETURN 1
      ENDIF

C-----------------------------------------------------------------------
----------------------------
C    PERFORM LAST CALL MANIPULATIONS
      IF (INFO(8).EQ.-1) THEN
        RETURN 1
      ENDIF

C-----------------------------------------------------------------------
----------------------------
C    PERFORM POST CONVERGENCE MANIPULATIONS
      IF(INFO(13).GT.0) THEN
        RETURN 1
      ENDIF

C-----------------------------------------------------------------------
----------------------------
C    PERFORM FIRST CALL MANIPULATIONS
      IF (INFO(7).EQ.-1) THEN
        !retrieve unit and type number for this component from the INFO
array
```

```
        IUNIT = INFO(1)
        ITYPE = INFO(2)
        !set some info array variables to tell the trnsys engine how
this type is to work
        INFO(6) = NO   !reserve space in the OUT array using INFO(6)
        INFO(9) = 0    !this TYPE does not depend explicitly on TIME

        INFO(10)=0 !

        MODE    = JFIX(PAR(1)+0.1)
        IF (MODE .EQ. 1) THEN
          NP = 35
        ELSE IF (MODE .EQ. 2) THEN
            NP = 40
        ENDIF

        !CALL THE TYPE CHECK SUBROUTINE TO COMPARE WHAT THIS TYPE
REQUIRES TO WHAT IS SUPPLIED IN
        !THE TRNSYS INPUT FILE
        CALL TYPECK(1,INFO,NI,NP,ND)
        !CALL THE INPUT-OUTPUT CHECK SUBROUTINE TO SET THE CORRECT
INPUT AND OUTPUT UNITS
        IF (MODE .EQ. 1) THEN
            CALL RCHECK(INFO,YCHECK,OCHECK1)
        ELSE IF (MODE .EQ. 2) THEN
            CALL RCHECK(INFO,YCHECK,OCHECK2)
        ENDIF
        !RETURN TO THE CALLING PROGRAM
        RETURN 1
      ENDIF

C-----------------------------------------------------------------------
----------------------------
C    PERFORM INITIAL TIMESTEP MANIPULATIONS
      IF (TIME.LT.(TIME0+DELT/2.)) THEN
        !set the UNIT and TYPE numbers for future calls
        IUNIT = INFO(1)
        ITYPE = INFO(2)

        MODE    = JFIX(PAR(1)+0.1)

        IF((MODE.LT.1) .OR. (MODE.GT.2))    CALL TYPECK(-4,INFO,0,1,0)


          ISCR    = PAR(2)
          VOCR    = PAR(3)
          TCR     = PAR(4)
          SUNR    = PAR(5)
          VMR     = PAR(6)
          IMR     = PAR(7)
          MISC    = PAR(8)
          MVOC    = PAR(9)
          SERCELL = PAR(10)
          NSER    = PAR(11)
          NPRL    = PAR(12)
          TCNOCT  = PAR(13)
```

```
          TANOCT  = PAR(14)
          SUNNOCT = PAR(15)
          AREA    = PAR(16)
          TAMAX   = DABS(PAR(17))
          EG_REF  = PAR(18)  !Band gap at reference temperature
          A_REF   = PAR(19)  !the following are the 5 reference
parameters for the DeSoto model
          IL_REF  = PAR(20)
          IO_REF  = PAR(21)
          RS      = PAR(22)
          RSH_REF = PAR(23)
          KL      = PAR(24)  !extinction coefficient
          Width   = PAR(25)
          Length  = PAR(26)
          EmisC   = PAR(27)
          EmisB   = PAR(28)
          MC      = JFIX(PAR(29)+0.1)
          MSO     = JFIX(PAR(30)+0.1)
          ML      = JFIX(PAR(31)+0.1)
          HTD     = JFIX(PAR(32)+0.1)
          W_gap   = PAR(33)
          Nrows   = PAR(34)
          Ncols   = PAR(35)

        IF (MODE .EQ. 2) THEN
          P_max_inv = PAR(36) !Inverter maximum power
          V_max_inv = PAR(37) !Inverter maximum voltage
          V_min_inv = PAR(38) !Inverter minimum voltage
              tare          = PAR(39)
          LU_inv    = jfix(PAR(40) +0.1)
        ENDIF

        IF(ISCR.LT.0.d0)    CALL TYPECK(-4,INFO,0,2,0)
        IF(VOCR.LT.0.d0)    CALL TYPECK(-4,INFO,0,3,0)
        IF(TCR.LT.0.d0)     CALL TYPECK(-4,INFO,0,4,0)
        IF(SUNR.LT.0.d0)    CALL TYPECK(-4,INFO,0,5,0)
        IF(VMR.LT.0.d0)     CALL TYPECK(-4,INFO,0,6,0)
        IF(IMR.LT.0.d0)     CALL TYPECK(-4,INFO,0,7,0)
        IF(SERCELL.LT.1.d0) CALL TYPECK(-4,INFO,0,10,0)
        IF(NSER.LT.1.d0)    CALL TYPECK(-4,INFO,0,11,0)
        IF(NPRL.LT.1.d0)    CALL TYPECK(-4,INFO,0,12,0)
        IF(TCNOCT.LT.0.d0)  CALL TYPECK(-4,INFO,0,13,0)
        IF(TANOCT.LT.0.d0)  CALL TYPECK(-4,INFO,0,14,0)
        IF(SUNNOCT.LT.0.d0) CALL TYPECK(-4,INFO,0,15,0)
        IF(AREA.LT.0.d0)    CALL TYPECK(-4,INFO,0,16,0)
        IF(TAMAX.EQ.0.d0)   CALL TYPECK(-4,INFO,0,17,0)
        IF(EG_REF.LT.0.d0)  CALL TYPECK(-4,INFO,0,18,0)


C      INITIALIZE OUTPUTS
        OUT(1)  = VOCR*NSER   !ARRAY VOLTAGE
        OUT(2)  = ISCR*NPRL   !ARRAY CURRENT
        OUT(3)  = 0.D0        !ARRAY POWER
        OUT(4)  = 0.D0        !ARRAY MAXIMUM POWERset to non-zero only
if DOPMAX (Par 23) > 0
        OUT(5)  = 0.D0        !RATIO P/PMAX
```

```
        OUT(6)  = VMR*NSER    !ARRAY VOLTAGE AT MAXIMUM POWER POINT
        OUT(7)  = IMR*NPRL    !ARRAY CURRENT AT MAXIMUM POWER POINT
        OUT(8)  = VOCR*NSER   !ARRAY OPEN CIRCUIT VOLTAGE
        OUT(9)  = ISCR*NPRL   !ARRAY SHORT CIRCUIT CURRENT
        OUT(10) = 0.D0        !ARRAY FILL FACTOR
        OUT(11) = 0.D0        !ARRAY TEMPERATURE
        OUT(12) = 0.D0        !ARRAY COLLECTION EFFICIENCY
        IF (MODE .EQ. 2) THEN
                OUT(13) = 0.D0
        ENDIF
        OUT(14) = 0.D0

      ENDIF

C-----------------------------------------------------------------
C    THIS IS AN ITERATIVE CALL TO THIS COMPONENT ***
C-----------------------------------------------------------------

C    RE-READ THE PARAMETERS IF ANOTHER UNIT OF THIS TYPE HAS BEEN
CALLED SINCE THE LAST
C    TIME THEY WERE READ IN
      IF(INFO(1).NE.IUNIT) THEN
        !reset the unit number
        IUNIT = INFO(1)
        ITYPE = INFO(2)
        !read the parameter values
        MODE    = PAR(1)
        ISCR    = PAR(2)
        VOCR    = PAR(3)
        TCR     = PAR(4)
        SUNR    = PAR(5)
        VMR     = PAR(6)
        IMR     = PAR(7)
        MISC    = PAR(8)
        MVOC    = PAR(9)
        SERCELL = PAR(10)
        NSER    = PAR(11)
        NPRL    = PAR(12)
        TCNOCT  = PAR(13)
        TANOCT  = PAR(14)
        SUNNOCT = PAR(15)
        AREA    = PAR(16)
        TAMAX   = DABS(PAR(17))
        EG_REF  = PAR(18)
        A_REF   = PAR(19)  !the following are the 5 reference
parameters for the DeSoto model
        IL_REF  = PAR(20)
        IO_REF  = PAR(21)
        RS      = PAR(22)
        RSH_REF = PAR(23)
        KL      = PAR(24)
        Width   = PAR(25)
        Length  = PAR(26)
        EmisC   = PAR(27)
        EmisB   = PAR(28)
        MC      = JFIX(PAR(29)+0.1)
```

```
        MSO     = JFIX(PAR(30)+0.1)
        ML      = JFIX(PAR(31)+0.1)
        HTD     = JFIX(PAR(32)+0.1)
        W_gap   = PAR(33)
        Nrows   = PAR(34)
        Ncols   = PAR(35)

        IF (MODE .EQ. 2) THEN
          P_max_inv = PAR(36) !Inverter maximum power
          V_max_inv = PAR(37) !Inverter maximum voltage
          V_min_inv = PAR(38) !Inverter minimum voltage
              tare          = PAR(39)
          LU_inv    = jfix(PAR(40) +0.1)
        ENDIF

      ENDIF

C    RETRIEVE THE CURRENT VALUES OF THE INPUTS TO THIS MODEL FROM THE
XIN ARRAY
      SUNTILT = XIN(1)/3.6d0        !total solar radiation on tilted
surface; Input in kJ/m2-hr converted to W/m^2
      TA      = XIN(2)+273.15       !ambient temperature in K but input
in °C {SAK 10/10/05}
      V       = XIN(3)                    !voltage
      SLOPE   = XIN(4)                    !slope of array
      SUNDIR  = XIN(5)/3.6D0        !beam radiation on tilted surface
Input in kJ/m2-hr converted to W/m^2
      SUNDIFF = XIN(6)/3.6D0        !sky diffuse radiation on tilted
surface; Input in kJ/m2-hr converted to W/m^2
      SUNGND  = XIN(7)/3.6D0        !ground diffuse radiation on tilted
surface; Input in kJ/m2-hr converted to W/m^2
      THETA   = XIN(8)                    !incidence angle on tilted
surface
      THETAZ  = XIN(9)                    !zenith angle
      V_WIND  = XIN(10)                   !Wind speed
      TDEW    = XIN(11)             !Dew Point Temp [C]
      P_atm   = XIN(12)*101325      !Atmospheric Pressure, convert
[atm] to [Pa]
      t_hr    = XIN(13)             !Time of Day [hr]
      WD      = XIN(14)             !Wind Direction [deg]
      T_attic = XIN(15)+273.15      !Attic Temperature in K but input
in C
      T_in    = XIN(16)+273.15      !Indoor Temperature in K but input
in C

       !Define backside temp based on mounting location (integrated
mounting configuration)
      IF (ML.EQ.1) T_back = TA
      IF (ML.EQ.2) T_back = T_attic
      IF (ML.EQ.3) T_back = T_in

      IF (THETAZ.GT. 86.0) THETAZ=86.0 !Zenith angle must be < 90°

C       INCIDENCE ANGLE MODIFIER CALCULATIONS
      IF (THETA.LE.0) THEN
        THETA=1
```

```
      ENDIF
      n2         = 1.526   !refractive index of glass

      RefrAng1   = asinD(sinD(THETA)/n2)
      TransSurf1 = 1-0.5*((sinD(RefrAng1-THETA))**2/(sinD(RefrAng1+
     &  THETA))**2+(tanD(RefrAng1-THETA))**2/(tanD(RefrAng1+THETA))**2)
      TransCoverAbs1 = Dexp(-KL/cosD(RefrAng1))
      tau1       = TransCoverAbs1*TransSurf1

C       Evaluating transmittance at angle Normal to surface (0), use 1
to avoid probs.
      THETA2     = 1
      RefrAng2   = asinD(sinD(THETA2)/n2)
      TransSurf2 = 1-0.5*((sinD(RefrAng2-1))**2/(sinD(RefrAng2+1))**2+
     & (tanD(RefrAng2-1))**2/(tanD(RefrAng2+1))**2)
      TransCoverAbs2 = Dexp(-KL/cosD(RefrAng2))
      tau2       = TransCoverAbs2*TransSurf2

C        Evaluating transmittance at equivalent angle for diffuse
!      THETA3     = 58
      THETA3 = 59.7 - 0.1388*SLOPE  + 0.001497*SLOPE**2
      RefrAng3   = AsinD(sinD(THETA3)/n2)
      TransSurf3 = 1-.5*((sinD(RefrAng3-THETA3))**2/(sinD(RefrAng3+
     & THETA3))**2 + (tanD(RefrAng3-THETA3))**2/(tanD(RefrAng3+
     & THETA3))**2)
      TransCoverAbs3 = Dexp(-KL/cosD(RefrAng3))
      TransCoverDiff = TransCoverAbs3
      tau3       = TransCoverAbs3*TransSurf3
      TADIR      = tau1/tau2
      TADIFF     = tau3/tau2
      THETA3X        = THETA3
C        Evaluating transmittance at equivalent angle for ground
reflected radiation
!      THETA3     = 58
      THETA3 = 90.0 - 0.5788*SLOPE  + 0.002693*SLOPE**2
      RefrAng3   = AsinD(sinD(THETA3)/n2)
      TransSurf3 = 1-.5*((sinD(RefrAng3-THETA3))**2/(sinD(RefrAng3+
     & THETA3))**2 + (tanD(RefrAng3-THETA3))**2/(tanD(RefrAng3+
     & THETA3))**2)
      TransCoverAbs3 = Dexp(-KL/cosD(RefrAng3))
      tau3       = TransCoverAbs3*TransSurf3
      TAGND     = tau3/tau2



C         Calculate HDKR COVER absorbed radiation for energy balance
      QDIFF = SUNDIFF*(1.-TransCoverDiff)
      QGND = SUNGND*(1.-TransCoverAbs3)
      QDIR = SUNDIR*(1.-TransCoverAbs1)
      QHDKR = QDIFF+QGND+QDIR

C         Calculate HDKR TOTAL absorbed radiaion for energy balance
      SHDKR = SUNDIFF*TADIFF*tau2+SUNGND*TAGND*tau2+SUNDIR*TADIR*
     &          tau2 + QHDKR

C         Calculation of Effective irradiance
```

```
      SUNDIFF=SUNDIFF*TADIFF
      SUNGND=SUNGND*TAGND
      SUNDIR=SUNDIR*TADIR
      SUNEFF = SUNDIFF+SUNGND+SUNDIR

      TAU_AL     = TAMAX
      IF (SUNTILT.GT.0) TAU_AL = TAMAX*SUNEFF/SUNTILT  !DAA: = TAMAX is
used for CEC study
      IF (SUNEFF.LT.0)  SUNEFF=0

C         Calculation of Air Mass Modifier
      IF (THETAZ.LE.0) THETAZ=0
      AMASS      = 1/(cosD(THETAZ)+0.5057*(96.080-THETAZ)**(-1.634))
      MAM        = a0+a1*AMASS+a2*AMASS**2+a3*AMASS**3+a4*AMASS**4
      !SUNEFF     = SUNEFF*MAM

C  Evaluation of cell temperature

C     Define heat transfer dimensions based on module or array size
      IF (HTD.EQ.2) THEN
      Length     = Nrows*Length
      Width      = Ncols*Width
      ENDIF

C     Define characteristic length
      L_char     = 4. * Length * Width / (2. * (Width + Length))

C     For gap mounting configuration, set characteristic length for
channel flow
      V_WIND = MAX(0.001,V_WIND)
      IF (MC.EQ.4) THEN
        IF (MSO.EQ.1) THEN
            L_charB = L_char
            L_str   = L_char
        ENDIF
        IF (MSO.EQ.2) THEN
            V_WIND  = MAX(0.001,abs(cosD(WD))*V_WIND)
            L_charB = Length
            L_str   = Width
        ENDIF
        IF (MSO.EQ.3) THEN
            V_WIND  = MAX(0.001,abs(cosD(WD+90))*V_WIND)
            L_charB = Width
            L_str   = Length
        ENDIF
      ENDIF

      Area       = Length * Width        !Surface area of module

      Fcg        = (1. - cosD(SLOPE))/2  !view factor between top of
tilted plate and horizontal plane adjacent to bottom edge of plate
      Fcs        = 1. - Fcg              !view factor between top of
tilted plate and everything else (sky)
      Fbs        = Fcg                   !view factor bewteen top and
ground = bottom and sky
```

```
      Fbg        = Fcs                    !view factor bewteen bottom
and ground = top and sky
      T_sky      = TA*(0.711+0.0056*TDEW+0.000073*TDEW**2+0.013*
     &             cosD(t_hr))**(0.25)   !Sky Temperature: Berdahl and
Martin
      T_ground   = TA                     !Set ground temp equal to
ambient temp
      T_rw       = TA                     !Initial guess for roof or
wall temp

      EFFREF     = IMR*VMR/(SUNR*AREA)   !Efficiency of module at SRC
conditions
      P_guess    = EFFREF * (SUNEFF*AREA)!Estimate performance based on
SRC efficiency

      TC         = TA+(SUNTILT*(TCNOCT-TANOCT)/SUNNOCT*(1.-
EFFREF/TAU_AL
     &                  ))*9.5/(5.7 + 3.8*V_WIND)     !Estimate cell
temp w/ Duffie and Beckman equation

      err_P      = 100.  !Set initial performance error. Must be >
tolerance for power error in do loop
      p_iter     = 0     !Set iteration counter (performance)

      DO WHILE ((p_iter .LT. 11).AND.(abs(err_P) .GT. 0.1))
      err_TC     = 100.  !Set initial temperature error. Must be >
tolerance for temp error in do loop
      h_iter     = 0     !Set iteration counter (temperature)

      IF (SUNEFF.LT.1) THEN
        TC       = TA
      ELSE
        IF (MC.EQ.1) THEN   !Rack Mounting Configuration
         DO WHILE ((h_iter .LT. 11).AND.(abs(err_TC) .GT. 0.1))
        rho_air    = P_atm*28.967/8314.34*(1./((TA+TC)/2.)) !density of
air as a function of pressure and ambient temp
        Re_forced  = MAX(0.1,rho_air*V_WIND*L_char/mu_air)  !Reynolds
number of wind moving across module
        Nu_forced  = 0.037 * Re_forced**(4./5.) * Pr_air**(1./3.)
!Nusselt Number (Incropera et al., 2006)
        h_forced   = Nu_forced * k_air / L_char
        h_sky      = (TC**2+T_Sky**2)*(TC+T_sky)
        h_ground   = (TC**2+T_ground**2)*(TC+T_ground)
        h_free_c   = FREECONVECTION194(TC,TA,SLOPE,RHO_AIR,Pr_air,
!Call function to calculate free convection on tilted surface (top)
     &               mu_air,Area,Length,Width,k_air)
        h_free_b   = FREECONVECTION194(TC,TA,180.-
SLOPE,RHO_AIR,Pr_air,!Call function to calculate free convection on
tilted surface (bottom)
     &               mu_air,Area,Length,Width,k_air)
        h_conv_c   = (h_forced**3.+h_free_c**3.)**(1./3.) !Combine free
and forced heat transfer coefficients (top)
        h_conv_b   = (h_forced**3.+h_free_b**3.)**(1./3.) !Combine free
and forced heat transfer coefficients (bottom)
```

```
        TC1 = ((h_conv_c+h_conv_b)*TA + (Fcs*EmisC+Fbs*EmisB)*sigma*
!Energy balance to calculate TC
     &       h_sky*T_sky +
(Fcg*EmisC+Fbg*EmisB)*sigma*h_ground*T_ground
     &       -(P_guess/AREA)+SHDKR)/(h_conv_c+h_conv_b+(Fcs*EmisC +
     &       Fbs*EmisB)*sigma*h_sky+(Fcg*EmisC+Fbg*EmisB)*sigma
     &        *h_ground)
C       Since some variables in TC1 calc are function of TC, iterative
solving is required
        err_TC     = TC1 - TC !Error between n-1 and n temp
calculations
        TC         = TC1      !Set cell temp to most recent calculation

        h_iter     = h_iter + 1 !+1 to iteration counter
         END DO

        ELSEIF (MC.EQ.2) THEN !Flush Mounting Configuration
         DO WHILE ((h_iter .LT. 11).AND.(abs(err_TC) .GT. 0.1))
        rho_air    = P_atm*28.967/8314.34*(1 / ((TA+TC)/2.)) !density
of air a function of pressure and ambient temp
        Re_forced  = MAX(0.1,rho_air*V_WIND*L_char/mu_air)  !Reynolds
number of wind moving across panel: function of L_char: array depen?
        Nu_forced  = 0.037 * Re_forced**(4./5.) * Pr_air**(1./3.)
        h_forced   = Nu_forced * k_air / L_char
        h_sky      = (TC**2+T_Sky**2)*(TC+T_sky)
        h_ground   = (TC**2+T_ground**2)*(TC+T_ground)
        h_free_c   = FREECONVECTION194(TC,TA,SLOPE,RHO_AIR,Pr_air,
     &               mu_air,Area,Length,Width,k_air)
        h_conv_c   = (h_forced**3.+h_free_c**3.)**(1./3.)

        TC1 = ((h_conv_c)*TA + (Fcs*EmisC)*sigma*
     &       h_sky*T_sky + (Fcg*EmisC)*sigma*h_ground*T_ground
     &       -(P_guess/AREA)+SHDKR)/(h_conv_c+(Fcs*EmisC)
     &        *sigma*h_sky+(Fcg*EmisC)*sigma
     &        *h_ground)

        err_TC     = TC1 - TC
        TC         = TC1

        h_iter     = h_iter + 1
         END DO

        ELSEIF (MC.EQ.3) THEN  !Integrated Mounting Configuration
         DO WHILE ((h_iter .LT. 11).AND.(abs(err_TC) .GT. 0.1))
        rho_air    = P_atm*28.967/8314.34*(1 / ((TA+TC)/2.)) !density
of air a function of pressure and film temp
        rho_bk     = P_atm*28.967/8314.34*(1 / ((T_back+TC)/2.))
        Re_forced  = MAX(0.1,rho_air*V_WIND*L_char/mu_air)  !Reynolds
number of wind moving across panel: function of L_char: array depen?
        Nu_forced  = 0.037 * Re_forced**(4./5.) * Pr_air**(1./3.)
        h_forced   = Nu_forced * k_air / L_char

        h_sky      = (TC**2+T_Sky**2)*(TC+T_sky)
        h_ground   = (TC**2+T_ground**2)*(TC+T_ground)
```

```
        h_radbk    = (TC**2+T_back**2)*(TC+T_back)!Using T_back now
instead of TA

        h_free_c   = FREECONVECTION194(TC,TA,SLOPE,RHO_AIR,Pr_air,
     &               mu_air,Area,Length,Width,k_air)

        h_free_b   = FREECONVECTION194(TC,T_back,180.-SLOPE,RHO_BK,
     &               Pr_air,mu_air,Area,Length,Width,k_air)

        h_conv_c   = (h_forced**3.+h_free_c**3.)**(1./3.)
        h_conv_b   = h_free_b !No forced convection on backside

        TC1 = (h_conv_c*TA+h_conv_b*T_back+Fcs*EmisC*sigma*h_sky*T_sky
     &        +Fcg*EmisC*sigma*h_ground*T_ground+
     &       EmisB*sigma*h_radbk*T_back-(P_guess/AREA)+SHDKR)/
     &       (h_conv_c+h_conv_b+Fcs*EmisC*sigma*h_sky+
     &        Fcg*EmisC*sigma*h_ground+EmisB*sigma*h_radbk)

        err_TC     = TC1 - TC
        TC         = TC1

        h_iter     = h_iter + 1
         END DO

      ELSEIF (MC.EQ.4) THEN !Gap (channel) Mounting Configuration
        DO WHILE ((h_iter .LT. 11).AND.(abs(err_TC) .GT. 0.1))
        rho_air    = P_atm*28.967/8314.34*(1 / ((TA+TC)/2.)) !density
of air a function of pressure and film temp
        Re_forced  = MAX(0.1,rho_air*V_WIND*L_char/mu_air)  !Reynolds
number of wind moving across panel: function of L_char: array depen?
        Nu_forced  = 0.037 * Re_forced**(4./5.) * Pr_air**(1./3.)
        h_forced   = Nu_forced * k_air / L_char
        h_sky      = (TC**2+T_Sky**2)*(TC+T_sky)
        h_ground   = (TC**2+T_ground**2)*(TC+T_ground)
        h_free_c   = FREECONVECTION194(TC,TA,SLOPE,RHO_AIR,Pr_air,
     &               mu_air,Area,Length,Width,k_air)
        h_conv_c   = (h_forced**3.+h_free_c**3.)**(1./3.)

        AR         = W_gap / L_str !Aspect Ratio of channel
        A_c        = W_gap * L_str !Cross Sectional area of channel

        Per_c        = 2.*(L_str + W_gap) !Perimeter of A_c of channel
        Per_cw       = 2.*L_str !Perimeter minus open sides
        D_h          = (4.*A_c)/Per_c !Hydraulic diameter
        e_r        = 0.005 !Estimate of surface roughness
        Re_dh        = rho_air*V_WIND*D_h / mu_air !Reynolds number for
channel flow
        T_cr       = (TC+T_rw)/2. !Average of cell and roof temp
assumed in correlations

        h_fo       = CHANNELFLOW194(e_r,D_h,Re_dh,AR,Pr_air,L_charB,
     &                  k_air) !Call function for forced heat transfer
coef.
        IF (MSO.EQ.3) THEN
        h_fr       = 0 !If E-W supports then assume no free convection
        ELSE
```

```
C       Call function for channel free convection
        h_fr       = CHANNELFREE194(W_gap,SLOPE,TA,T_cr,k_air,
     &                  rho_air,cp_air,mu_air,Length)
        ENDIF

        m_dot        = V_WIND*rho_air*A_c !mass flow rate through
channel
C       Calculate air temperature at the end of the channel
        T_m        = T_cr-(T_cr-TA)*Dexp(-Per_cw*L_charB*h_fo/
     &               (m_dot*cp_air))
C       Heat transfer from backside
        Q_fo         = max(0.0001,cp_air*m_dot*(T_m - TA))
        Q_fr       = max(0.0001,h_fr*Per_cw*Length*(T_cr - TA))
C       Combine heat transfer from free and forced convection
C       Must be completed this way because using 'h' would be
C       inappropriate because the heat transfer calculations
C       operate between two different temperature differences
        Q_conv     = (0.5*(Q_fo**3+Q_fr**3)**(1./3.))/Area

        h_radbk    = (TC**2+T_rw**2)*(TC+T_rw)
C       Energy Balance to calculate roof/wall temperature
        T_rw       = TC - Q_conv/(EmisB*sigma*h_radbk)

        TC1 = (h_conv_c*TA + Fcs*EmisC*sigma*h_sky*T_sky
     &
+Fcg*EmisC*sigma*h_ground*T_ground+sigma*EmisB*h_radbk*T_rw
     &       -Q_conv-(P_guess/AREA)+SHDKR)/(h_conv_c+Fcs*EmisC
     &       *sigma*h_sky+Fcg*EmisC*sigma*h_ground+sigma*EmisB*h_radbk)

        err_TC     = TC1 - TC
        TC         = TC1

        h_iter     = h_iter + 1
         END DO

        ENDIF
      ENDIF

C       Evaluation of IL and IO at operating conditions, for one module
      IL   = (SUNEFF/SUNR)*(IL_REF+MISC*(TC-TCR))

      IF (IL.LT.0.0) IL=0.0
      EG   = EG_REF*(1-0.0002677*(TC-TCR))
      IO   = IO_REF*((TC/TCR)**3)*DEXP((1/KB)*(EG_REF/TCR-EG/TC))
      A    = A_REF*TC/TCR
      RSH  = 1E6
      IF (SUNEFF.GT.0.d0) RSH=RSH_REF*(SUNR/SUNEFF) !Shunt resistance
relation in DeSoto paper

C         Open circuit voltage, short circuit current for 1 module
      VOC = OPENVOLTN194(VOCR,SUNEFF)
      ISC = IL/(1+RS/RSH)


C****   all calculations are being skipped during time periods
C****   with no insolation
```

```
      IF(SUNEFF.EQ.0.d0)THEN
        V    = 0.d0
        I    = 0.d0
        IMP  = 0.d0
        VMP  = 0.d0
        PMAX = 0.d0
        UTIL = 0.d0
        FF   = 0.d0
      ELSE
C****     check on operation mode
        IF(V.LT.0.)THEN
          V=0.d0
          I=0.d0
        ELSE
C****         normal operation
C****         check if voltage greater than open circuit voltage
          IF((V/NSer).GT.VOC)THEN
            V=VOC*NSer
            I=0.d0
          ELSE
            I=CURRENT5194(V,0.9*IL, NSER, NPRL)  !CURRENT FOR ENTIRE
ARRAY
          ENDIF
        ENDIF

1000    P=I*V     !POWER FOR ENTIRE ARRAY

c     MAXIMUM POWER FOR THE ARRAY
        PMAX=0
        VMP=0
        IMP=0
          VMP=(VMR+MVOC*(TC-TCR))/2
          DO WHILE (PMAX.LE.(IMP*VMP).AND. (VMP.LT.VOC))
            PMAX=IMP*VMP
           VMP=VMP+0.01
            IMP=CURRENT5194(VMP,0.9*IL, 1, 1)  !IMP PER MODULE
          END DO

        PMAX = IMP*VMP*NSER*NPRL  !PER ARRAY

        IF(PMAX.NE.0.)THEN
          UTIL=P/PMAX
        ELSE
          UTIL=0.d0
        ENDIF

C      Fill factor
        IF ((VOC.GT.0.d0).AND.(ISC.GT.0.d0)) THEN
          FF=VMP*IMP/VOC/ISC
        ELSE
          FF=0.d0
        ENDIF
      ENDIF

      err_P     = PMAX - P_guess !Performance error
      P_guess   = PMAX !Set performance to most recent calc
```

```
      p_iter    = p_iter + 1 !+1 to iteration counter

      END DO

C-----------------------------------------------------------------

C     INVERTER
C     This section modifies the operating voltage of the modules
C     in order to couple them with the inverter

      P_mp_array = PMAX       !Array power at maximum power point
      V_mp_array = VMP*NSER   !Array voltage at maximum power point
      I_mp_array = IMP*NPRL   !Array current at maximum power point
      V_oc_array = VOC*NSER   !Array open circuit voltage

      IF (MODE .EQ. 2) THEN
        eta_inverter = 1            !Initialization value

        if (P_mp_array<P_max_inv) then
          if (V_mp_array > V_max_inv) then
              V=V_max_inv
              I =  CURRENT5194(V,0.9*IL,NSER,NPRL)
              if ( (V.lt.V_min_inv) .or. (V.gt.V_max_inv) .or.
     .              (P.gt.P_max_inv) ) then
                eta_inverter = 0.d0
              else
                !Interpolation routine for inverter efficiency
                X(1) = V
                X(2) = P_mp_array
                NX(1) = 3
                NX(2) = 7
                call DynamicData(LU_inv,2,NX,1,X,Y,INFO,*101)
                call LINKCK('Type198','DynamicData',3,198)
101             if (ErrorFound()) return 1
                eta_Inverter = Y(1)
            endif
                P=V*I*eta_Inverter
          else
            if ((V_min_inv<V_mp_array) .and. (V_mp_array< V_max_inv))
then
                  I=I_mp_array
                  V=V_mp_array
                if ( (V.lt.V_min_inv) .or. (V.gt.V_max_inv) .or.
     .              (P.gt.P_max_inv) ) then
                  eta_inverter = 0.d0
                else
                  !Interpolation routine for inverter efficiency
                    X(1) = V
                    X(2) = P_mp_array
                    NX(1) = 3
                    NX(2) = 7
                    call DynamicData(LU_inv,2,NX,1,X,Y,INFO,*102)
                    call LINKCK('Type198','DynamicData',3,198)
102                 if (ErrorFound()) return 1
                    eta_Inverter = Y(1)
                  endif
```

```
                P=I*V*eta_inverter
            else ! "V < V_min"

                if(V_oc_array > V_min_inv) THEN
                  V=V_min_inv
                  I = CURRENT5194(V,0.9*IL,NSER,NPRL)
                if ( (V.lt.V_min_inv) .or. (V.gt.V_max_inv) .or.
     .              (P.gt.P_max_inv) ) then
                  eta_inverter = 0.d0
                else
                  !Interpolation routine for inverter efficiency
                    X(1) = V
                    X(2) = P_mp_array
                    NX(1) = 3
                    NX(2) = 7
                    call DynamicData(LU_inv,2,NX,1,X,Y,INFO,*103)
                    call LINKCK('Type198','DynamicData',3,198)
103                 if (ErrorFound()) return 1
                    eta_Inverter = Y(1)
              endif
                  P=V*I*eta_inverter
                else
                  V=V_oc_array
                  I=0
                  P=0
                  eta_inverter=0
                endif
            endif
        endif

    else !"P_mp>P_max_inv"
    P=0
    eta_inverter=1000

    if (V_oc_array<V_min_inv) then
        P=0
        I=0
        V=0
    else !"V_oc>V_min"
        V = V_min_inv
      I = CURRENT5194(V,0.9*IL,NSER,NPRL)
        I_vmin = I
        P_vmin=V_min_inv*I_vmin
        if (V_oc_array>V_max_inv) then
          V = V_max_inv
          I_vmax = I
          P_vmax=V_max_inv*I_vmax
        else
          P_vmax=0
          V_max_prime=V_oc_array
        endif

        if (V_mp_array<V_min_inv) then
          P=P_vmin
        else
          if (V_mp_array>V_max_inv) then
```

```
                if ((P_vmin>P_max_inv) .and. (P_vmax>P_max_inv)) then
                  P=0
                else
                  P=dmax1(P_vmin, dmin1(P_max_inv, P_vmax))
                endif
            else !"V_min < V_mp < V_max"
                if ((P_vmin>P_max_inv) .and. (P_vmax>P_max_inv)) then
                  P=0
                else
                  P=P_max_inv
                endif
            endif
          endIf
      endIf
      eta_inverter=P_max_inv/P_mp_array
    endif

    P = eta_inverter * P_mp_array

    ENDIF

C*****  Update power during the night - inverter on, so it consumes
power
    IF(SUNEFF.EQ.0.d0)THEN
      P = -tare
      eta_inverter = 0
    ENDIF

C**** SET OUTPUTS  ************************************
    OUT(1)  = V             !ARRAY VOLTAGE
    OUT(2)  = I             !ARRAY CURRENT
    OUT(3)  = P             !ARRAY POWER
    OUT(4)  = PMAX          !ARRAY MAXIMUM POWERset to non-zero only
if DOPMAX (Par 23) > 0
    OUT(5)  = UTIL          !RATIO P/PMAX
    OUT(6)  = VMP*NSER      !ARRAY VOLTAGE AT MAXIMUM POWER POINT
    OUT(7)  = IMP*NPRL      !ARRAY CURRENT AT MAXIMUM POWER POINT
    OUT(8)  = VOC*NSER      !ARRAY OPEN CIRCUIT VOLTAGE
    OUT(9)  = ISC*NPRL      !ARRAY SHORT CIRCUIT CURRENT
    OUT(10) = FF            !ARRAY FILL FACTOR
    OUT(11) = TC            !ARRAY TEMPERATURE
    IF (SunTilt.GT.0) THEN
      OUT(12) = P/(Area*NSER*NPRL*SunTilt) !ARRAY COLLECTION
EFFICIENCY
    ELSE
      OUT(12)= 0.D0
    ENDIF
    IF (SunTilt.GT.0) THEN
      OUT(13) = PMAX/(Area*NSER*NPRL*SunTilt) !ARRAY COLLECTION
EFFICIENCY at MPP
    ELSE
      OUT(13)= 0.D0
    ENDIF
    IF (MODE .EQ. 2) THEN
          OUT(14) = eta_inverter
    ENDIF
```

```
1010  RETURN 1
      END SUBROUTINE TYPE299

C*************************************************************
      FUNCTION CURRENT5194(V,IMR,NSER,NPRL)

C     Iterative solution for current as a function of voltage using
C     equations from the five-parameter model.  Newton's method is used
C     to converge on a value.  Max power at reference conditions is
initial
C     guess.

      IMPLICIT NONE

      COMMON /ARRAY194/ A, IL, IO, RS, RSH

      DOUBLE PRECISION IOLD,INEW,F,FPRIME, I, CURRENT5194,V_MODULE,V
      DOUBLE PRECISION A, IL,IO,RS,RSH,IMR
      INTEGER NSER,NPRL

      IOLD = 0.0
      V_MODULE    = V/NSer
C**** first guess is max.power point current
      INEW = IMR
      DO WHILE (DABS(INEW-IOLD).GT.1.E-4)
        IOLD   = INEW
        F      = IL-IOLD-IO*(DEXP((V_MODULE+IOLD*RS)/A)-1.0)-
     &             (V_MODULE+IOLD*RS)/RSH
        FPRIME = -1.-IO*(RS/A)*DEXP((V_MODULE+IOLD*RS)/A)-(RS/RSH)
        INEW   = MAX(0.d0,(IOLD-(F/FPRIME)))
      END DO
      I           = INEW       !CURRENT FOR ONE MODULE
      CURRENT5194 = I*NPRL !CURRENT FOR ENTIRE ARRAY

      END FUNCTION CURRENT5194

C*************************************************************
      FUNCTION OPENVOLTN194(VOCR,SUN)

C     Function added by BF and modified by SAK
C     Iterative solution for open-circuit voltage.  Explicit algebraic
solution
C     not possible in 5-parameter model

      IMPLICIT NONE

      COMMON /ARRAY194/ A, IL, IO, RS, RSH

      DOUBLE PRECISION VOCOLD,VOCNEW,OPENVOLTN194,I
      DOUBLE PRECISION A,IL,IO,RS,RSH,VOCR,SUN
      DOUBLE PRECISION VOCUP,VOCLOW

      IF (SUN.LT.1) THEN
        OPENVOLTN194=0
```

```
      ELSE
        VOCUP=VOCR*1.5
        VOCLOW=0
        VOCOLD=0
        VOCNEW=VOCR
        DO WHILE (DABS(VOCUP-VOCLOW).GT.1.E-3)
          VOCOLD=VOCNEW
          I=IL-IO*(DEXP(VOCOLD/A)-1)-VOCOLD/RSH
          IF (I.LT.0) VOCUP=VOCOLD
          IF (I.GT.0) VOCLOW=VOCOLD
          VOCNEW=(VOCUP+VOCLOW)/2
        END DO
        OPENVOLTN194=VOCNEW
      ENDIF

      END FUNCTION OPENVOLTN194

C*****************************************************************
      FUNCTION FREECONVECTION194(TC,TA,SLOPE,RHO_AIR,Pr_air,mu_air,
     & Area,Length,Width,k_air)

C     Function added by TN (2010)
C     Solution for free convection coefficienet as presented in Nellis
and Klein (2008)
C     and EES

      IMPLICIT NONE

      DOUBLE PRECISION FREECONVECTION194,TC,TA,SLOPE,RHO_AIR,Pr_air,
     & mu_air,Area,Length,Width,k_air,grav,L_ch_f,nu,Beta,g_spec,
     & Gr,Ra,C_lam,
     & Nu_lam,
     & C_turb,Nu_turb,Nu_bar,h_up,h_vert,h_down

      DATA grav/9.81/

      L_ch_f    = Area/(2.*(Length+Width))  !Eq. 6-54 (Nellis&Klein)

C     Properties Constant for Each Plate Scenario
      nu        = mu_air / rho_air          !Kinematic Viscosity
      Beta      = 1. / ((TA+TC)/2.)         !volumetric coefficient of
thermal expansion

C     Horizontal Heated Upward Facing Plate (L_ch_f)
      g_spec    = grav*MAX(0.,cosD(SLOPE))  !Adjustment of gravity
vector
      Gr        = g_spec*Beta*ABS(TC-TA)*L_ch_f**3./nu**2.    !Grashof
Number
      Ra        = max(0.0001,Gr*Pr_air)                 !Rayleight
Number

      C_lam     = 0.671/(1.+(0.492/Pr_air)**(9./16.))**(4./9.)  !Eq. 6-
49 (Nellis&Klein)
      Nu_lam    = 1.4/log(1.+(1.4/(0.835*C_lam*Ra**0.25)))!Eq. 6-56
(Nellis&Klein)
```

```
      C_turb    = 0.14*((1.+0.0107*Pr_air)/(1.+0.01*Pr_air)) !Eq. 6-58
(Nellis&Klein)
      Nu_turb   = C_turb*Ra**(1./3.)        !Eq. 6-57  (Nellis&Klein)
      Nu_bar    = (Nu_lam**10. + Nu_turb**10.)**(1./10.) !Eq. 6-55
(Nellis&Klein)
      h_up      = Nu_bar*k_air/L_ch_f

C     Vertical Plate (Length)
      g_spec    = grav*sinD(SLOPE)          !Adjustment of gravity
vector
      Gr        = g_spec*Beta*ABS(TC-TA)*Length**3/nu**2
      Ra        = max(0.0001,Gr*Pr_air)

      Nu_bar    = (0.825+(0.387*Ra**(1./6.))/(1+(0.492/Pr_air)**
     &            (9./16.))**(8./27.))**2  !(Incropera et al.,2006)
      h_vert    = Nu_bar*k_air/Length

C     Horizontal Heated Downward Facing Plate
      g_spec    = grav*MAX(0.,-cosD(SLOPE))
      Gr        = g_spec*Beta*ABS(TC-TA)*L_ch_f**3/nu**2
      Ra        = max(0.0001,Gr*Pr_air)

      Nu_bar    = 2.5/log(1.+(2.5/(0.527*Ra**0.2))*(1.+(1.9/Pr_air)
     &            **0.9)**(2./9.))    !Eq. 6-59  (Nellis&Klein)
      h_down    = Nu_bar*k_air/L_ch_f

C     Take Maximum of 3 Calculated Heat Transfer Coefficients

      FREECONVECTION194 = MAX(h_down,h_vert,h_up)  !Fig. 6-12
(Nellis&Klein)

      END FUNCTION FREECONVECTION194

C*****************************************************************
      FUNCTION CHANNELFLOW194(e,D_h,Re_dh,AR,Pr_air,Length,k_air)

C     Function added by TN (2010)
C     Solution for internal forced convection as presented in Nellis
and Klein (2008)
C     and EES.

      IMPLICIT NONE

      DOUBLE PRECISION CHANNELFLOW194,e,D_h,Re_dh,AR,Pr_air,Length,
     & k_air,f_fd,Nus,h_f

      f_fd  = (-2.*log10(max(0.01,((2.*e/(7.54*D_h)-5.02/Re_dh*log10(2.
     &         *e/(7.54*D_h)+13./Re_dh))))))**(-2)
      if (Re_dh < 2300) then
        Nus = 7.541*(1.-2.610*AR+4.970*AR**2-5.119*AR**3+2.702*AR**4
     &        -0.548*AR**5)
      else
            Nus = (f_fd/8.*(Re_dh -
1000.)*Pr_air)/(1.+12.7*(Pr_air**(2./3.)-1.)
     &               *sqrt(f_fd/8.))*(1.+(Length/D_h)**(-0.7))
      endif
```

```
      h_f   = Nus*k_air/D_h

      CHANNELFLOW194 = h_f

      END FUNCTION CHANNELFLOW194

C*****************************************************************

      FUNCTION CHANNELFREE194(W_gap,SLOPE,TA,T_cr,k_air,rho_air,
     & cp_air,mu_air,Length)

C     Function added by TN (2010)
C     Solution for internal forced convection as presented in Nellis
and Klein (2008)
C     and EES

      IMPLICIT NONE

      DOUBLE PRECISION CHANNELFREE194,grav,W_gap,SLOPE,TA,T_cr,
     & k_air,rho_air,cp_air,mu_air,Length,g_spec,Beta,alpha,
     & nu_air,Ra,Nu,h

      DATA grav/9.81/

      nu_air    = mu_air / rho_air          !Kinematic Viscosity

      g_spec    = max(0.1, sinD(SLOPE)*grav)
      Beta        = 1./((T_cr+TA)/2.)
      alpha       = k_air / (rho_air * cp_air)
      Ra        = max(0.001,g_spec*W_gap**3*Beta*(T_cr-
TA)/(nu_air*alpha))
      Nu          = Ra/24.*W_gap/Length*(1.-Dexp(-
35./Ra*Length/W_gap))**.75

      h         = Nu*k_air/W_gap

      CHANNELFREE194 = h

      END FUNCTION CHANNELFREE194
```